University of Zurich[UZH]

Department of Geography

The Effect of Cold Ice on the Ablation of the Grenzgletscher

GEO 511 Master's Thesis

Author
Michael Thalmann
13-767-066

Supervised by
Dr. Martin Lüthi

Faculty Representative
Prof. Dr. Andreas Vieli

30.09.2019
Department of Geography, University of Zurich

Abstract

Glaciers and ice sheets are increasingly melting due to climate change. Albedo is one of the most important factors controlling the energy balance at the glacier surface and therefore ice melt. Glacier-wide albedos decrease with receding snowlines. However, also bare-ice surfaces in the ablation zones tend to darken in different places in the world. The aim of this Master's Thesis is to study the influence of cold ice on the bare-ice albedo. For this purpose, the Grenzgletscher in the European Alps was chosen as study site, because it is a large and well-studied polythermal glacier. Large supraglacial channels and strikingly bright ice indicate cold ice at the glacier surface in the lower ablation zone. A borehole temperature measurement revealed cold ice in the surface layer of the glacier.

Multi-annual ablation measurements were compared with albedo images computed from Landsat TM and OLI data. Additionally, temporal and spatial changes in the bare-ice albedo of the Grenzgletscher were analysed. The albedo is subject to great seasonal fluctuations, which are mainly linked to the presence of liquid water on the glacier surface. In order to minimize the impact of seasonality, the selection of the Landsat images was limited to end-of-summer scenes (August and September) for the detection of long-term trends. Since 1990, the bare-ice albedo increased in the study area. Furthermore, the albedo is raised higher up on the glacier what is possibly linked to an earlier emergence of the cold ice at the glacier surface. However, this study did not find a correlation between albedo and ablation. More extensive investigations of the ice temperature at the surface as well as the comparison of more ablation measurements with high-resolution albedo images could give further insight about the influence of cold ice on the ablation of the Grenzgletscher. In the global context, this knowledge potentially helps to understand the ablation of the ice shields, which is of great importance for people and environment on our planet.

Contents

1 Introduction **11**

1.1 Glacier Melt and its Consequences 11

1.2 State of Knowledge 13

1.3 Study Area 14

1.4 Research Questions 15

1.5 Content of this Master's Thesis 17

2 Theoretical Background **19**

2.1 Glaciers 19

2.1.1 Glacier Motion 19

2.1.2 Thermal Regimes 19

2.1.3 Mass Balance 20

2.1.4 Surface Energy Balance 21

2.1.5 Shortwave Radiation and Glacier Albedo 22

2.2 Albedo of Ice, Snow and Glaciers 23

2.2.1 The Albedo of Clean Ice and Snow 23

2.2.2 Light-absorbing Impurities (LAIs) 24

2.2.3 Ice temperature, Glacier Hydrology and Albedo 27

2.2.4 Glacier Albedo Variations in Space and Time 30

2.2.5 Glacier Darkening Related to Climate Change 30

2.2.6 Darkening Ice in Greenland 32

2.3 Glacier Albedo in Remote Sensing 34

2.3.1 History of Satellite-derived Glacier Albedo Measurements . . 34

2.3.2 Difficulties of Space-born Albedo Retrieval 36

2.3.3 Landsat Data and Glacier Albedo 38

2.3.4 Narrow-to-broadband Conversion for Landsat Bands 40

3 Study Area **43**

3.1 Cold Firn and Ice in the European Alps 43

3.2 Cold Firn in the Accumulation Area of Grenzgletscher 44

3.3 Gorner-/Grenzgletscher System 45

3.4 Polythermal Structure of the Lower Ablation Zone of Grenzgletscher 46

3.5 Study Area on the Lower Ablation Zone of the Grenzgletscher 48

4 Materials and Methods **50**

4.1 Ablation Data 50

4.1.1 Pre-existing Measurements 50

4.1.2 Additional Measurements in Autumn 2018 50

4.1.3 Computation of Degree-day Factors 51

4.2 Albedo Data 52

4.2.1 Data Selection 52

4.2.2 Albedo Computation 53

4.3 Comparison of Albedo and Ablation 54

4.4 Temporal Change in the Albedo 55

4.5 Spatial Change in Albedo Patterns 56

4.6 Ice Temperature Measurement 56

5 Results **57**

5.1 Albedo and Ablation 57

5.1.1 Wires 57

5.1.2 Stakes 57

5.2 Temporal Change in the Albedo 59

5.3 Spatial Change of Albedo Patterns 62

5.4 Ice Temperature Measurement 66

6 Discussion **67**

6.1 Albedo 67

6.1.1 Albedo Values 67

6.1.2 Albedo Computation 68

6.2 Ablation 69

6.2.1 Ablation Values 69

6.2.2 Comparison of Albedo and Ablation 69

6.3 Ice Temperature at the Glacier Surface 71

6.4 Seasonality of the Bare-Ice Albedo 74

6.5 Brightening and Changing Albedo Patterns 75

7 Conclusion and Outlook **77**

8 Acknowledgements **78**

9 Bibliography **79**

10 Appendix **94**

10.1 Appendix 1: Degree-Day-Factors 94

10.1.1 Appendix 1.1: Degree-Day-Factors for the Wires 94

10.1.2 Appendix 1.2: Degree-Day-Factors for the Stakes 106

10.2 Appendix 2: Additional Material 118

11 Personal Declaration **121**

List of Figures

1 Map of the study area. . . . 14
2 Supraglacial lakes and channels on the Grenzgletscher. . . . 15
3 Albedo of Grenzgletscher, Gornergletscher and Findelgletscher. . . . 17
4 Spectral reflectance curves for snow and ice in different formation stages. . . . 25
5 Cryoconite holes on the Grenzgletscher. . . . 28
6 Dark ice zone . . . 34
7 Comparison of bandwidth of Landsat sensors. . . . 40
8 Gorner-/Grenzgletscher system in the Little Ice Age, on the Dufourkarte (1863). . . . 46
9 Study area on the Grenzgletscher. . . . 47
10 Solar radiation between July 1 and September 31 on the lower ablation area of Grenzgletscher. . . . 48
11 Field work. . . . 51
12 Map of the location of the test areas. . . . 54
13 1-cell environment and 4-cell environment. . . . 55
14 Photograph of the borehole ice temperature measurement next to 'bh3-07'. . . . 56
15 Albedo and DDF of the wires. . . . 58
16 Wires positions. . . . 59
17 Albedo and DDF of the stakes. . . . 60
18 Stake positions. . . . 61
19 Comparison between 'bh1-05' and 'bh4-05'. . . . 61
20 Albedo change in the test areas. . . . 63
21 Albedo change boxplots: 5 years. . . . 64
22 Spatial change in albedo patterns. . . . 65
23 Borehole ice temperature next to 'bh3-07'. . . . 66
24 Cold ice at the surface of the Grenzgletscher. . . . 73

25 Degree-Day-Factor 'bh1-05'. 94
26 Degree-Day-Factor 'bh3-05'. 95
27 Degree-Day-Factor 'bh4-05'. 96
28 Degree-Day-Factor 'center'. 97
29 Degree-Day-Factor 'hut'. 98
30 Degree-Day-Factor 'lake'. 99
31 Degree-Day-Factor 'temp1-07'. 100
32 Degree-Day-Factor 'temp1-08'. 101
33 Degree-Day-Factor 'temp3-07'. 102
34 Degree-Day-Factor 'temp4-08'. 103
35 Degree-Day-Factor 'temp4-10'. 104
36 Degree-Day-Factor 'temp5-10'. 105
37 Degree-Day-Factor 'st13'. 106
38 Degree-Day-Factor 'st14'. 107
39 Degree-Day-Factor 'st23'. 108
40 Degree-Day-Factor 'st24'. 109
41 Degree-Day-Factor 'st28'. 110
42 Degree-Day-Factor 'st34'. 111
43 Degree-Day-Factor 'st35'. 112
44 Degree-Day-Factor 'st36'. 113
45 Degree-Day-Factor 'st37'. 114
46 Degree-Day-Factor 'st53'. 115
47 Degree-Day-Factor 'st62'. 116
48 Degree-Day-Factor 'st63'. 117
49 Albedo change of end-of-summer scenes (boxplots): 10 year interval. . 118
50 Albedo change of all scenes (boxplots): 5 year interval. 118
51 Albedo change of all scenes (boxplots): 10 year interval. 119
52 Comparison of albedo image and SwissImage. 120

List of Tables

1 Ice sheets and glaciers: area and sea-level rise 13
2 Snow and ice densities 21
3 Albedos for snow and ice 32
4 Impact of anisotropy effect for different glacier surface types 39
5 Landsat Bandwidths 41
6 Lower boundaries of cold firn occurrence in the European Alps 45
7 Test areas 53
8 Mean albedo categorized by month. 62
9 Ablation 'bh1-05' 94
10 Ablation 'bh3-05' 95
11 Ablation 'bh4-05' 96
12 Ablation 'center' 97
13 Ablation 'hut' 98
14 Ablation 'lake' 99
15 Ablation 'temp1-07' 100
16 Ablation 'temp1-08' 101
17 Ablation 'temp3-07' 102
18 Ablation 'temp4-08' 103
19 Ablation 'temp4-10' 104
20 Ablation 'temp5-10' 105

Abbreviations

A1	Test Area 1
A2	Test Area 2
A3	Test Area 3
A4	Test Area 4
AIS	Antarctic Ice Sheet
AVHRR	Advanced Very High Resolution Radiometer
BRDF	Bi-directional Reflectance Distribution Function
DDF	Degree-day Factor
ELA	Equilibrium Line Altitude
ETH	Eidgenössische Technische Hochschule
ETM+	Enhanced Thematic Mapper Plus
GLOF	Glacial Lake Outburst Flood
GrIS	Greenland Ice Sheet
IPCC	Intergovernmental Panel on Climate Change
LAIs	Light-Absorbing Impurities
LaSRC	Landsat 8 Surface Reflectance Code
LEDAPS	Landsat Ecosystem Disturbance Adaptive Processing System
MAFT	Mean Annual Firn Temperature
MODIS	Moderate-Resolution Imaging Spectroradiometer
OLI	Operational Land Imager
SLE	Sea-level Equivalent
TM	Thematic Mapper
USGS	United States Geological Survey
WGMS	World Glacier Monitoring Service

1 Introduction

1.1 Glacier Melt and its Consequences

Retreating glaciers are one of the most visible signs of a changing climate (Benn and Evans, 2010; IPCC, 2013). Glacier retreat leaves behind large amounts of unconsolidated sediments, unstable rock walls and ice-marginal lakes (Evans and Clague, 1994; Kääb et al., 2007). Catastrophic events linked to glacier recession, like landslides (Huggel et al., 2012), debris flows (Chiarle et al., 2007; Stoffel and Huggel, 2012) and glacial lake outburst floods (GLOFs) (Frey et al., 2010; Worni et al., 2012), are an often studied subject in mountainous areas (Benn and Evans, 2010).

Glaciers play a critical role for the environment and people on larger scales, too. On a local and regional scale, glaciers provide water resources for drinking water, agriculture, energy production by hydro-power plants, industries and recreational purposes (Sorg et al., 2012; Radić and Hock, 2014; Soruco et al., 2015; Huss et al., 2017). Glacial runoff is often high during hot periods with low precipitation (Soruco et al., 2015; Huss and Hock, 2018). About half of the earth's population uses mountain water (Beniston, 2003). However, quantification of glacial influence on runoff is still a subject of research (Radić and Hock, 2014; Huss and Hock, 2018).

On a global scale, the role of glaciers seems negligible as they cover only 0.5% of the total land surface[1], without including the ice sheets of Antarctica and Greenland[2] (IPCC, 2013). The enormous importance of glaciers in terms of the rising sea-level was first noticed by Meier (1984). Despite making up only a very small part of the Earth's total ice volume (e.g. Radić and Hock, 2014), the mass loss rate of glaciers was equal or even exceeded the mass loss rates of each of the ice sheets during the last decades (IPCC, 2013). Thus, melted glacial ice makes up between one-third and one-half of global sea-level rise in this period (Dyurgerov and Meier, 2005; Kaser et al., 2006; Cogley, 2009b,a; Gardner et al., 2013). Water from melting glaciers is expected to contribute 0.06 to 0.15 m to sea-level rise in the 21$^{\text{th}}$ century, depending on the emission scenario. Despite their relatively small volume in the global context,

---

[1] Calculated for IPCC (2013) from glacier outlines by Arendt et al. (2012), which include glaciers around Greenland and Antarctica.

[2] For more information about the differentiation between ice sheets and glaciers see IPCC (2013).

they are likely to be one of the major cryospheric contributors to sea-level rise in the near-future (IPCC, 2013).

The sea-level rise that would occur if all the ice of an ice body melted is called *sea-level equivalent* (SLE). The SLE of all glaciers is about 160 times smaller than the aggregated SLE of both ice sheets (Tab. 1). The Antarctic Ice Sheet (AIS) is by far the largest cryospheric entity on planet Earth (IPCC, 2013). Its future contributions to sea-level rise are highly uncertain (Deconto and Pollard, 2016). The Greenland Ice Sheet (GrIS) is much smaller. Nevertheless, the GrIS mass loss was higher than the AIS mass loss during the last decades (IPCC, 2013). Until the end of the 21$^{\text{th}}$ century, the GrIS is expected to contribute more than 0.2 m to the global sea-level rise (Dumont et al., 2014).

According to Benn and Evans (2010), size is not the only difference between the ice sheets, but they also differ in the ablation mechanisms. There is hardly any surface melt in the cold and dry Antarctic climate. The major ice loss of the AIS is towards the ocean by calving and submarine melting at the bottom of ice shelves. On the contrary, the mass loss of the GrIS is approximately equally divided into ice discharge and surface melt that becomes runoff (van den Broeke et al., 2009). With a trend towards higher air temperatures over Greenland (Benn and Evans, 2010) and increasing amounts of absorbed solar energy (Box et al., 2012), surface melt is likely to constitute an important part of the GrIS mass loss in the next decades.

Sea-level rise affects millions of people living in coastal regions (e.g. Strauss et al., 2015). Coastal lowlands[3] are densely populated. Despite the extent of only about 2% of the global land surface, this area is home to about a tenth of the Earth's population (McGranahan et al., 2007). Sea-level rise leads to flooding, more coastal erosion, salinization and changes in ecosystems (Nicholls et al., 2011). These changed conditions can be countered with expensive construction measures or migration away from the affected coastal zones (McGranahan et al., 2007). Migration towards land-locked areas (Hauer, 2017; Aerts, 2017) makes sea-level rise a subject that concerns a large part of humanity.

---

[3] Coastal lowlands are defined as land that is less than 10 m above sea level (McGranahan et al., 2007).

Tab. 1: Comparison of the Antarctic Ice Sheet, the Greenland Ice Sheet (GrIS) and glaciers (including glaciers around Greenland and Antarctica) concerning size and sea-level equivalent (SLE) (IPCC, 2013).

	Percent of Global Land Surface	SLE (m)
Antarctic Ice Sheet	8.3	58.3
Greenland Ice Sheet	1.2	7.36
Glaciers	0.5	0.41

1.2 State of Knowledge

The accurate prediction of glacier melt is important to be prepared for the changes arising from it. This master thesis focusses on the surface melting of polythermal ice bodies and thus contributes to the understanding of the melting behaviour of glaciers.
Surface melt is largely modulated by the albedo, especially in places where solar radiation is the most important component of the surface energy balance (Bøggild et al., 2010; Braithwaite and Olesen, 1990; Braithwaite et al., 1998). Therefore, the albedo is an important element for modelling melt and even the climate (Gardner and Sharp, 2010).

The decline of glacier surface albedo is a phenomenon that has been observed in various places on Earth in recent decades (Tedesco et al., 2011; Box et al., 2012; Stroeve et al., 2013; Dumont et al., 2014; Takeuchi et al., 2001; Oerlemans et al., 2009; Fugazza et al., 2019). Albedo decline is often associated with the increased presence of particles on the glacier surface which have a lower albedo than the ice itself (Wientjes and Oerlemans, 2010; Tedstone et al., 2017; Ryan et al., 2018). These particles are often grouped under the term *light-absorbing impurities* (LAIs) (e.g. Tedstone et al., 2017). Supraglacial runoff is able to relocate LAIs (Ryser et al., 2013). These redistribution processes are able to reduce the glacier albedo (Bøggild et al., 2010).

The temperature of glacial ice can be at the pressure melting temperature and is then called *temperate ice*. If the ice has a temperature lower than the pressure melting temperature, it is called *cold ice*. Cold ice is impermeable to water as long as there are no crevasses or fractures (Hodgkins, 1997; Boon and Sharp, 2003; Ryser et al., 2013). Therefore, distinct supraglacial runoff is typical for cold ice bodies (Knap and Oerlemans, 1996; Suter et al., 2001).

The connection between supraglacial runoff and albedo leads to the assumption that the occurrence of cold ice could increase albedo. Furthermore, small cavities in the impermeable cold ice are often filled with air instead of water (e.g. Suter et al.,

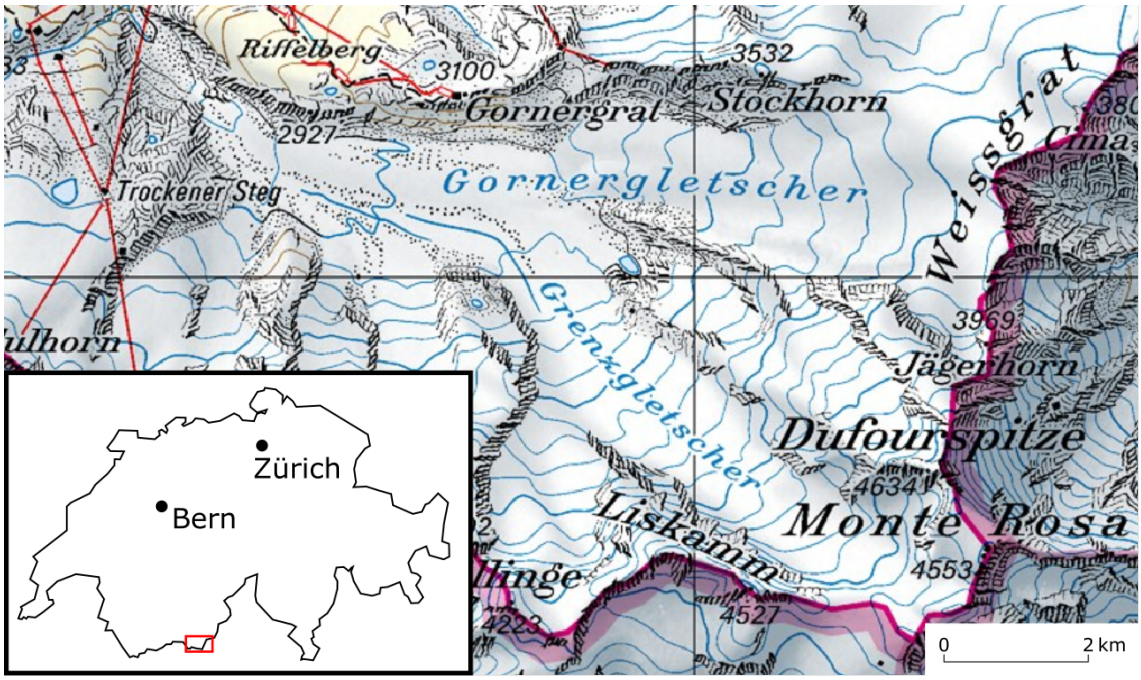

Fig. 1: Map of the study area and its location in Switzerland. The lower part of the Grenzgletscher is still named Gornergletscher on the the swisstopo map (swisstopo, 2019).

2001). These air bubbles further increase the albedo (Gardner and Sharp, 2010). In conclusion, the ablation of cold ice is likely to be reduced due to these albedo effects.

1.3 Study Area

The Grenzgletscher is a large polythermal glacier in the south of Switzerland, near the border to Italy (Fig. 1). The upper accumulation area of the Grenzgletscher lies in the heart of the Monte Rosa, which is Switzerland's highest mountain massif. The cold high-altitude conditions allow the formation of cold firn and ice (Suter et al., 2001). Further down the valley the temperatures are higher, but the accumulation still outweighs the ablation. Temperate ice is formed here, which buries the cold ice underneath. Below the *equilibrium line altitude* (ELA) (Section 2.1.3), the glacier begins to melt and the temperate layer becomes thinner. The cold ice emerges at the glacier surface in the lower ablation zone (Eisen et al., 2009). This relatively flat part of the glacier has been well known for large supraglacial channels and lakes (Fig 2) for a long time (Renaud, 1936). The ice in this particular area appears to be much cleaner and brighter than the surrounding ice of the upper ablation zone and the neighbouring glaciers (Ryser et al., 2013).

The Grenzgletscher has been the subject of various studies since the 1970s because of its size, accessibility and a glacier-dammed lake and that poses a risk to the valley

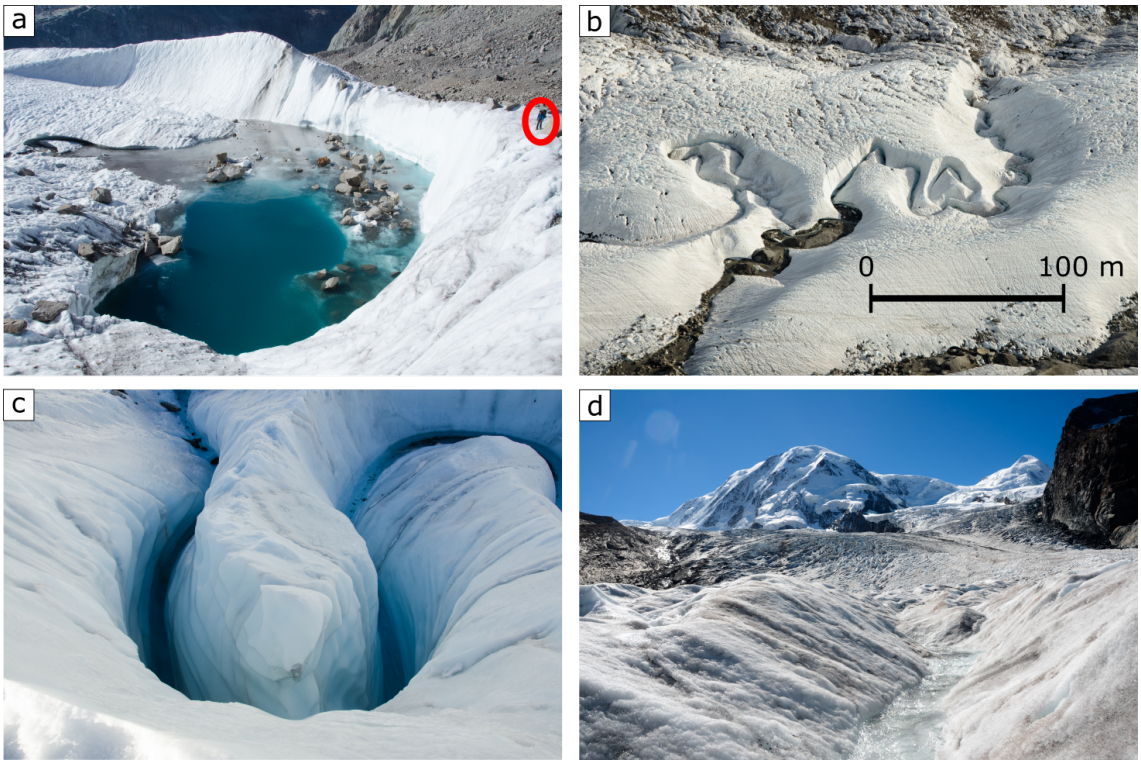

Fig. 2: Several supraglacial hydrological features on the Grenzgletscher: (a) shows the largest (compare with the human in the red outlines) and presumably deepest supraglacial lake on the Grenzgletscher. The length of the lake is almost 100 m. Due to its multi-annual existence, the lake is even found in the topographic map of Switzerland (swisstopo, 2019). It is located about 1.3 km from the glacier terminus; (b) shows some of the large meltwater channels. The scale-bar is roughly derived from aerial photographs; (c) shows a narrow and deeply incised meander of one of the large channels. The channels can have a depth of 10-30 m (Ryser et al., 2013); (d) shows a smaller channel in the confluence area. Further back a part of the large crevasse zone in the upper ablation zone can be seen.

downstream (Benoit et al., 2018). Therefore, some data and information about the glacier are already available. Additionally, there is also a meteo station on the Gornergrat, about one kilometre from the glacier margin. Due to all these factors, the Grenzgletscher is a very suitable place for this study.

According to Ryser et al. (2013), studies addressing the polythermality of the Grenzgletscher possibly help to understand the influence of polythermal temperature regimes on the ablation of the ice sheets. The advantage of research on alpine glaciers compared to research on the ice sheets are the much simpler logistics and the associated lower costs.

1.4 Research Questions

The clear visual differences on the bare-ice glacier surface of the Grenzgletscher (Ryser et al., 2013) raised the question, if the ablation is affected through albedo

effects. As the differences between clean ice and dirty ice are highest in the visual part of the solar spectrum and diminish towards longer wavelengths (Fig. 4) (Naegeli et al., 2017), there is consequently a difference in the albedo. Furthermore, Landsat bands of the visible spectrum showed higher reflectance values towards the glacier tongue. The Grenzgletscher stands out among the glaciers in this region because of the extraordinary high albedo in the lower ablation zone which is preceded by lower albedo values higher up on the glacier (Fig. 3). The lower ablation zone is defined as the relatively flat part of the ablation zone which extends from the terminus up to about 2600 m a.s.l. in this study. Based on these observations, the following research questions were elaborated:

1. **Has there been a difference in the ablation rate between zones of cold ice and zones of temperate ice?**

Question 1 analyses the influence of cold ice on the ablation of the Grenzgletscher. Albedo is used as a proxy for identifying cold bare-ice zones. Thus, ablation point measurements are compared with the albedo. For bare-ice, this paper uses the definition by Naegeli et al. (2019, p. 398) as "glacier surfaces covered neither by snow nor by thick debris".

2. **Has there been a change in the albedo of the glacier surface during the last decades?**

Question 2 investigates the temporal change of the bare-ice albedo of the Grenzgletscher. Does the glacier surface experience darkening as other glaciers in many parts of the world (see Section 2.2.4 and 2.2.6)?

3. **Has there been a spatial change in albedo patterns of the glacier surface during the last decades?**

Question 3 examines the temporal evolution of spatial patterns of the bare-ice albedo on the Grenzgletscher. The thermal structure of cold and polythermal glaciers will presumably be altered by a changing climate (e.g. Gusmeroli et al., 2012). For Grenzgletscher, glacier recession could result in an upwards movement of the cold-ice zone at the glacier surface, because the temperate ice, which covers the cold ice, melts faster.

The answers to these question could help to better comprehend the influence of cold ice on the melting of polythermal glaciers. Knowledge of polythermal Alpine

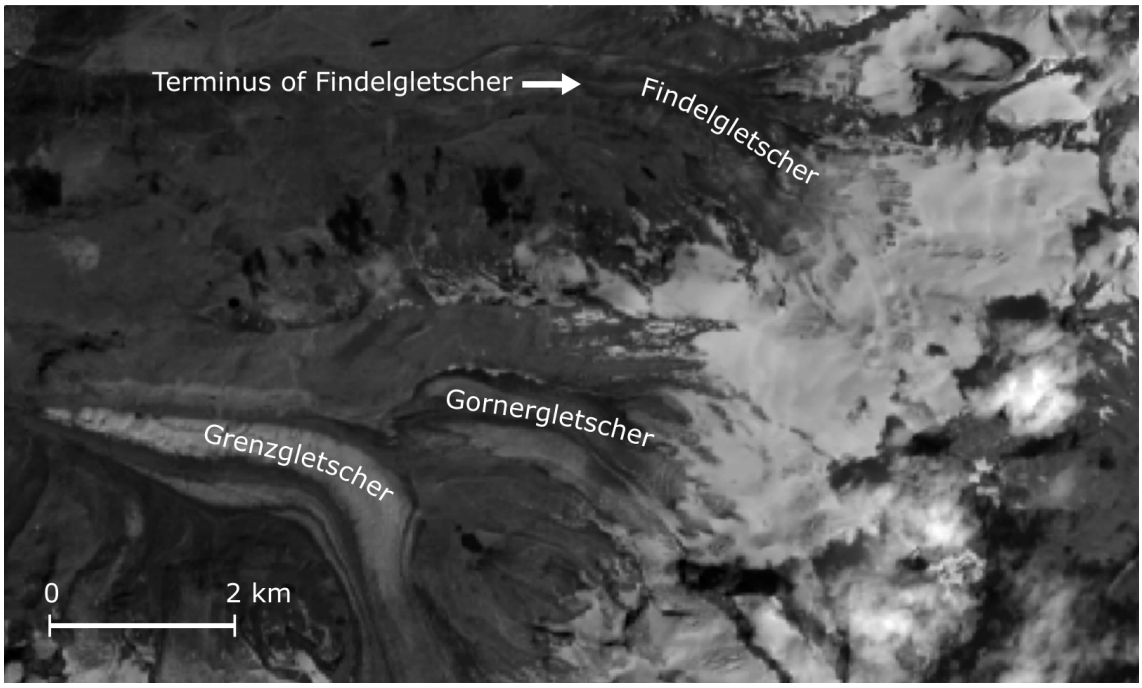

Fig. 3: This picture shows the albedo of the region west of Zermatt on 30 July 2018. Bright parts of the image represent zones with a higher albedo. The ablation area of the Grenzgletscher gets brighter towards the tongue. Meanwhile, the ablation areas of the neighbouring Gornergletscher and Findelgletscher are much darker. The snow-covered accumulation areas of Gorner- and Findelgletscher have a clearly higher albedo than the bare-ice surfaces. Some clouds, which cast shadows, have a very high albedo. The picture is calculated from different Landsat scenes with Eq. 7.

glaciers could potentially help to predict ablation rate and ablation patterns of the GrIS and the Antarctic Ice Sheet. While the technical advance in remote sensing over the last decades helped to attain more and better data, research at site is still costly and determined by logistical difficulties (Benn and Evans, 2010). Polythermal Alpine glaciers represent a nice opportunity to do research in this field at much lower expenses, as they are a lot easier to reach than the ice sheets (Ryser et al., 2013).

1.5 Content of this Master's Thesis

Chapter 1 shows the effects of glacier melt for humanity and underlines the importance of understanding, predicting and quantifying the processes which are involved in this topic. The subject of this Master's Thesis is outlined in the context of climate change and glacier melt. The research questions and the study area are presented.

Chapter 2 contains theoretical background knowledge about glaciers in general, glacier albedo and space-born glacier albedo retrieval.

Chapter 3 presents the characteristics of the study area, properties of the Grenzgletscher and information about its thermal structure.

Chapter 4 contains information about the data used for this work, which is the previously existing data and the data acquired during field trips. The methods which were used for the processing of the data are introduced.

Chapter 5 presents the results of the comparison between albedo and ablation, the albedo change as well as changing albedo patterns.

Chapter 6 discusses the results and compares them with findings in the literature. The chapter also highlights uncertainties which influence the results.

Chapter 7 contains the conclusion and an outlook on possible future research.

2 Theoretical Background

2.1 Glaciers

2.1.1 Glacier Motion

The following section is based entirely on the work of Benn and Evans (2010). Glacier motion is probably the most fascinating aspect of glaciers. In the past, advancing glaciers threatened settlements, while nowadays the retreat of glaciers is the main concern.

Glacier motion is driven by gravitational forces. The ice develops at higher altitudes and flows to lower altitudes, where the glacier melts or calves into water bodies. The acceleration of the ice by gravity, also named the driving stress, is counteracted by resistive stresses. Resistive stresses are basal and lateral drag as well as longitudinal stress gradients. Driving and resisting stresses usually are in balance and acceleration can be ignored in most glaciological situations.

The stresses that influence glacier flow are influenced by several interacting factors such as ice temperature, debris and water content of the ice, debris at the glacier bed, bed roughness and water pressure. The exact processes that explain the flow rate are still a topic of research.

2.1.2 Thermal Regimes

The difference between cold ice and temperate ice was already introduced in Section 1.2. Ice bodies can consist only of tempered or cold ice. However, both ice temperatures can coexist in different zones in the same glacier. This results in the following threefold classification for thermal regimes of glaciers (Benn and Evans, 2010):

Temperate glaciers: The ice in temperate glaciers is everywhere at the pressure-melting-point. The only exception are the uppermost metres close to the surface, which are influenced by seasonal temperature fluctuations as long as there is no insulating snow layer.

Cold glaciers: The ice in cold glaciers is throughout below the pressure-melting-point. Cold glaciers are frozen to the glacier bed. None of the large valley glaciers in the European Alps are cold (Section 3.1). However, there exist for example small high-altitude hanging glaciers which are cold (e.g. Faillettaz et al., 2011).

Polythermal glaciers: Polythermal glaciers contain temperate and cold ice. There exist various types of polythermal glaciers with a wide range of different thermal structures. The factors which are responsible for the thermal structure are heat diffusion, heat advection by the moving ice, frictional heating, percolating water and active moulins (Phillips et al., 2010).

The ice temperature is an important factor for mass flux by influencing ice viscosity (Hutter, 1983; Blatter and Hutter, 1991) and for the glacier hydrology (Knap and Oerlemans, 1996; Eisen et al., 2009; Ryser et al., 2013).

2.1.3 Mass Balance

The following section is based entirely on the work of Benn and Evans (2010). Glaciers are in a constant exchange of energy and mass with their environment. The interplay between gain and loss of ice is called *mass balance*. All the processes which add mass to the glacier are processes of *accumulation*. Processes of mass loss are collectively termed *ablation*.

The zone, where annual accumulation exceeds annual ablation is referred to as *accumulation zone*. Conversely, the zone where annual ablation exceeds annual accumulation is called *ablation zone*. The *equilibrium line* separates the accumulation zone from the ablation zone and represents the line on which accumulation and ablation are perfectly balanced. The mean elevation of the equilibrium line is called *equilibrium line altitude* (ELA).

The main source of accumulation in most regions is snowfall. Avalanches, wind transported snow from the surrounding area as well as freezing of wind transported and cold water droplets, rain or groundwater represent other types of accumulation.

The density of fresh snow is low compared to glacier ice. The duration of the transformation from snow to ice depends on the pressure of the layers accumulating above as well as on melting and refreezing processes. Therefore, this process takes much longer in cold, arid climate than in maritime climate.

Melting is the primary process of ablation on most glaciers which are not terminating into water bodies. When glaciers end in the sea or in lakes, calving can make up a significant part of the ablation. Furthermore, there are more ablation processes like evapotranspiration, sublimation, scouring by wind and ice break-offs in steep terrain (dry calving). Certain processes are only relevant if special conditions are given (e.g. sublimation in cold, arid climates).

Tab. 2: Densities for different types of snow and ice (Paterson, 1994; Benn and Evans, 2010). In general, with increasing density the specific surface decreases (Gardner and Sharp, 2010).

	Density (kg m^{-3})
Fresh snow	50-200
Firn	400-830
Glacier ice	830-910
Pure ice	917
Water	1000

Glacier in maritime regions tend to have larger mass turnover rates than glaciers in continental regions. The reasons for this are, amongst others, higher precipitation rates and higher average annual air temperatures in the maritime climate.

2.1.4 Surface Energy Balance

According to Benn and Evans (2010), melting snow and ice requires energy. 334 Joules is the amount of energy to melt 1 gram of ice at the temperature of 0 °C. If the ice is colder than 0 °C, the ice has to be heated up before it melts. The specific heat capacity of ice is dependent on the ice temperature. The warmer ice gets, the more energy is needed to raise the ice temperature further. However, the amount of energy which is needed to raise the temperature of ice by 1 °C is many times lower than the amount of energy needed to melt 1 gram of ice. 2 Joules of energy is enough to heat 1 g of ice from -10 °C to -9 °C (Benn and Evans, 2010).

The melting at the glacier surface is dependent on the surface energy balance, which is determined by atmospheric energy fluxes (Sicart et al., 2008) and the intrinsic properties of glacier ice (e.g. Cierniewski et al., 2012). Solar and terrestrial radiation are the most important energy fluxes on most glaciers (Hock, 2005).

The main part of solar radiation has wavelengths from 0.2 to 4.0 µm. The highest energy fluxes from the sun are in the visible part of the spectrum (0.4 to 0.7 µm), with significant parts in the ultra-violet and the near infra-red part, too. However, a significant amount of the incoming shortwave radiation is reflected on its way through the atmosphere and on the surface. The amount which is available for ablation is called net shortwave radiation (SW).

Terrestrial material usually have a temperature which is much lower than the temperature of the sun. Thus, their wavelengths are lower, mainly between 4 and 120 µm. Terrestrial radiation includes radiation emitted from the atmosphere and the earth surface. The glacier itself emits long wave radiation, too. These energy fluxes are summarized under the term of net long wave radiation (LW).

The energy flux that exists through direct contact of atmospheric molecules with the ice is called sensible heat transfer (QH) (Benn and Evans, 2010). A positive sensible heat flux is enhanced by warm and strong winds as well as high surface roughness, resulting in more turbulence (Paterson, 1994). Energy transfer also takes place during evaporation and condensation as well as sublimation and deposition. This flux is the latent heat transfer (QE). Relatively warm rain (QR), falling on the glacier and delivering energy for melting, provides a special case of latent heat transfer.

Within the glacier-meltwater system, energy used for the change of the ice temperature (QT) and for melt (M) alters the energy balance. According to the laws of energy conservation, all these components can be combined in the following equation for the surface energy balance (Benn and Evans, 2010):

$$SW + LW + QH + QE + QR - QT - M = 0 \tag{1}$$

2.1.5 Shortwave Radiation and Glacier Albedo

Shortwave radiation provides most energy for the surface energy balance in continental climates with a high probability for clear skies (Braithwaite and Olesen, 1990; Braithwaite et al., 1998). Location factors that amplify shortwave radiation are low latitude, because of the high midday solar angle, and high altitude, because of less filtering and scattering by the atmosphere. The northern and central Andes as well as the Himalayas are home to such conditions (Kayastha et al., 1999; Benn et al., 2001). On the contrary, frequent hazy or overcast weather conditions as often found in maritime climates, weaken the role of shortwave radiation and intensify the role of longwave radiation (Hock, 2005).

The Earth's atmosphere attenuates shortwave radiation. A surface that is perpendicular to the incoming solar radiation receives $\sim 1368\,\mathrm{W\,m^{-2}}$ at the top of the atmosphere. The sun rays are scattered by air molecules, cloud droplets and other particles during its way through the atmosphere. Thus, the intensity of radiation closer to the earth surface is lower. Beside the direct, but filtered radiation there is also diffuse, scattered radiation that can reach the Earth's surface from different angles than the direct radiation. The extreme case of dominating diffuse radiation is found in thick fog, when the illumination is uniform and the location of the sun as the light source cannot be seen (Benn and Evans, 2010).

On the surface, factors that modulate the incoming radiation are slope angle, aspect, topographic shading (Benn and Evans, 2010; Tedstone et al., 2017) and reflection

by terrain (Gardner and Sharp, 2010). A substantial part of the incoming radiation that reaches the glacier surface is reflected. A surface's ability to reflect incoming radiation is characterized by the *albedo* (e.g. Braithwaite and Olesen, 1990; Knap and Oerlemans, 1996; Brock et al., 2000; Van den Broeke et al., 2011). The albedo (α) is defined as

$$\alpha = SW_{out}/SW_{in} \tag{2}$$

with SW_{in} and SW_{out} connoting the incoming and outgoing radiation, respectively. Therefore, the net shortwave radiation, the part that is available for ablation, is given by the following equation (Benn and Evans, 2010):

$$SW = SW_{in} * (1 - \alpha) \tag{3}$$

2.2 Albedo of Ice, Snow and Glaciers

2.2.1 The Albedo of Clean Ice and Snow

Absorption and reflection by a surface at a specific wavelength (λ) is characterized by the *spectral albedo* (α_λ). The spectral albedo of pure snow and ice is greatly variable across the solar spectrum. α_λ is close to 1 in the near-ultraviolet and in the visible range but decreases to much lower values at higher wavelengths (Gardner and Sharp, 2010).

Gardner and Sharp (2010) explained the radiative transfer as a statistical process. For their radiative transfer model, they made the assumptions that all scattering events take place at air-ice interfaces and absorption only happens in the ice. Internal scattering in the ice and absorption by the air were neglected. Larger snow grain size or less air bubbles in the ice lead to longer travel paths for photons in the ice, making absorption more probable, and scattering at air-ice interfaces less probable.

Thus, fresh snow usually has the highest albedo of all snow types (Röthlisberger and Lang, 1987; Paterson, 1994). After snowfall, in the course of destructive metamorphism, the highly structured snow grains get rounded and some snow grains get bigger at the cost of others (LaChapelle, 1969). This process decreases the specific surface area[4] (Gardner and Sharp, 2010) and therefore the albedo (e.g. Tedesco

[4] The specific surface area is the surface area per unit mass.

et al., 2011; Box et al., 2012). Modellings by Gardner and Sharp (2010) showed a very good logarithmic correlation of snow and ice albedo with specific surface area.

Ice has a much higher density than snow (Tab. 2) and air-ice interfaces are restricted to air bubbles and fractures (Gardner and Sharp, 2010). Therefore, the albedo of ice is much smaller than the albedo of snow (Tab. 3). Water on the glacier surface further reduces the albedo (Knap and Oerlemans, 1996).

The surface roughness is another factor influencing the albedo. Pfeffer and Bretherton (1987) list three reasons why surface roughness affects albedo and melt. First, indentations possibly act as traps for radiation. Second, indentations enable access for radiation to deeper parts of the glacier. Third, surface roughness enlarges the surface and exposes ice to radiation at different angles. Crevasses are the most obvious surface structures on a glacier and they can occupy large proportions of the glacier surface (e.g. Meier et al., 1985). Crevasses lead to an albedo decrease of 10-25% according to Pfeffer and Bretherton (1987) and Cathles et al. (2011). Absorption by crevasses is determinted by the size, orientation, density and presence of water in the crevasse (Ryan et al., 2015). Rippin et al. (2015) found correlations between high densities of supraglacial water channels and low reflectance values. They also observed distinct variations in reflectivity along channel pathways, which they assume to be either caused by presence of water or shading.

In conclusion, albedos of snow and ice are determined by the respective specific surface area (Gardner and Sharp, 2010). The specific surface area is strongly influenced by the presence of liquid water in and on top of the medium. Surface roughness is an additional factor which modulates the albedo.

2.2.2 Light-absorbing Impurities (LAIs)

Snow and glacier ice always contain a certain amount of impurities. There are three processes, which add impurities to snow. First, snow flakes form around an ice nuclei (Warren and Wiscombe, 1980). Second, they entrain particles in the air while falling (Magono et al., 1979). Third, impurity concentrations in snow laying on the ground are further raised by fallout (e.g. Falconer and Hogan, 1971). Dry fallout and melting out of particles (Kohno and Maeno, 1979) result in a dirtier layer which forms every melt season (Warren and Wiscombe, 1980). Dust concentrations in these kind of layers can be many times higher than in the intervening clean layers, depending on the length of the melt season assuming constant dust deposition (Körner, 1977). These layers help to differentiate between annual layers in snow (Langway et al., 1977; Hammer, 1977) and glacier ice (Körner, 1977).

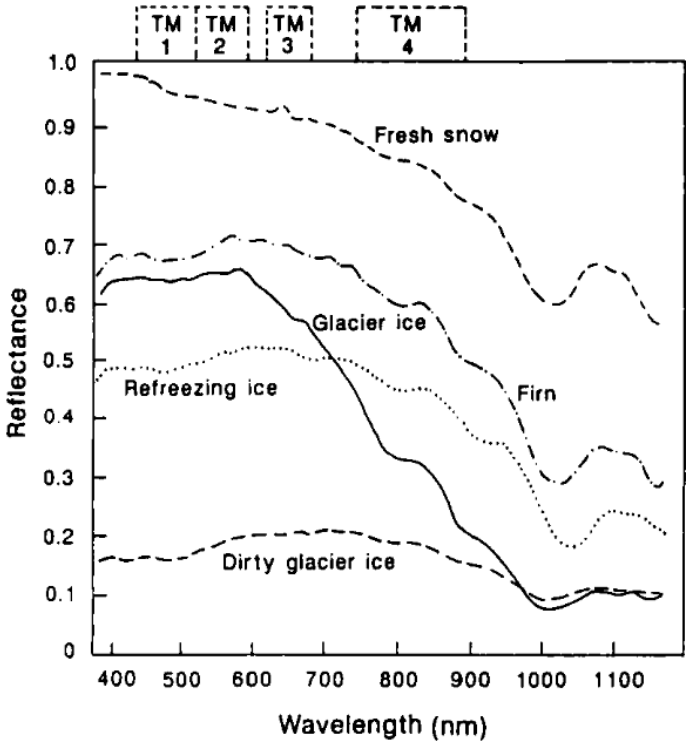

Fig. 4: Spectral reflectance curves for snow and ice in different formation stages. Bandwidths of Landsat TM bands 1-4 are given on top (Winther, 1993, fig. 5).

Outcropping of ice from past time periods with pronounced aeolian deposition can have significant effects on dust accumulation at the glacier surface (Oerlemans et al., 2009; Wientjes et al., 2012; Dumont et al., 2014). A similar effect can be produced by high melt rates, which lead to more englacial particles emerging at the surface (Tedstone et al., 2017).

Impurities often have different absorption properties than snow and ice. Thus, their presence at or close to the surface of the glacier can greatly reduce the albedo (e.g. Dumont et al., 2014; Naegeli et al., 2015; Tedstone et al., 2017), because they reduce the spectral albedo at wavelengths where most solar irradiation occurs (Gardner and Sharp, 2010). This is due to the fact that photons in the near-ultraviolet ($0.3 < \lambda < 0.4$ (e.g. Gardner and Sharp, 2010)) and visible ($0.4 < \lambda < 0.7$ (e.g. Bøggild et al., 2010)) range travel greater distances in the ice and are therefore more likely to be affected by LAIs. At higher wavelengths ($\lambda > 0.9\,\mu m$), the ice itself already absorbs more photons (Warren and Wiscombe, 1980). The closer the LAIs are located to the surface, the more they reduce the albedo (Aoki et al., 2000; Grenfell et al., 2002). Furthermore, Chylek et al. (1983) and Bohren (1986) state that LAIs which are in the ice grain are about 1.4 times as effective for albedo reduction than LAIs in interstitial air. They also note that the closer to the centre of the ice grain the LAI is located, the more it raises the absorption because irradiation gets

refracted towards the centre of the ice grain.

The type of LAI is also of vital importance for the albedo reduction. Not all particles in snow and ice work as light-absorbing impurities. In coastal regions, sea salt can make up a significant part of the total amount of dust (Warren and Wiscombe, 1980). However, sea salt is almost transparent for wavelengths in the solar spectrum (Toon et al., 1976). Where the marine influence is less pronounced, clay minerals are often predominant in snow (Kumai, 1976, 1977; Warren and Wiscombe, 1980). The effect of clay minerals on snow albedo is also relatively small, but they often contain very absorptive inclusions like iron oxide, carbon or organic material (Lindberg, 1976). Soot[5] is by far the most efficient absorptive particle (Warren, 1982; Dumont et al., 2014). Warren and Wiscombe (1980) observed that it needs mineral dust concentrations about 100 times higher than soot concentrations to have a similar effect on the snow albedo.

Fugazza et al. (2019) found a significant correlation between albedo decrease and debris cover increase in ablation areas of mountain glaciers in the European Alps. However, although the low albedo of the debris reduces the glacier albedo, the debris does not necessarily lead to more melt. If the debris layer reaches a critical thickness, it has an insulating effect and reduces the melt rates of the underlying ice (Bocchiola et al., 2015).

A very important group of LAIs has a biological origin. Biological activity in snow and ice has long been considered extremely low (Takeuchi et al., 2001). However, snow and ice algae, bacteria and their products substantially reduce the albedo of snow and ice (Gajda, 1958; Kohshima et al., 1993; Takeuchi et al., 2001; Tedstone et al., 2017; Ryan et al., 2018).
Ice algae can inhabit the upper few centimetres of melting bare-ice (Tedstone et al., 2017). In order to protect the photosynthetic apparatus from too much radiation, ice algae develop specialist pigments which absorb radiation in the ultraviolet and visible wavelengths (Dieser et al., 2010; Yallop et al., 2012; Remias et al., 2012). Thus, ice algae possess the ability to significantly reduce the albedo of bare-ice surfaces (Yallop et al., 2012; Lutz et al., 2014; Stibal et al., 2017).

Some of these micro-organisms form together with organic matter and mineral par-

---

[5] Soot is a solid substance that mainly consists of carbon (Choi et al., 1994). Light-absorbing carbon is often ambiguously referred to as 'soot' or 'black carbon' (Gardner and Sharp, 2010). Black carbon origins from incomplete combustion processes and it is emitted in natural and anthropogenic soot (Amann et al., 2012).

ticles an aggregate called *cryoconite* (Wharton et al., 1985; Takeuchi et al., 2001; Hodson et al., 2008; Cook et al., 2016). Cryoconite means ice dust and origins from the greek words *kruos* meaning ice and *konis* meaning dust (Gajda, 1958). The albedo of cryoconite depends on its composition (Takeuchi, 2002a; Fountain et al., 2004). Cryoconite can be spread out (Kohshima et al., 1993; Takeuchi et al., 2001) or trapped in *cryoconite holes*, which can have diameters as little as a few centimetres up to several meters (Macdonell and Fitzsimons, 2008; Bøggild et al., 2010).

Cryoconite holes were already described by the Nordenskiöld (1883), who encountered these water-filled obstacles while crossing Greenland in 1870. Cryoconite hole formation is associated with flushing of cryoconite into depressions (Bøggild et al., 2010). The albedo is decreased locally what promotes that the cryoconite melts into the ice (Takeuchi et al., 2001; Takeuchi, 2002a). The cryoconite gets less exposed to solar radiation in the hole and at the equilibrium depth, melt rates in the hole are more or less equal to melt rates on the surface (Ryan et al., 2018). A change of the conditions from short-wave dominated to long-wave dominated can lead to a melting out of the cryoconite and redistribution on the surface (Fountain et al., 2004; Chandler et al., 2015).

The concentration of LAIs in cryoconite holes raises the glacier albedo through different effects. First, a large part of the glacier surface is relatively clean and high LAI concentrations are spatially very restricted (Kohshima et al., 1993). Second, LAIs are effectively hidden from solar radiation (Bøggild et al., 2010). Third, cryoconite holes are often water-filled (Macdonell and Fitzsimons, 2008). Thus, the specular reflection of the water layer enhances the albedo compared to wet cryoconite without a water layer on top (Bøggild et al., 2010). The water layer possibly freezes and the ice layer sometimes contains air bubbles (Fig. 5), what further enhances the albedo reducing effect of cryoconite holes (Section 2.2.1).

In summary, the influence of LAIs depends on their type, distribution, position, and quantity. In addition, factors such as irradiation angle, radiation intensities in different wave ranges or properties of the medium also have an influence on the effectiveness of LAIs.

2.2.3 Ice temperature, Glacier Hydrology and Albedo

The ice temperature is critical for glacier hydrology. In temperate ice, water does not immediately refreeze and it can form a network of intragranular veins that transport water within the ice (Nye and Frank, 1973) unless they are not blocked

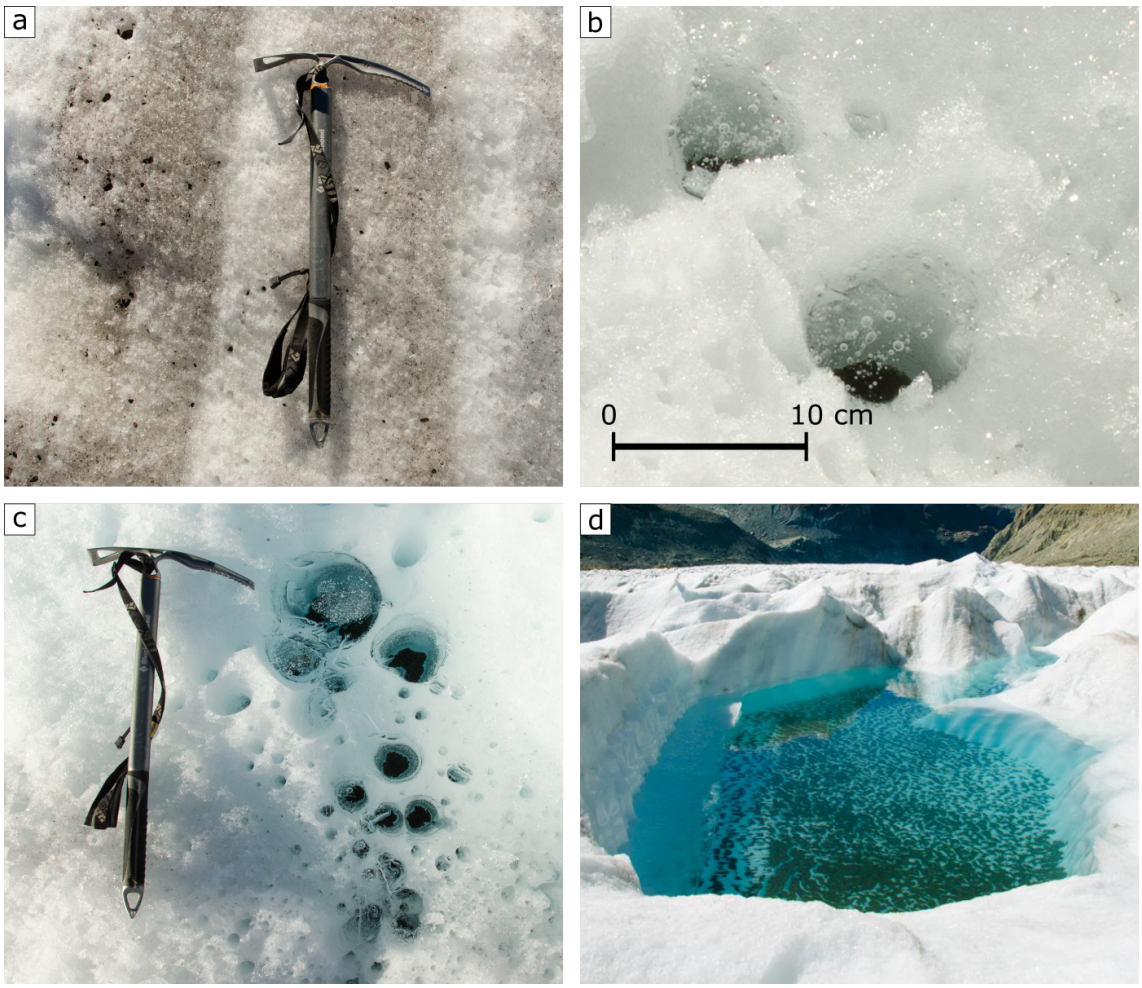

Fig. 5: Four images of the glacier surface in the lower ablation zone of the Grenzgletscher: (a) shows a glacier surface which is dirty compared to the other three images; (b) shows cryoconite holes whose water layer is frozen and contains air bubbles; (c) shows several cryoconite of different sizes whose water layer is also partly frozen and sometimes contains air bubbles. The dirty cryoconite layer at the bottom of the holes is only visible from a point of view which is relatively straight above the hole; (d) shows a large cryoconite hole which measures several meters in diameter. Bøggild et al. (2010) call these wide holes, whose diameter is greater than their depth, 'cryoconite basins'. Note that a thin ice layer is partly covering the hole. All photographs were taken by M. Thalmann in the course of the field trips.

by air bubbles (Lliboutry, 1996). In contrast, cold ice is impermeable to water. As long as there are no crevasses and fractures, water stays at the glacier surface and often forms deeply incised channels and lakes (Hodgkins, 1997; Boon and Sharp, 2003; Ryser et al., 2013). Fractures, veins containing liquid water and boreholes commonly refreeze in some hours (Ryser et al., 2013) unless there are large amounts of flowing water (Zwally et al., 2002; Das et al., 2008; Catania et al., 2008).

The most important effects related to glacier hydrology and ice temperature on the albedo are listed here:

Concentrating LAIs in cryoconite holes: The surface water flow on cold ice entrains LAIs, which are transported into depressions (Ryser et al., 2013). There, cryoconite holes (Fig. 5) form, which partly hide LAIs from direct sunlight (Bøggild et al., 2010). The concentration of LAIs in these depressions makes the other parts of the glacier surface cleaner and raises the albedo on average (Section 2.2.2) (Takeuchi et al., 2001; Bøggild et al., 2010).

Water in interstital pores: Air-bubble-rich ice is typical for cold glaciers (Suter et al., 2001). As long as the ice remains cold, water cannot seep through the ice. Thus, the bubbles remain air-filled as long as there are no fractures in the ice. The larger air-ice interface in cold ice raises the albedo (Section 2.1.2).

Supraglacial water: The presence of liquid water on the glacier surface can lower the albedo effectively (Zuo and Oerlemans, 1996; Greuell, 2000; Greuell et al., 2002). Ryan et al. (2018) observed albedo values of supraglacial water in the range of 0.19 to 0.26. However, the albedo of supraglacial water depends also on the material beneath the water layer (Naegeli et al., 2015) as well as the water depth (Fitzpatrick et al., 2014; Legleiter et al., 2013). Gardner and Sharp (2010) mainly attribute the albedo reduction in zones with surface water to the decreased number of air-ice interfaces near the ice surface. Hanson (1965) observed melt rates 2 to 3 times higher below surface ponds than on bare-ice surfaces next to the ponds. Lüthje et al. (2006) obtained similar results with modelling.

Extensive supraglacial hydrological features indicate cold ice (Ryser et al., 2013). Additionally, cold ice reduces glacier dynamics and crevasse development (Etzelmüller et al., 1993). As crevasses often represent the sole possibility for water to get in the glacier and to the glacier bed in cold glacier, supraglacial water presence is further enhanced in cold ice zones (Rippin et al., 2015).

Channel networks: Dense supraglacial channel networks enhance surface roughness and lower the albedo (Rippin et al., 2015).

2.2.4 Glacier Albedo Variations in Space and Time

Albedos are constantly changing. The diurnal and seasonal cycles of the sun have a continuous effect on the albedo through changing sun elevation. The more acute the angle at which the photon hits the surface, the longer the photon is near the surface, where it is more likely to be sent out of the snow (Gardner and Sharp, 2010). However, sun elevation is by far not the only factor affecting albedos at diurnal time scales. Cloud cover can change within minutes (Gardner and Sharp, 2010) and pronounced melting can produce a thin water film which effectively lowers the albedo (Naegeli et al., 2017). Furthermore, freeze-thaw cycles change the surface properties of supraglacial ponds on diurnal or seasonal scales (Macdonell and Fitzsimons, 2008).

Rain has a different effect on the albedo depending on the type. Heavy precipitation can reduce surface roughness and flush away fine debris, what can raise the albedo drastically (5-20% according to Brock (2004); Azzoni et al. (2016)) on a short-term (Azzoni et al., 2016). On the other side, light rain covers the glacier surface with a thin water film, which absorbs more radiation than the underlying ice (Naegeli et al., 2019).

Krimmel and Meier (1975) observed that increased crevassing, caused by a surge, resulted in darkening due to enhanced surface roughness (Section 2.2.1).

During the melt season, more and more parts of the glacier surface lose their snow cover and bare ice is exposed. Therefore, under the assumption of constant incoming shortwave radiation, the amount of energy that is available for ablation increases throughout the ablation season as more parts of the ablation zone gets free of snow (Benn and Evans, 2010). This decrease of snow surfaces at the expense of bare-ice surfaces triggers a positive feedback mechanism and fastens melt processes (e.g. Box et al., 2012).

2.2.5 Glacier Darkening Related to Climate Change

Climate change influences glacier-wide albedos, albedos of clean snow and glacier ice as well as processes concerning LAIs. The most obvious influence of climate change on the glacier-wide albedo is by decrease of snow-covered areas on the glacier (Naegeli et al., 2017).

Atmospheric warming enhances growth of snow grains (Tedesco et al., 2011; Box et al., 2012) by enhancing the availability of liquid water (Gardner and Sharp, 2010). Water films can develop on glaciers in warm periods (Naegeli et al., 2017). As

temperatures rise, spatial and temporal extent of these water films is likely to raise. Furthermore, as thermal structures of polythermal glaciers are likely to change(Ryser et al., 2013), less extent of air-bubble-rich cold ice zones potentially lowers albedos .

Climate change has various effects on dust deposition and accumulation on snow and ice surfaces. Higher melt rates cause higher dust accumulation rates at the glacier surface (Tedstone et al., 2017). Increased proportions of snow and ice free areas in space and time enhance dust availability (Oerlemans et al., 2009; Dumont et al., 2014). Warmer temperatures possibly cause an increase in wild fires (Westerling et al., 2006), which increase black carbon concentrations in the atmosphere (Tedesco et al., 2016). Combustion of fossil fuels by humans enhances dust concentrations (Warren and Wiscombe, 1980). Furthermore, dust is often rained out of the atmosphere by storms (Warren and Wiscombe, 1980) and the frequency of such extreme events as well as precipitation patterns are likely to change (IPCC, 2013).

Studies concerning mass balance and sea-level rise should address the spatiotemporal patterns of albedo (Brock et al., 2000; Brock, 2004; Ryan et al., 2018). Tedesco et al. (2016) highlight the vital importance of LAIs and see the reason for the differences between measured and modelled albedos in the missing integration of processes with LAIs in models. Naegeli et al. (2019) argue for a clear distinction between albedo changes due to differences in snow cover and albedo trends within snow and ice surfaces in studies concerning glacier albedo. This distinction is necessary to find out which processes impact the albedo and what are the dependencies between these processes.

Recent studies indicate a darkening of glaciers at different places in the world, for example the Greenland Ice Sheet (GrIS) (Section 2.2.6) (Tedesco et al., 2011; Box et al., 2012; Stroeve et al., 2013; Dumont et al., 2014), the Himalayas (Takeuchi et al., 2001) and the European Alps (Oerlemans et al., 2009; Fugazza et al., 2019) over recent years and decades. Trends of darkening bare-ice surfaces has also been observed (Tedstone et al., 2017; Fugazza et al., 2019) but are not always clear (Naegeli et al., 2019). Bare-ice surfaces usually are much more heterogeneous than snow surfaces (Naegeli et al., 2015). Different reasons were presented to explain the darkening of bare-ice surfaces like melt water accumulation on the surface (Knap and Oerlemans, 1996), increased dust deposition on the glacier surface due to larger ice and snow free areas (Oerlemans et al., 2009; Dumont et al., 2014), emerging of ancient, dust-rich ice at the surface (Wientjes and Oerlemans, 2010; Bøggild et al., 2010; Wientjes et al., 2012), or activity of micro-organisms (Takeuchi et al., 2001; Benning et al., 2014; Tedstone et al., 2017). Fugazza et al. (2019) state that also

Tab. 3: Albedos for snow and ice (Paterson, 1994).

	Range
Dry snow	0.80-0.97
Melting snow	0.66-0.88
Firn	0.43-0.69
Clean ice	0.34-0.51
Slightly dirty ice	0.26-0.33
Dirty ice	0.15-0.25
Debris-covered ice	0.10-0.15

increased extent of supraglacial debris lowers albedos of ablation areas. However, when a certain threshold in thickness is reached, debris has an insulating effect on glacier ice (Bocchiola et al., 2015).

2.2.6 Darkening Ice in Greenland

The importance of the GrIS concerning sea-level rise was emphasized in chapter 1.1. The GrIs is polythermal. The ice in the central part is cold (Greve, 1997), except some parts that experience high geothermal heat flux (Dahl-Jensen et al., 1997). In the marginal areas of the ice sheet, the ice is temperate at the base in large zones (Greve, 1997).

Short-wave radiation provides the major part of the melt energy for the GrIS (Braithwaite and Olesen, 1990; Braithwaite et al., 1998). Thus, the melt rates are often largely controlled by the albedo (van den Broeke et al., 2009; Bøggild et al., 2010; Box et al., 2012). The albedo of the GrIS is decreasing in recent years, allowing more shortwave radiation to be absorbed (Tedesco et al., 2011; Box et al., 2012; Stroeve et al., 2013). The beginning of the albedo reduction is located in the 1990s (Tedesco et al., 2016). This is in line with the finding of Rignot et al. (2008) that the GrIS was in relative balance between 1961 and 1990. Several sectors of the GrIs showed significantly lower albedos after 2000 than in the 1990s (He et al., 2013). Between 2000 and 2012, GrIS summer albedo tended to decline (Stroeve et al., 2013).

Parts of the albedo reduction can be linked to the spatial and temporal decrease of snow cover (Bøggild et al., 2010; Box et al., 2012). The bare-ice ablation area shows a growth trend, however with high interannual variability (Shimada et al., 2016). The albedo reduction cannot be explained only by vanishing snow cover. Snow albedo decreases because of stronger snow metamorphism earlier in the season (Box et al., 2012). In recent years, the development of so called ”dark” ice zones has been observed on bare-ice surfaces in some ten kilometres of distance from the margin

of the icesheet (Oerlemans, 1993a; Bøggild et al., 1996). The dark ice zone is a band of, compared to the surrounding ice, darker ice in the ablation zone with a width of tens of kilometres (Fig. 6) (Wientjes et al., 2011; Tedstone et al., 2017). Oerlemans (1993a) was the first describing this phenomenon, which was conspicuous because until then it had been assumed that the albedo on glaciers gets smaller with decreasing altitude, as more and more debris is deposited (e.g. Koelemeijer et al., 1993; Knap et al., 1999), or is relatively constant with altitude (e.g. Greuell et al., 1997).

Different reasons were presented to explain the decreasing bare-ice albedo and the dark-ice zones. Oerlemans (1993a) and Knap and Oerlemans (1996) connected the low albedo with a maximum accumulation of melt water on the cold and therefore impermeable ice. The maximum occurs because of a lower melt rate higher up on the GrIS and steeper slopes lower down, which lead to higher runoff and less accumulation. Greuell (2000) supported this thesis as he found a significant correlation between the mean annual albedo reduction in the dark-ice zone and the melt measured at stakes in the same location.
Wientjes and Oerlemans (2010) suggested that ice containing dust from older periods emerges at the surface and supposed that the melt water accumulation is induced by the darker ice. Deposition by wind and rain is unlikely the cause, because it cannot explain the distance to the margin and the sharp transition.

Several studies assume that biological processes are responsible for the dark zone. Tedstone et al. (2017) suggest that the dust in the ancient ice provides nutrients for pigmented ice algae assemblages. However, these algae can only prosper when conditions as liquid meltwater presence, sufficient radiation fluxes for photosynthesis and high enough air temperatures are met.
Stibal et al. (2017) refer to algae growth as one of the controlling variables of bare-ice darkening. Algae caused a greater albedo reduction than nonalgal LAIs in their study area located in the southwestern sector of the GrIS.
Ryan et al. (2018) quantify possible causes for albedo variations. They identify distributed LAIs of organical and anorganical origin as the main factor for the dark zone, explaining 73 % of the spatial variability. On the contrary, cryoconite concentrated in large holes and fluvial deposits has a very little impact because of its spatially very limited extent (<0.5 %). Supraglacial water (<1 %) and crevasses (<0.2 %) are also only present in a small part of the dark ice zone and account for about 12 to 15 % of the spatial variability. Ryan et al. (2018) expect the dark ice zone to extend further in the future.

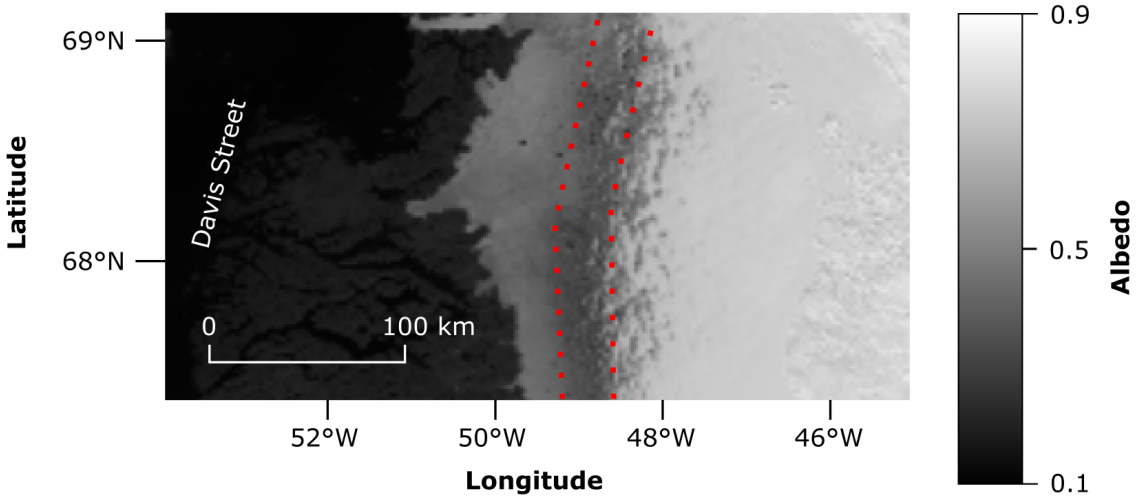

Fig. 6: Albedo map showing an area in the south-western part of Greenland. In the west (left side of the image) is the sea (Davis Street), in the east (right side of the image) is the GrIs. In between is the tundra area cut by fjords. The dark ice zone is clearly visible as a north-south extending band around 49 °W (in between the two dotted red lines). The acquisition date of the of the satellite images is 2 July 1995. The sensor is the AVHRR (Advanced Very High Resolution Radiometer) (modified after Greuell, 2000, fig. 1)

2.3 Glacier Albedo in Remote Sensing

2.3.1 History of Satellite-derived Glacier Albedo Measurements

Albedo measurements on glaciers is labour-intensive when performed in-situ. Access is often difficult and ice flow as well as processes of ablation continuously alter the glacier surface. Dangers like snow-covered crevasses and avalanches possess danger for life and hinder work on the glacier (Knap et al., 1999). Bare-ice surfaces are highly heterogeneous (Naegeli et al., 2015) and therefore the use of spatial extrapolation is limited (Gratton et al., 1993). Consequently, a high number of measuring points is needed to adequately represent the glacier surface (Knap et al., 1999; Naegeli et al., 2015). Thus, glacier-wide albedo measurements are rare (Knap et al., 1999) and albedo is often only measured at a few points (e.g. Oerlemans, 1993b).

The potential of remote sensing for surface mass balance studies was already recognized in the 1980s. A study by Hall et al. (1988) used reflectance values computed by Landsat 5 TM data to identify zones of similar glacier facies, which are a proxy for mass balance. A big problem they faced was the oversaturation of certain TM bands over snow and ice surfaces.

In the 1990s, there were already quite a lot of studies concerning glaciers and satellite-derived glacier reflectance and albedos. Hall et al. (1990) compared reflectance values computed by Landsat TM data with field measurements on a glacier

in the east of Greenland. They emphasize the importance of the atmospheric correction, as it raised the reflectance values by 5-17% relative to the uncorrected at-satellite reflectance. These corrected values were within 6% deviation of the field measurements. The field measurements were performed with a portable spectrometer held at nadir viewing angle. Koelemeijer et al. (1993) performed a similar analysis in the European Alps. They note that reflectance usually decreases from the glacier head to the terminus. However, they highlight the pronounced heterogeneity of the glacier surface, which they mainly attribute to the physical state of the glacier surface. While the presence of crevasses, dust and debris material from moraines tend to decrease the reflectance, air bubbles in the ice tend to increase the reflectance (Mullen and Warren, 1988; Pfeffer and Bretherton, 1987; Warren and Wiscombe, 1980; Wiscombe and Warren, 1980). Winther (1993) noticed large variations in the albedo over short time periods as well as high spatial heterogeneity.

An important study was conducted by Knap et al. (1999). They investigated relationships between spectral albedos, representing the Landsat TM bands, and broadband albedos. They described this relationship with a narrow-to-broadband conversion for Landsat TM data (see Section 2.3.4). The conversion formula is used in several other studies for example in Liang (2000), Greuell et al. (2002), Paul et al. (2005), Fugazza et al. (2016), Pope et al. (2016) and Naegeli et al. (2017). It is the only conversion formula that is frequently used in glaciological studies (Naegeli et al., 2017). The formula is said to be accurate for snow and ice surfaces (e.g. Liang, 2000; Greuell et al., 2002).

In the 21th century, data acquired by MODIS (Moderate-resolution Imaging Spectroradiometer) on board the satellites of Aqua and Terra (e.g. Fuentes et al., 2019) was used for several studies concerning the ice sheets (e.g. Wientjes and Oerlemans, 2010; Box et al., 2012; Tedesco et al., 2011; Dumont et al., 2014; Casey et al., 2017; Tedstone et al., 2017; Ryan et al., 2018). MODIS data is available as a product tailored for snow cover and albedo, which is often used in ice sheet studies (e.g. Box et al., 2012; Alexander et al., 2014; Dumont et al., 2014; Brun et al., 2015). Despite the moderate spatial resolution (mostly 500 m), Davaze et al. (2018) used MODIS data even for Alpine glaciers. They enhanced the spatial resolution with the method of image fusion proposed by Sirguey et al. (2008). Thus, they obtained a spatial resolution of 250 m. Furthermore, all pixels that not fully show the glacier were removed. They detected a good correlation between summer minimum albedo and glacier-wide annual surface mass balance.

On ice sheets, satellite imagery with even lower spatial resolution than MODIS was used. For example, Greuell and Knap (2000) used AVHRR (Advanced Very High

Resolution Radiometer) data with a spatial resolution of 1.1 km. They detected the line that separates areas uniformly covered with snow higher up on the GrIS from areas with a higher spatial variability lower down. The higher spatial variability is associated with a mixture of snow patches, slush and ice in this area.

Despite the higher temporal resolution of MODIS and AVHRR data, Landsat data was still often used, especially for studies of mountain glaciers. Paul et al. (2005) analysed glaciers in Landsat TM scenes of the European Alps in the context of the extreme heat in summer 2003. They used Eq. 4 by Knap et al. (1999) for the narrowband-to-broadband conversion. They observed large variabilities in the albedo between different years. They also noticed albedos of about 0.15 in the ablation area instead of the often used value of 0.35.

Naegeli et al. (2017) used the formulae by Knap et al. (1999) and Liang (2000) (see Section 2.3.4). For latter, their study was the first one to validate the formula. Furthermore, they adapted both formulae for Landsat 8 (Eq. 6) and Sentinel-2 data (Eq. 7). They state that the bare-ice albedo of glaciers received relatively little interest so far compared to snow albedo. They emphasize the importance of addressing the spatial and temporal variations of bare-ice albedos for the melting of glaciers.

Fugazza et al. (2019) use Landsat TM and ETM+ images to detect albedo trends in the ablation area of glaciers in the European Alps. Their results confirmed negative albedo trends on the surface of the investigated glaciers, which they attribute mostly to changes in supraglacial debris cover. Naegeli et al. (2019) aimed to analyse bare-ice albedo trends of glaciers in the European Alps. In contrast to Fugazza et al. (2019), they could not detect a significant trend in bare-ice albedos.

Future research can rely on Sentinel-2 data. This satellite mission was just launched in 2015 and therefore there is not so much data available yet. The aim of the mission, however, is to ensure long-term continuity (Naegeli et al., 2017).

2.3.2 Difficulties of Space-born Albedo Retrieval

The importance of the albedo for the surface energy balance was introduced in Section 2.1.4. This section aims to explain the term albedo in the context of remote sensing and show the difficulties that are encountered for albedo retrieval.

Radiation always consists of direct, non-scattered radiation and diffuse, scattered radiation (see Section 2.1.4). Thus, the incident radiant flux and the exitent radiant flux have a directional component and need to be integrated over the whole

hemisphere to represent adequately for energy balance purposes (Schaepman-Strub et al., 2006). Space-born radiometric instruments measure the exitent radiant flux of a certain spectral range in a specific direction and also altered by the atmosphere at a certain point in time. This results in some difficulties for albedo retrieval:

Atmospheric influence: The atmosphere alters the radiant flux. Therefore, a space-born spectrometer does not measure the same as a similar spectrometer close to the glacier surface. The atmospheric correction addresses scattering for example by aerosols, water vapor and ozone. In some cases, data from other satellites is used for the atmospheric correction (e.g. USGS, 2019b). There are some products available on which the atmospheric correction already is performed, for example the *Landsat Surface Reflectance Level-2 science product* (see Section 2.3.3).

Effects of topography: According to Gardner and Sharp (2010), topography has different effects on the albedo. First, the aspect and slope angle determine the amount of incoming solar radiation. If the satellite overflies the glacier in the morning, slopes exposed towards the east show higher reflectance values than slopes exposed towards the west, which may still be shaded. Second, varying surface angles change the angle of incidence and consequently the albedo. Third, shading and reflection by surrounding topographic features alter the albedo.

Anisotropic reflection: Surfaces on glaciers often have non-Lambertian reflection properties (Naegeli et al., 2015). Thus, the *bi-directional reflectance distribution function* (BRDF) becomes increasingly more important with more acute angles of irradiation (Greuell and de Ruyter de Wildt, 1999). Additionaly, the characteristics of the reflectance anisotropy vary for different materials (Naegeli et al., 2015). Freshly fallen snow has properties which are close to a Lambertian reflector. However, the snow metamorphosis causes more forward-scattering of the reflected radiation (Winther, 1993). Ice surfaces also act as forward-scattering reflectors (Pellikka and Rees, 2010). Thus, nadir observations can lead to albedo underestimation for these kind of surfaces (Klok et al., 2003).

Paul et al. (2005) state that albedo corrections up to +0.1 are possible. Naegeli et al. (2017) compared corrected and uncorrected albedo values for various glacier surface types. They observed that darker ice surfaces are more strongly affected by the anisotropy correction than clean ice surfaces and snow. Debris surfaces were not affected at all on average.

Spatial resolution: Satellite imagery used for albedo retrieval on glaciers and ice shields usually has a spatial resolution of a few decametres up to several hundred meters. Glaciers are often smaller and such spatial resolutions do not appropriately represent the glacier outlines, but often include spectral information from glacier marginal areas. Furthermore, the highly heterogeneous bare-ice surfaces are not adequately represented (Naegeli et al., 2015).

Temporal resolution: Space-born remote sensing systems that have sufficient spatial resolution have temporal resolutions between a day at lower spatial resolution and more than two weeks at higher spatial resolution (see Chapter 2.3.3. Too much cloud coverage makes images unusable for albedo retrieval and cloud shadows cause problems, too (USGS, 2019a,b). Ablation seasons usually have durations of a few weeks (Körner, 1977) to a few months (Paul et al., 2005). Thus, depending on the sensor of choice and the study area, there are not too many opportunities for bare-ice albedo retrieval. Additionally, summer snowfall events possibly occur and change the albedo of the glacier significantly (Naegeli et al., 2015).

Spectral coverage: Spectrometers on satellites usually measure the amount of radiation in distinct wavelength bands (see Fig. 7). These band albedos are often called spectral albedos in glaciological studies, despite not representing the albedo at a single wavelength band (α_λ) but at a narrow range of wavelengths (Cogley et al., 2011). These bands only cover a small part of the solar spectrum. The energy fluxes in the unmeasured wavelength ranges between the bands of the spectrometer must be estimated. This is usually done with a so-called *narrowband-to-broadband conversion* (see Section 2.3.4), where spectral bands are weighted and aggregated. The result of this conversion is called *broadband albedo* (Naegeli et al., 2015).

Oversaturation: Space-born spectrometers can encounter problems when trying to acquire data over snow and ice surfaces (e.g. USGS, 2019a,b). Cells representing snow and ice can be oversaturated. This problem is common and has been known since early glaciological studies with satellite data (e.g. Hall et al., 1988; WGMS, 1989). Cells affected by oversaturation are unusable for albedo retrieval.

2.3.3 Landsat Data and Glacier Albedo

Landsat satellites provide space-born images of the earth surface. Landsat satellites orbit the earth at an altitude of about 700 km. The swath width for the sensors

Tab. 4: Impact of anisotropy effect for different glacier surface types calculated on two Alpine glaciers. The impact of anisotropy effects is given as the difference between corrected and uncorrected values (Naegeli et al., 2017)

	Impact of Anisotropy Effects (%)
Snow	2.6
Bright Ice	3.9
Ice	10.8
Dirty Ice	8.5
Debris	0

onboard Landsat 4-8 is about 185 km. The goal of the Landsat mission is to acquire data for land change research (USGS, 2016).

The first Landsat (Landsat 1) mission started in 1972. Landsat 5 operated from March 1984 to January 2013 and was the longest operating earth observation satellite. Landsat 7 (since April 1999) and Landsat 8 (since February 2013) are currently in use. A technical incident occured on Landsat 7 in May 2003. The instruments on Landsat 7 still acquire data after this incident but every scene has data gaps (USGS, 2016).
Besides the long time series, Landsat sensors offer a decent spatial resolution (mainly 30 m) (Fuentes et al., 2019). A decent spatial resolution is important to represent spatial heterogeneity on the glacier surface (Naegeli et al., 2015). The temporal resolution is low (Fuentes et al., 2019). Each Landsat satellite acquires data of the whole earth in 16-day cycles. Landsat 7 and Landsat 8 as well as Landsat 7 and Landsat 5 have an offset orbit, effectively resulting in 8-day cycles in the time period where both satellites where in space (USGS, 2016).

Other sensors offer much higher temporal resolution than Landsat sensors. For example, MODIS (Moderate-resolution Imaging Spectroradiometer) on board of the satellites of Aqua and Terra offers daily temporal resolution (Fuentes et al., 2019). MODIS data is often used for studies of the ice sheets (Wientjes and Oerlemans, 2010; Box et al., 2012; Tedesco et al., 2011; Dumont et al., 2014; Casey et al., 2017; Tedstone et al., 2017). On large ice shields, the moderate spatial resolution of MODIS (250 m to 1000 m) is sufficient. A lot of studies used the MOD10A1 product for snow cover and albedo at a resolution of 500 m (Box et al., 2012; Alexander et al., 2014; Dumont et al., 2014; Brun et al., 2015). However, for mountain glaciers for example in the European Alps, only a small number of MODIS pixel represent pure glacier surfaces (swisstopo, 2019). Naegeli et al. (2019) state that the MODIS data (500 m resolution) is not suitable for Alpine glaciers because of their limited extent and the complex small-scale topography which the Alpine glaciers are embedded in.

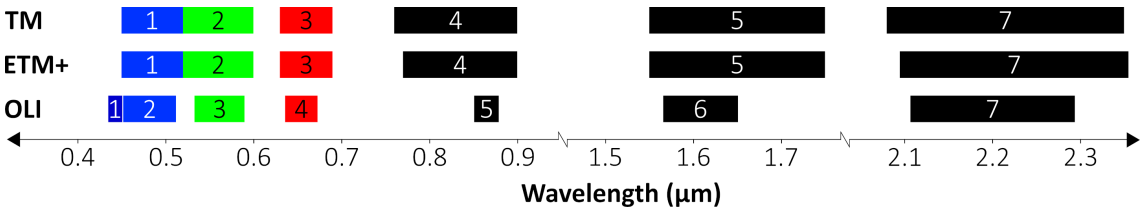

Fig. 7: Bandwidths for the Landsat sensors Thematic Mapper (TM), Enhanced Thematic Mapper Plus (ETM+) and Operational Land Imager (OLI). The bands in the visible part of the solar spectrum (0.4-0.7 µm) are coloured according to their band name (blue band, green band, red band as well as the ultra-blue band 1 of OLI). Notice that not all bands are included (compare with Tab. 5) and the x-axis is broken between 0.9 and 1.5 µm and 1.7 and 2.1 µm.

However, studies exist which use MODIS data for the analysis of Alpine glaciers, for example Davaze et al. (2018) (see Section 2.3.1).

Landsat, as other satellites that carry high-resolution spectrometers, does not offer an albedo product (Naegeli et al., 2019). However, Landsat offers the *Landsat Surface Reflectance Level-2 science product* that shows the fraction of incoming solar radiation that is reflected from the Earth's surface to the sensor onboard the Landsat satellite. The surface reflectance is computed by the LEDAPS code for Landsat 4 - 7 (USGS, 2019a) and by the LASRC code for Landsat 8 (USGS, 2019b), both containing atmospheric correction partly on the basis of MODIS data.

Naegeli et al. (2019) used the Landsat Surface Reflectance Level-2 science product to compute broadband albedo, which they used to look for darkening Alpine glaciers. The suitability of the product for temporal analysis is the subject of several studies. Claverie et al. (2015) analysed the surface reflectance product computed by the *LEDAPS* (Landsat Ecosystem Disturbance Adaptive Processing System) code and found neither trends nor significant annual variabilities. This underlines the suitability of this product for temporal analysis Naegeli et al. (2019). Vermote et al. (2016) state that the surface reflectance product computed by the LaSRC performs even better than the one computed by the LEDAPS code. The product is georeferenced and intercalibrated between the Landsat sensor TM, ETM+ and OLI but it does not include correction for topography or cloud shadows (Young et al., 2017).

2.3.4 Narrow-to-broadband Conversion for Landsat Bands

Landsat TM bands only represent the spectral albedo for the wavelength ranges of the respective bands (Fig. 7). Narrow-to-broadband conversion is used to compute the broadband albedo. Two different narrow-to-broadband conversions and their respective adapted versions are presented in the following section.

Tab. 5: Landsat Bandwidths.

Band Number	TM (µm)	ETM+ (µm)	OLI (µm)
1	0.45-0.52	0.45-0.52	0.433-0.453
2	0.52-0.60	0.53-0.61	0.450-0.515
3	0.63-0.69	0.63-0.69	0.525-0.600
4	0.76-0.90	0.78-0.90	0.630-0.680
5	1.55-1.75	1.55-1.75	0.845-0.885
6	10.4-12.5	10.4-12.5	1.560-1.660
7	2.08-2.35	2.09-2.35	2.100-2.300
8		0.52-0.90	0.500-0.680
9			1.360-1.390
10			10.30-11.30
11			11.50-12.50

Knap et al. (1999) conducted fieldwork with specifically designed spectrometers that use similar wavelength intervals as band 2 and band 4 of the Thematic Mapper (TM). Their conversion formula describes the empirical relationship between these spectral albedos and the broadband albedos (0.3-3.0 µm) measured by a conventional albedometer. The field measurements were conducted on Morteratschgletscher, Switzerland. This conversion formula is the most used one in glaciological literature (Naegeli et al., 2017), for example by Paul et al. (2005), Fugazza et al. (2016) and Pope et al. (2016). The albedo computation by Knap et al. (1999) is suitable for snow and ice surfaces but performs bad on other surface types (Liang, 2000).

$$\alpha_{Knap} = 0.726b_2 - 0.322b_2^2 - 0.051b_4 + 0.581b_4^2 \tag{4}$$

Liang (2000) used modeling to determine an empirical relationship between five Landsat TM bands. This approach works well independent of the surface type. Naegeli et al. (2017) were the first ones using and validating this approach in glaciological literature.

$$\alpha_{Liang} = 0.356b_1 + 0.130b_3 + 0.373b_4 + 0.085b_5 + 0.072b_7 - 0.0018 \tag{5}$$

Both formulas were developed for TM bands. Naegeli et al. (2017) adapted these formulas for the OLI of Landsat 8. They substituted the TM bands with the most similar OLI bands (Fig. 7).

$$\alpha_{Knap,L8} = 0.726b_3 - 0.322b_3^2 - 0.051b_5 + 0.581b_5^2 \tag{6}$$

$$\alpha_{Liang,L8} = 0.356b_2 + 0.130b_4 + 0.373b_5 + 0.085b_6 + 0.072b_7 - 0.0018 \quad (7)$$

According to Naegeli et al. (2017), the problem of these adapted versions are the substantial band shifts from TM and ETM+ to OLI. Especially the very narrow band 5 of OLI (Fig. 7), which substitutes band 4 of TM and ETM+, is likely to cause higher discrepancies. The formula of Liang (2000) relies on five Landsat bands in contrast to the formula of Knap et al. (1999), which solely relies on two Landsat bands. Thus, the former is more robust towards these band shifts and its adapted version is still able to produce albedo images of high accuracy.

3 Study Area

3.1 Cold Firn and Ice in the European Alps

Cold ice is common in the ice sheets (Greve, 1997; Braithwaite et al., 1998) and glaciers of high-latitude (e.g. Fountain et al., 2006). On the contrary, glaciers in the European Alps were generally thought to be temperate for a long time (Suter et al., 2001), despite observations of cold firn in the Mont Blanc massif in the late 19th century by Vallot (1913).

In the 1950s, observations of cold firn and ice in the Monte Rosa massif (Fisher, 1953, 1954) and in the Jungfrau area (Haefeli and Brentani, 1955) got debates about the occurrence of cold firn and ice in the European Alps going again (Suter et al., 2001). Measurements were mostly conducted in the context of construction work (Haefeli and Brentani, 1955; Haeberli et al., 1979) or high-Alpine core drillings (Oeschger et al., 1978; Alean et al., 1983; Haeberli and Funk, 1991; Vincent et al., 1997). Haeberli (1976) and Lliboutry et al. (1976) were the first to look into the distribution of cold firn and ice in a systematic manner. Since a few decades, the existence of cold ice in the European Alps is undisputed (Suter et al., 2001).

Cold ice is formed from cold firn. In the European Alps, cold firn exists only in very high elevated accumulation areas (Haeberli, 1976; Suter et al., 2001; Eisen et al., 2009). The firn temperature is very sensitive to percolating melt water. Therefore, firn temperature gradients (-1.2 °C (100 m)$^{-1}$) are much more pronounced than air temperature gradients (-0.65 °C (100 m)$^{-1}$) with respect to altitude (Suter et al., 2001). Consequently, firn warming is likely to exceed atmospheric warming, what possibly amplifies the expected change in the thermal structures of polythermal glaciers due to atmospheric warming (Suter et al., 2001).

Suter et al. (2001) conducted ice and firn temperature measurements at different high-altitude sites in the European Alps in the first half of the 1990s. The measurements were used as input data for modelling cold-firn distribution in the European Alps. The model uses the altitude as a proxy for the air temperature and the aspect as a proxy for the direct solar radiation to define areas where cold firn is possible or probable (Tab. 6). According to this model, about 120 glaciers (area $> 1\,km^2$) have cold-firn areas.

3.2 Cold Firn in the Accumulation Area of Grenzgletscher

The coldest firn temperatures measured by Suter et al. (2001) were found in the upper accumulation area of the Grenzgletscher, which is a part of the Gorner- / Grenzgletscher system (Section 3.3). The upper accumulation area of Grenzgletscher is located in a high-altitude basin south of the Dufourspitze in the middle of the Monte Rosa massif. The Dufourspitze (4634 m a.s.l.) is Switzerland's highest mountain and the Monte Rosa massif is home to several more peaks rising higher than 4500 m a.s.l. (e.g. swisstopo, 2019).

According to Suter et al. (2001), the climate is dominated by high-altitude conditions. Temperatures seldom rise higher than 0 °C and precipitation is high. Strong winds modulate snow accumulation patterns. At wind-exposed saddles, snow accumulation is only about 0.3 m w.e. y^{-1}. Meanwhile, at wind-protected sites, accumulation is almost about one order of magnitude higher (0.2-0.3 m w.e. y^{-1}).

The uppermost part of the accumulation zone is located at the Colle Gnifetti (4455 m a.s.l.), which is a relatively flat and strongly glacierized saddle. Before the first measurements were conducted at this site, Haeberli (1976) expected the *mean annual firn temperature* (MAFT) close to the surface to be in the range from -10 °C to -15 °C. He based his predictions on temperature data from other high-altitude sites and ice temperature measurements in boreholes at the tongue of the Grenzgletscher. The *mean annual air temperature* (MAAT) is usually higher than the MAFT because of the above-mentioned percolating melt water (Section 3.1) which refreezes (Suter et al., 2001).

First borehole temperature measurements were conducted in 1976 and revealed ice temperatures of -14.4 °C at 15 m depth and -14 °C at 33 m depth (Oeschger et al., 1978). In summer 1977, two more boreholes were drilled with similar results (-14.5 °C at 20 m depth and -13.8 °C at 50 m depth) (Blatter and Haeberli, 1984). In 1982, the first borehole reaching the glacier bed was completed. The temperature at the bed 124 m below the surface was -12.2 °C Haeberli and Funk (1991). Here, the glacier is frozen to the bed (Haeberli and Funk, 1991; Lüthi and Funk, 2001; Suter et al., 2001). Further down the valley, the ice at the glacier bed is warmed to the pressure melting temperature by processes such as the geothermal energy flux and the release of frictional heat due to ice deformation (Benn and Evans, 2010).

Suter et al. (2001) conclude that the upper accumulation area of Grenzgletscher is cold throughout. The aspect has the most pronounced influence on the MAFT as it modulates inputs of direct solar radiation. The snow pack slowly transforms into

Tab. 6: Lower boundaries of possible or probable cold-firn occurence in the European Alps according to FirnMap. Notice that the measurements, on which the modeling base on, were conducted in the 1990s (Suter et al., 2001).

Aspect	Cold firn possible above (m a.s.l.)	Cold firn probable above (m a.s.l.)
N	3000	3400
NE/NW	3000	3600
E/W	3300	3800
SE/SW	3550	3950
S	3700	4150

firn and ice. The ice of the upper accumulation area emerges at the surface of the lower ablation area (see Section 3.4 and 3.5). It visually differs clearly from the surrounding ice as it is brighter and full of air bubbles (Suter et al., 2001; Ryser et al., 2013). This type of ice is an indicator for cold-firn metamorphosis in the accumulation area (Suter et al., 2001).

3.3 Gorner-/Grenzgletscher System

The Gorner-/Grenzgletscher system is located south-east of Zermatt (Valais, Switzerland) and covers an area of almost 50 km^2 (Sugiyama et al., 2010). The two largest glaciers are the Gornergletscher, originating from the southern part of the Weissgrat at $\sim$3500 m a.s.l., and the Grenzgletscher, originating from a high-altitude basin south of the Dufourspitze (4634 m a.s.l.). There are several smaller glaciers in the region. Some of them are still part of the glacier system, others are not or just barely connected anymore due to strong glacier recession in the last decades since the Little Ice Age (Fig. 8) (swisstopo, 2019).

The glacier system showed a relatively stable trend of slight mass loss in the time period between the 1930s and until the the early 1980s. Only in the 1940s the mass loss was stronger (Huss et al., 2012), presumably due to increased solar radiation (Huss et al., 2009). Since the 1980s, the glacier system shows accelerated mass loss (Huss et al., 2012). This continuing trend towards mass loss can probably be explained by higher local annual mean temperatures causing the equilibrium line altitude, which is at the moment at about 3300 m a.s.l. according to studies on the nearby Findelgletscher, to rise. Currently, the glacier system is expected to be out of equilibrium and to retreat further (Sold et al., 2016).

The Gorner-/Grenzgletscher system has been a subject of studies since the 1970s. This is mainly due to its size as one of Europe's largest glaciers, relatively easy access and a glacier-dammed lake possessing danger through GLOFs (Sugiyama et al., 2010;

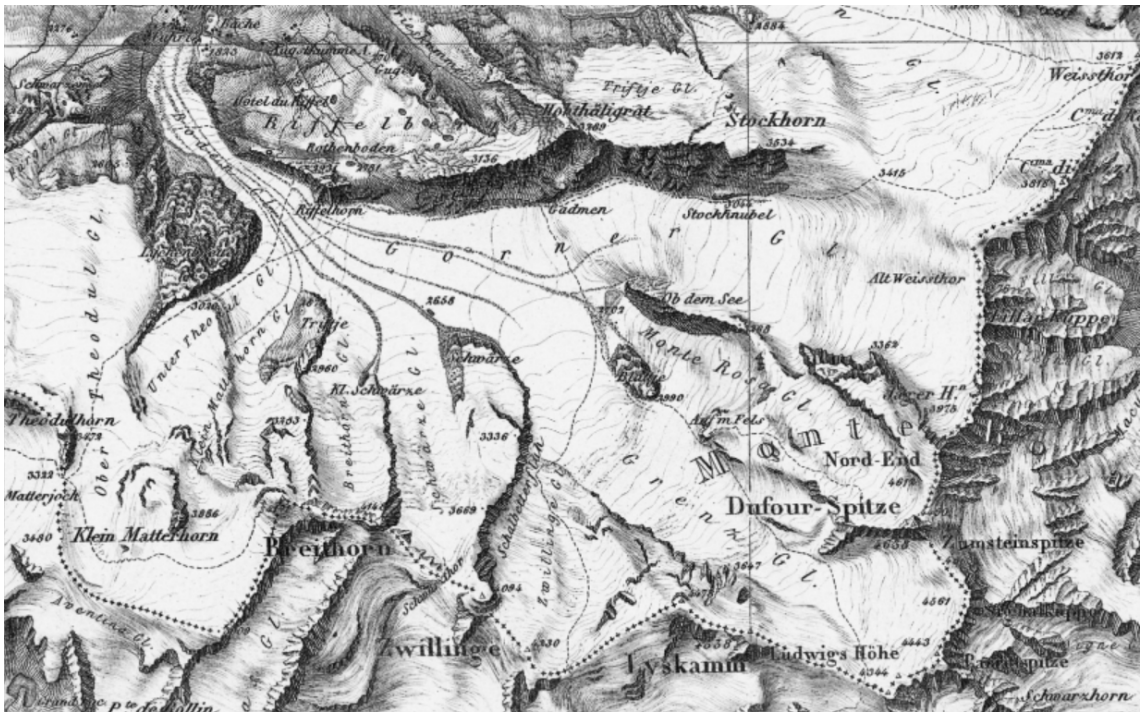

Fig. 8: Gorner-/Grenzgletscher system in the Little Ice Age, on the Dufourkarte (1863). The smaller glaciers originating from the northface of the Breithorn were part of the glacier system. The lowermost part was called Bodengletscher and reached down to almost 1800 m a.s.l. to the houses of Furi.

Werder et al., 2009, 2013). The longest individual branch of the glacier system is the Grenzgletscher, which measures about 12 km in length (Sugiyama et al., 2010). It is also the one covering the largest altitude difference, with the glacier head located above 4550 m a.s.l. and the terminus located at roughly 2300 m a.s.l. (swisstopo, 2019). The Grenzgletscher retreated roughly 3 km since the Little Ice age, as the terminus was close to the houses of Furi at about 1800 m a.s.l. (Fig. 8) (swisstopo, 2019).

3.4 Polythermal Structure of the Lower Ablation Zone of Grenzgletscher

The Grenzgletscher is a polythermal glacier (Suter et al., 2001; Eisen et al., 2009; Ryser et al., 2013). The cold ice of the upper accumulation zone (Section 3.2) is buried under temperate firn and ice of the lower accumulation zone. In the ablation zone, the temperate ice melts and the cold ice emerges at the surface (Suter et al., 2001). As cold ice is impermeable to water, supraglacial hydrological features like large and deeply incised melt-water channels, lakes and water-filled cryoconite holes are frequent (Suter et al., 2001). Grenzgletscher is well known for these features since a long time (Renaud, 1936). The multi-annual persistence of the large channels

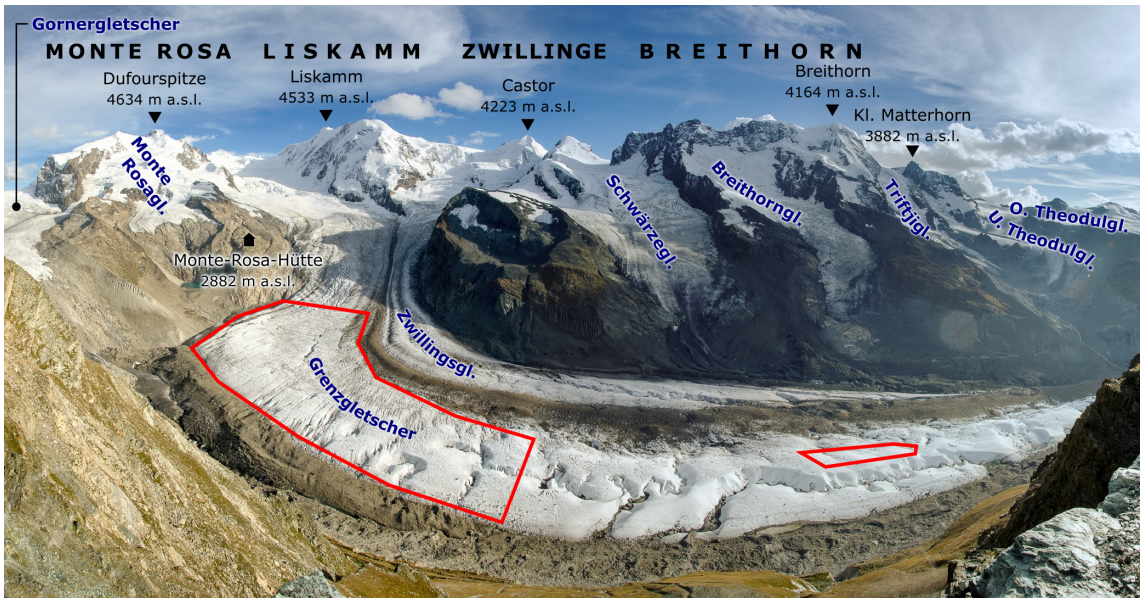

Fig. 9: View from Gornergrat (3133 m a.s.l.) southwards to the study area on the late afternoon of the 10th of September 2018. The uppermost accumulation area of the Grenzgletscher is not visible in the photograph. The terminus is also not visible. It is located a few hundred meters further down the valley from the point where the clearly visible melt water stream of the Unterer Theodulgletscher reaches the ice. The red polygon on the left indicates the area were most stakes and wires are located. Area 1-3 are also located in this area. The red polygon on the right represents roughly the extent of Area 4. There are some huge supraglacial water channels in the lower ablation zone of Grenzgletscher and Zwillingsgletscher. The snow line altitude on Grenzgletscher is about 3000 m a.s.l. in the photograph (Photograph by M. Thalmann).

even leads to their appearance on the topographic map of Switzerland. The glacier surface is also very slippery, even in warm summer weather (Ryser et al., 2013). Ice temperature measurements confirm the existence of cold ice in the lower ablation zone of Grenzgletscher. The coldest ice temperature measured by Haeberli (1976) was -2.8 °C at 44 m depth. Eisen et al. (2009) measured -2.65 °C at 70 m depth.

A temperate layer forms at the glacier bed due to the loss of altitude and the resulting strain heating as well as the geothermal heat flux (Benn and Evans, 2010). The exact starting point of this temperate layer is unknown for Grenzgletscher. Borehole measurements by Eisen et al. (2009) and Ryser et al. (2013), which were conducted in the confluence area, revealed the thickness of the temperate bottom layer to be in the range of a few to several decametres. Generally, the temperate bottom layer is thicker towards the glacier margins and further down along the flowline. The ice close to the medial moraines is expected to be temperate, because it was exposed to the bedrock earlier (Eisen et al., 2009). This is in line with the previously described borehole measurements, which are temperate throughout close to the medial moraine (Eisen et al., 2009; Ryser et al., 2013).

In their comprehensive study about the polythermal structure of the Grenzgletscher,

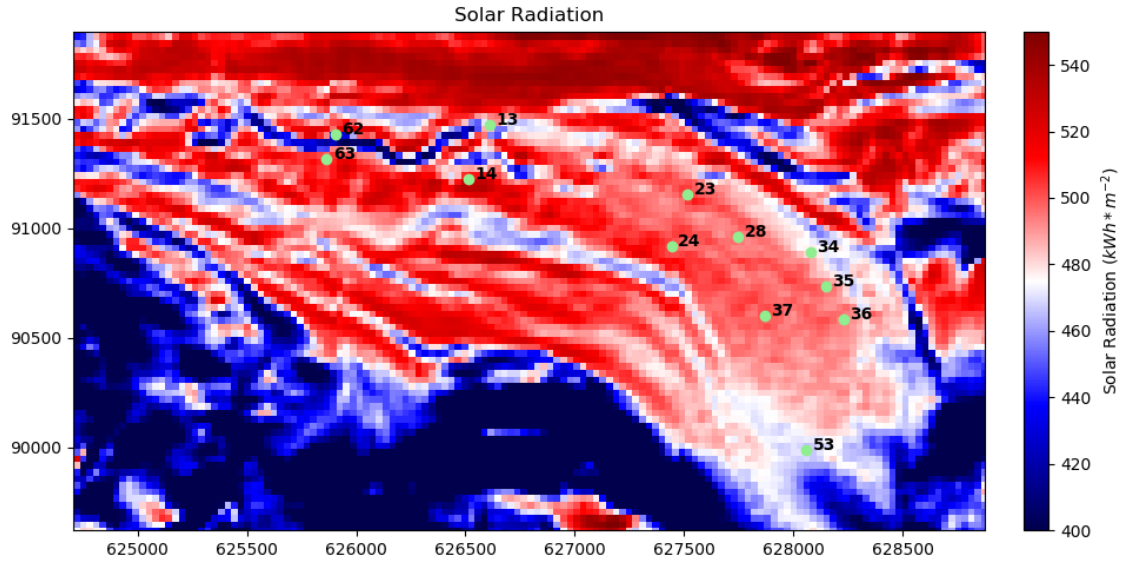

Fig. 10: Solar radiation between July 1 and September 31 on the lower ablation area of Grenzgletscher.

Ryser et al. (2013) also used an air-borne ice radar to map zones of cold ice. Cold ice has a very low content of liquid water in contrast to ice at pressure-melting-point. Liquid water in the ice scatters back the radar. Thus, low backscattering indicates the presences of cold ice. They validated the data of the ice radar with the above-mentioned temperature measurements in 15 deep boreholes. They identified a massive layer of cold ice along the central flow line that amounts for about 80-90% of the total ice thickness. This band of cold ice has a width of about 400 m in the confluence zone. In summary, it can be said that an essential part of the ice in the lower ablation zone is cold.

3.5 Study Area on the Lower Ablation Zone of the Grenzgletscher

The focus of this study is on the lower ablation zone of Grenzgletscher. In this study, the lower ablation zone is defined as the relatively flat partly of about 4 km of length, which begins in the confluence area of Grenz- and Gornergletscher. In the confluence area, the flow direction changes from northwards to westwards. From here, the glacier flows relatively straight, parallel to the Gornergrat, and its surface incline is only about 6% (Benoit et al., 2018). The average flow velocity is about 30 m $year^{-1}$ (Ryser et al., 2013).

Due to the characteristics of the surrounding mountain range and the relatively wide valley, the spatial variations in incoming solar radiations are in the range of

only 10-15% during the summer months. The sole exception from this range is the system of deeply incised melt water channels, which receives much less solar radiation at the bottom of the channels. The channel system is clearly recognizable on the solar radiation map (Fig. 10). The evenly distributed solar irradiation and the even surface incline favour incomparability between measurements conducted on the lower ablation zone of Grenzgletscher.

The surface appearance undergoes a strong visual change along the flowline (see Fig. 9). The surface of the confluence zone is much dirtier than the ice closer to the terminus. While the confluence zone is crevassed and has only weakly formed melt water channels, lower down the glacier has very few crevasses and huge melt water channels. Moulins are nearly absent (Ryser et al., 2013). The ice in this part is bright white.

The measurements which were used or conducted for this study are all but one located in the lower ablation zone of Grenzgletscher. The only exception is stake measurement 'st53', which is located higher up. The locations of the measurements are outside the channels, thus they are not affected by these strong variations in solar irradiation.

4 Materials and Methods

4.1 Ablation Data

4.1.1 Pre-existing Measurements

This study uses pre-existing ablation data acquired during previous research projects. These data can be divided into two datasets according to the type of measurement. The first dataset contains stake measurements. Stake measurements are the common type of in-situ point measurements of ablation (e.g Jouvet et al., 2011). The stake measurements in the study area were conducted in the middle of the 2000s over a few years. The stakes comprise segments, which each are 2 meters in length. The ablation at the measuring point can be determined by the number of segments that completely melted out and the length of the segment part sticking out of the ice. Some measurement points had unlikely jumps in their data series. The melt at the affected measuring points was modelled with degree-day factors (Section 4.1.3). It was highly likely that certain measurements had discrepancies of 2 m due to incorrect counting of the stake segments. These errors were corrected by M. Lüthi.

The second dataset contains measurements at wires. The wires were inserted between 2004 and 2010 in the context of studies conducted by the University of Zurich and the Eidgenössische Technische Hochschule (ETH). They were originally used to measure temperature and pressure. However, they offer a good opportunity for long-term (more than 10 years) ablation measurements, too. The place where the wire reaches the glacier surface is marked with tape. Thus, after a certain period of time, the ablation can be determined as the distance between the current ice surface and the bottom side of the tape representing the old position of the ice surface. The ablation measurements of the wires were performed by M. Lüthi and C. Ryser.

4.1.2 Additional Measurements in Autumn 2018

In the course of two field trips in autumn 2018, the data series of the wires were updated. The first field trip took place on September 10^{th} and 11^{th}. The ablation measurements were conducted on September 11. The second field trip took place about one month later between the 12^{th} and 14^{th} October. The ablation measurements were conducted on October 13^{th} and 14^{th}. The wires are hard to spot on the strongly heterogeneous glacier surface. The search parameters are given by the coordinates of former known positions, the ice flow velocity and the flow direction. Once the wire is found, the length is measured in meters as described in Section 4.1.1.

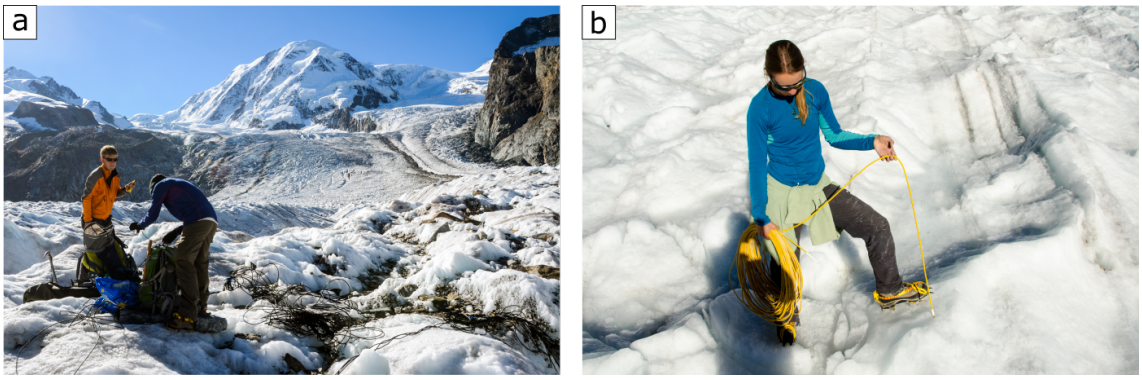

Fig. 11: Field work on the Grenzgletscher: (a) Unsorted cable at the borehole 'center' on the strongly heterogeneous glacier surface (September 11th, 2018) ; (b) The cable of 'bh3-05' which is already collected and marked at the glacier surface (October 13th, 2018) (photographs by M. Thalmann).

Occasionally, a knot was placed above the tape to make the identification of the marking easier. The molten out cable is collected and fixed with cable ties (Fig. 11). During both field trips, photographs were taken which help to interpret the results.

4.1.3 Computation of Degree-day Factors

The measurements of the wires and the stakes, respectively, differ in start and end date. *Degree-day factors* (DDFs) were calculated to make the measurements easily comparable. They were used to compare ablation and albedo. Furthermore, DDFs helped to spot errors in the measurements as described in Section 4.1.1. As a so-called *melt-index method*, DDFs describe the statistical relationship between melt rates and air temperature (Hock, 2003). The mean daily temperatures in degrees Celsius of all days with a positive mean daily temperature are added up (e.g. Braithwaite, 1995). The sum of the positive degree days is fitted to the cumulative melt. The constant which describes the fit is called DDF (Hock, 2003).

The weather station on the Gornergrat (3129 m a.s.l.) delivers continuous air temperature measurements. The ablation measurements are located within 3 km of the weather station. The air temperature data set from Gornergrat was calibrated with data from a weather station in the study area from the year 2005. The difference between the data of the Gornergrat station and the data of the weather station in the study area was minimized by addressing the offset and the amplitude. The calibration optimized for the year 2005 was applied to the entire data set. Thus, temperature data for the study area are available for the entire investigation period and in high temporal resolution. The DDFs for the wires and the stakes are presented in Appendix 1.

4.2 Albedo Data

4.2.1 Data Selection

Landsat data was chosen as input data for the albedo computation as it provides long time series and a decent spatial resolution, which is suitable for the study of Alpine glaciers (e.g. Naegeli et al., 2017). Landsat offers the *Landsat Surface Reflectance Level-2 science product*, which already includes an atmospheric correction (see Section 2.3.3). The *Landsat Surface Reflectance Level-2 science product* is provided by the *United States Geological Survey* (USGS). The product can be purchased via *Earth Explorer* (earthexplorer.usgs.gov). However, it is not readily available for downloading. The selected scenes are proceeded within a few days as long as the U.S. government is working. During shut-downs of the U.S. government, surface reflectance products of Landsat cannot be downloaded by the Earth Explorer. After processing, the scenes are available for download for several days.

The preferential months of acquisition were July, August and September, as the lower ablation zone usually is already free of snow and the durability of snow fall events is likely to be lower in these warm months. In some years, however, all scenes in this time period were affected by cloud cover or snow cover. Thus, the search mask was extended to the time period from June to October. Scenes from October were included because there was no snow on the glacier during the field trip in October.

There are two different scenes which show the study area, because the swath widths of the Landsat flight paths are overlapping. On *flight path 194*, the study area is close to the western, or left, margin of the image. The distance from the study area to nadir is about 90 km. On *flight path 195*, the study area is closer to nadir. The distance from the study area to nadir is only about 30 km. These differences change the sensor viewing angle slightly, but scenes of both flight paths were included.

The final selection of Landsat scenes was refined in several steps. In the first step, the Landsat scenes where checked for cloud-free conditions. It was often already visible in the preview image of Earth Explorer, if the study area is affected by clouds. If cloud-free scenes were already available in the required period, partially cloudy scenes were ignored. However, in some years the required scenes were scarce. Thus, scenes were often downloaded even though clouds were present in the study region. In the second step, scenes were visually checked for cloud cover after the download of the full-resolution version. Furthermore, some images were excluded by Landsat's own quality assessment due to high aerosol cocentrations over the study area. In

Tab. 7: Extent and mean altitude of the test areas.

	Extent (km^2)	Mean Altitude (m a.s.l.)
A1	0.1197	2565
A2	0.2385	2512
A3	0.1827	2477
A4	0.0513	2412

the third step, the corresponding band images of each scene were controlled for overexposure. However, most scenes contained enough bands that were not affected by this problem to perform the albedo computation with at least one formula. In the fourth step, it was controlled if there is fresh snow on the glacier surface. A thin layer of fresh snow is hard to spot on the glacier surface on satellite images (Naegeli et al., 2015). Two approaches help to decide whether there is snow on the glacier surface or not. The visual approach checks the area surrounding the glacier for fresh snow. If there is fresh snow on the slopes a few hundred meters above the glacier, it is likely that fresh snow is also located on the glacier. The meteorological approach checks temperature and precipitation data of the weather station on the Gornergrat for possible snowfall events shortly before the acquisition of conspicuous scenes. If scenes affected by snow were not detected with these approaches, they revealed unusually elevated albedo values after the albedo computation. They were excluded from the analysis as the aim of this study is to analyse the bare-ice albedo. Finally, the scenes which passed all these checks were cropped to the extent of the study area in the geospatial processing program *ArcMap*.

4.2.2 Albedo Computation

A narrow-to-broadband conversion was performed on the remaining Landsat scenes. The basis for the conversion are the conversion formulae which are presented in Section 2.3.4. The conversion was carried out with the *Raster Calculator* in ArcMap. Equation 4 was used to compute the albedo images from TM and ETM+ data. Equation 5 was not used for TM data, because these sensors are prone to overexposure in band 1 (blue band). Equation 7 is used to process OLI data. The advantages of Eq. 7 over Eq. 6 are presented in Section 2.3.4. A total of 93 Landsat scenes, which were acquired between 1990 and 2018, were processed to albedo images. 28 of them were OLI scenes, the other 65 scenes were TM scenes.

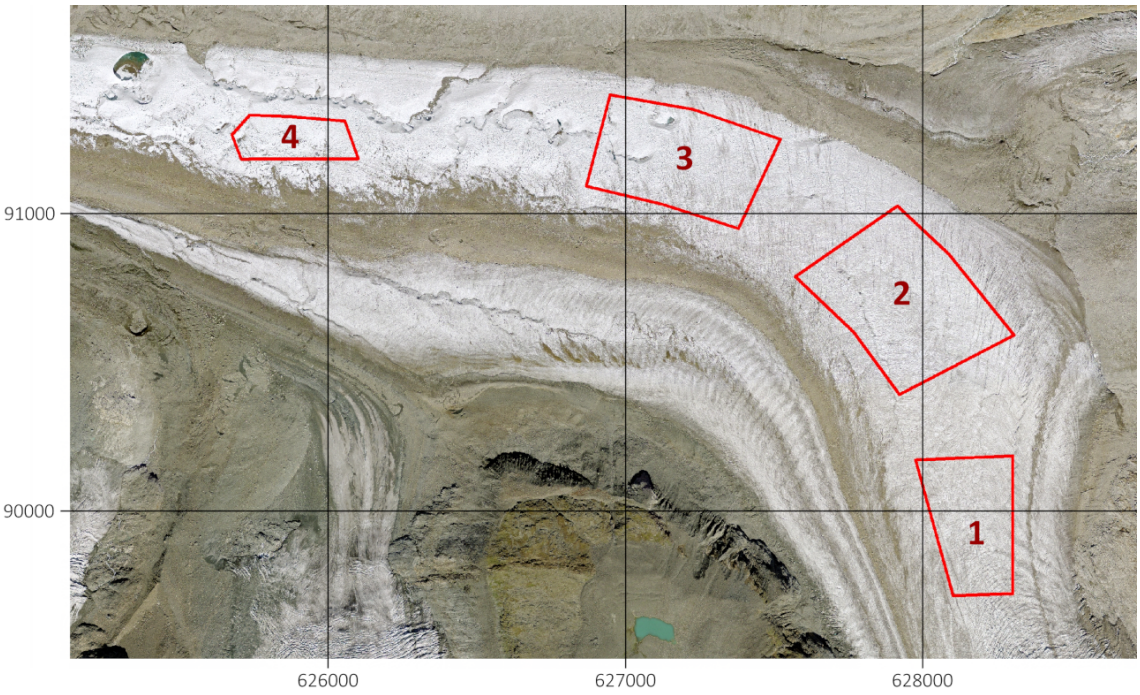

Fig. 12: Location of the four test areas on an aerial image of Swisstopo (SwissImage). Aquisition year: 2015 (swisstopo, 2019).

4.3 Comparison of Albedo and Ablation

The albedo images and the ablation measurements were compared to each other. For this comparison, the scene with the lowest mean albedo of each year ($\bar{\alpha}_{\text{annual min}}$) is chosen. For ablation measurements over several years, the albedo image was calculated as the average of several $\bar{\alpha}_{\text{annual min}}$. The lowest albedo was chosen according to the lowest mean albedo in the test areas. It is assumed that the scene that has the lowest mean albedo in the test areas also has the lowest mean albedo in the entire ablation zone. The selection of the $\bar{\alpha}_{\text{annual min}}$ images is done because a lower albedo favours a high melt rate. Thus, albedo images with low albedo values are more important for melt than albedo images with high albedo values.

The positions of the measurements move with the glacier. The mean location of all measuring sites was calculated for the stakes (Fig. 18). For the wires, the positions of the year 2013 (Fig. 16) were used, because the coordinates of all wires are known for this year and it is approximately in the middle of the observation period.

The albedo value at the position of the ablation measurement is then selected. Two methods were introduced for the retrieval of the albedo value from the albedo image. The first method is called the *1-cell environment method*. The albedo is taken solely from the cell in which the position of the measurement is situated. The second method is called the *4-cell environment method*. It uses the mean albedo

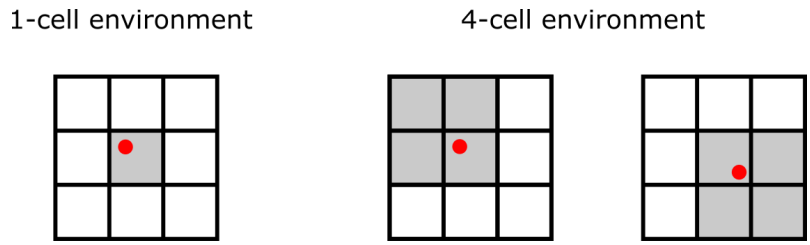

Fig. 13: Two different methods for the retrieval of the albedo at the position of the albedo measurement (red dot). The 1-cell environment solely uses the cell (grey) in which the position of the albedo measurement is. The 4-cell environment uses the four cells (grey) which are closest to the measurement.

value of the four cells which are closest to the measurement (Fig. 13). The DDFs (Section 4.1.3) represent the ablation. Finally, albedo and ablation were plotted against each other. The results of the comparison between albedo and ablation are found in Section 5.1.

4.4 Temporal Change in the Albedo

The albedo images were additionally analysed for temporal change in the bare-ice albedo. Two different selections of the albedo images were made. The first selection uses all 93 albedo images. The advantage of this selection is the higher number of albedo images. The second selection only uses end-of-summer images (from August and September) according to Naegeli et al. (2019), which improves the comparison over several years. In contrast, using all images highlights seasonal differences. 56 images are end-of-summer images.

Four areas on the lower ablation zone of the Grenzgletscher were defined (Fig. 12) entirely on bare-ice. Thus, medial and side moraines have been excluded in order to minimize the effect of supraglacial debris. Additionally, the large supraglacial melt water channels of the lower ablation zone were mostly excluded, too, in order to minimize topographic effects.

Area 1 is the uppermost area. Area 2 and Area 3 are both located in the former confluence zone with Gornergletscher. A small part of Area 3 is already affected by supraglacial channels. Area 4 is closest to the tongue. As a huge supraglacial channel makes up a significant part of the glacier width in this part of the glacier, Area 4 has the smallest extent.

Zonal statistics were calculated for all four test areas on all the calculated albedo images, using the feature 'Zonal Statistics as Table' in ArcMap. The mean values of each of the four test areas were checked for trends. The diagrams and boxplots which show the mean albedo values of the test area are presented in Section 5.2.

Fig. 14: Photograph of the temperature measurements in the borehole next to 'bh3-07'.

4.5 Spatial Change in Albedo Patterns

The end-of-summer images provided the basis for identifying long-term trends in the spatial patterns of the ice albedo. In order to further reduce the influence of seasonal fluctuations, the images were divided into groups defined by a 5-year interval. The average albedo of all images in a group was calculated with the Raster Calculator in ArcMap. The resulting images are shown in Section 5.3. In order to identify features visible in the albedo images, they were compared to an aerial image of SwissImage.

4.6 Ice Temperature Measurement

Several temperature measurements of near-surface ice were conducted with Thermistor strings produced by GeoPrecision. The Thermistor string is calibrated in an ice bath. Boreholes with a depth of a few metres were drilled into the ice with a Kovacs ice drill. The Thermistor string was inserted into the borehole and left there for about an hour to adapt to the ice temperature. The distance between the sensors on the string is 50 cm.
Due to technical issues, only one borehole temperature measurement was recorded correctly. This successful measurement is presented in the results (see Section 5.4).

5 Results

5.1 Albedo and Ablation

5.1.1 Wires

The results of the comparison between the albedo and the ablation at the wires are plotted in Fig. 15. The locations of the wires are from the year 2013 and they are marked in the albedo composite image (Fig. 16).
Fig. 15a shows the results of the 1-cell environment method. The data points are all but one located within the albedo range of 0.26-0.36 and within the degree-day factor range of 4.5-6.5 mm $°C^{-1}$ d^{-1}. The sole clear outlier is 'bh1-05'. At this point, the ablation between June 2005 and October 2018 was almost 100 m. Accordingly, the degree-day factor is 8.67 mm $°C^{-1}$ d^{-1}. The location is close to the medial moraine and the albedo at 'bh1-05' is also the lowest of all wires with about 0.22.
Fig. 15b shows the results of the 4-cell environment method. The point distribution of the 1-cell environment method and the 4-cell environment method are very similar. The results of both methods show a slight negative correlation between the albedo and the ablation. However, the determination coefficient is bad (R^2=0.32 and R^2=0.35) and the correlation is dependent on the outlier of 'bh1-05'. There is no correlation without 'bh1-05' (R^2<0.01).

5.1.2 Stakes

The results of the comparison between the albedo and the ablation at the stakes are plotted in Fig. 17. Fig. 17a shows the results of the 1-cell environment method and Fig. 17b shows the results of the 4-cell environment method. The point distribution is relatively similar for both methods. The biggest difference is found in 'st13', whose albedo is almost 0.07 lower in the 4-cell environment method due to its proximity to the glacier margin.
It is noticeable that 'st53' has the lowest albedo value and clearly the lowest ablation rate. The measurement at 'st53' is also the one at the highest altitude and it receives much less solar radiation (Fig. 10). Thus, 'st53' is an outlier concerning the general conditions. However, even when 'st53' is ignored, there is absolutely no significant correlation between the albedo and the ablation measured at the stakes (R^2<0.036).

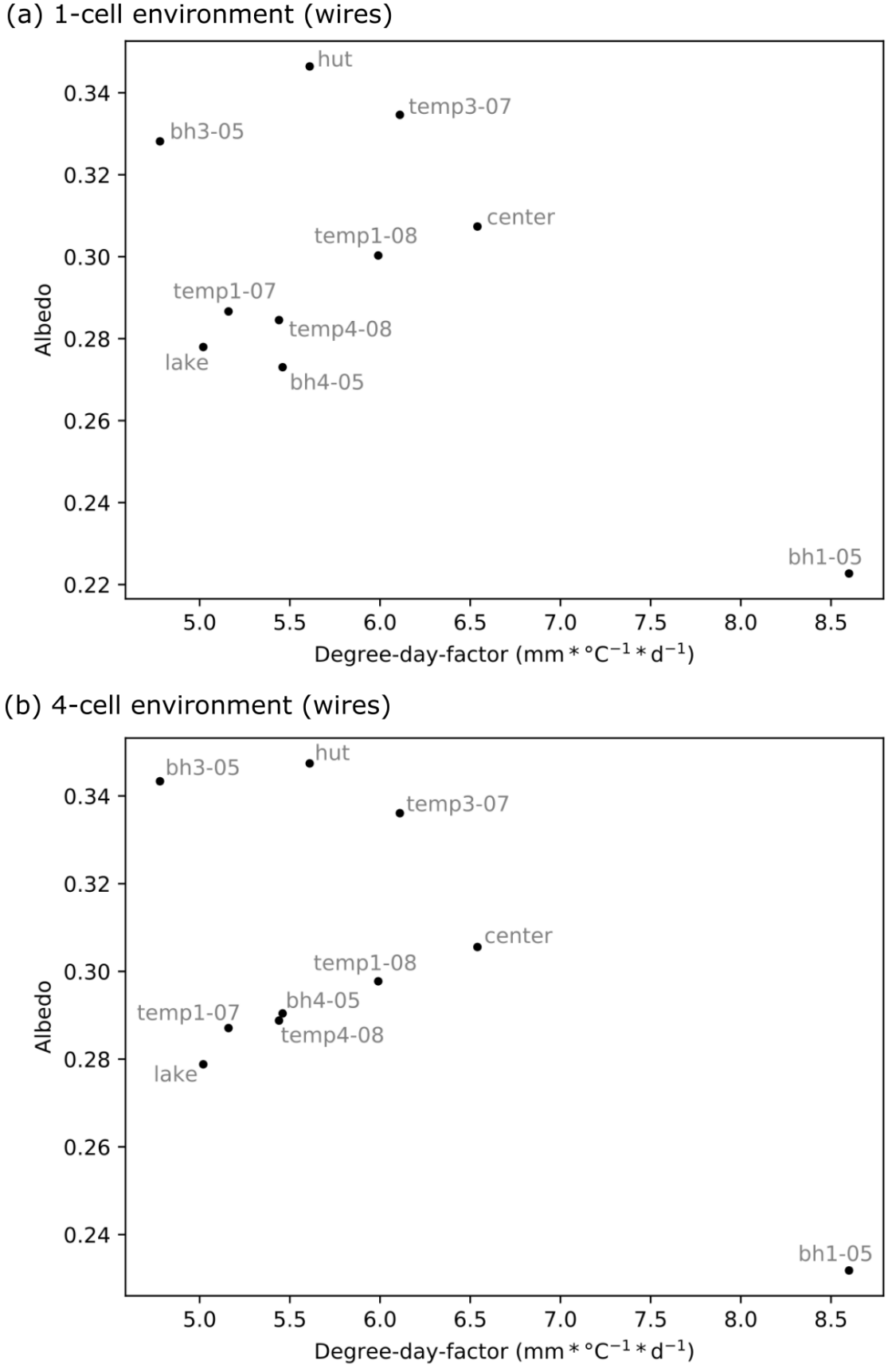

Fig. 15: Albedo and DDF of the wires: (a) shows the results of the 1-cell environment method; (b) shows the results of the 4-cell environment method.

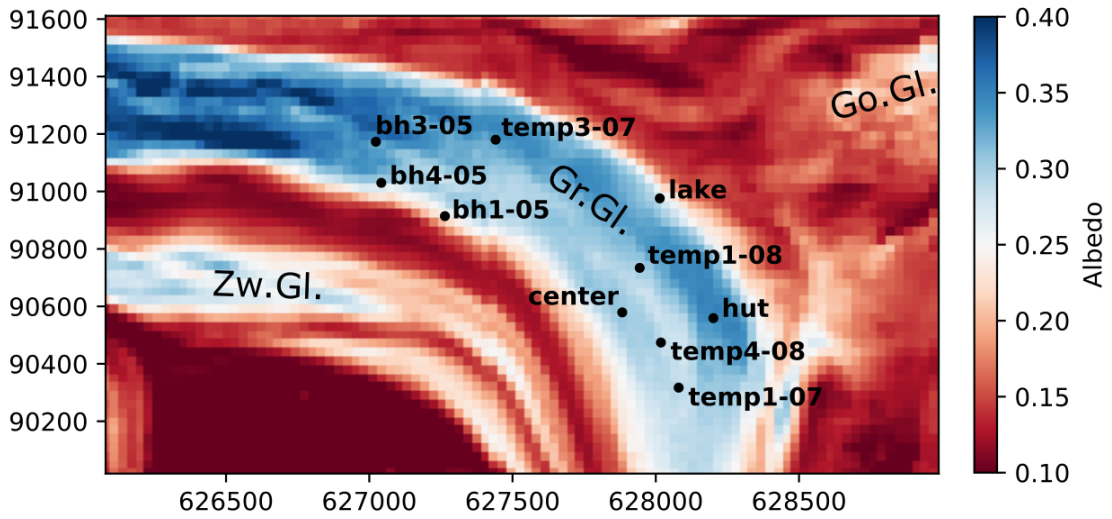

Fig. 16: The positions of the wires on the Grenzgletscher (Gr. Gl.). The albedo is from a composite image featuring the scene with the lowest albedo of each ablation season ($\bar{\alpha}_{\text{annual min}}$). Parts of the Zwillingsgletscher (Zw. Gl.) and the tongue of Gornergletscher (Go. Gl.) are visible.

5.2 Temporal Change in the Albedo

The mean albedos in the four test areas between 1990 and 2018 were plotted in Fig. 20. No data is available for the years 1996 and 2012. Fig. 20a includes all scenes which favours the representation of seasonal albedo fluctuations. Fig. 20b contains only the end-of-summer scenes, where multi-annual trends can be detected better (Naegeli et al., 2019).

The albedo is subject to great seasonal fluctuations (Tab. 8). Changes of more than 0.1 are possible on bare-ice surfaces within one season (Fig. 20a). On average, the lowest albedo values are obtained in the summer months, especially in July. The albedo values are becoming increasingly larger in the course of the season. The values in October are in the range of 0.06-0.09 higher than the values in July.

In all analysed scenes, the albedo is highest in A4, which is the lowermost test area. The average of the mean albedo values of all scenes in A4 in the time period 1990-2018 is 0.40. As in all test areas the albedo is lowest in July. However, even in July the albedo in A4 is higher than the albedo of A1 and A2 in October.

In almost all scenes, the albedo is lowest in A1, which is the test area highest up on the glacier. There is only one scene in which the albedo is lower in A2 than in A1 (10.09.2016). Furthermore, there are two scenes in which the albedo in Area 1 is almost equal to the albedo in A2. The mean albedo values in A1 are always lower than in A3. The average albedo of all scenes in A1 in the time period 1990-2018 is 0.27.

The mean albedos in A3 are always higher (0.03 on average) than in A2, except in

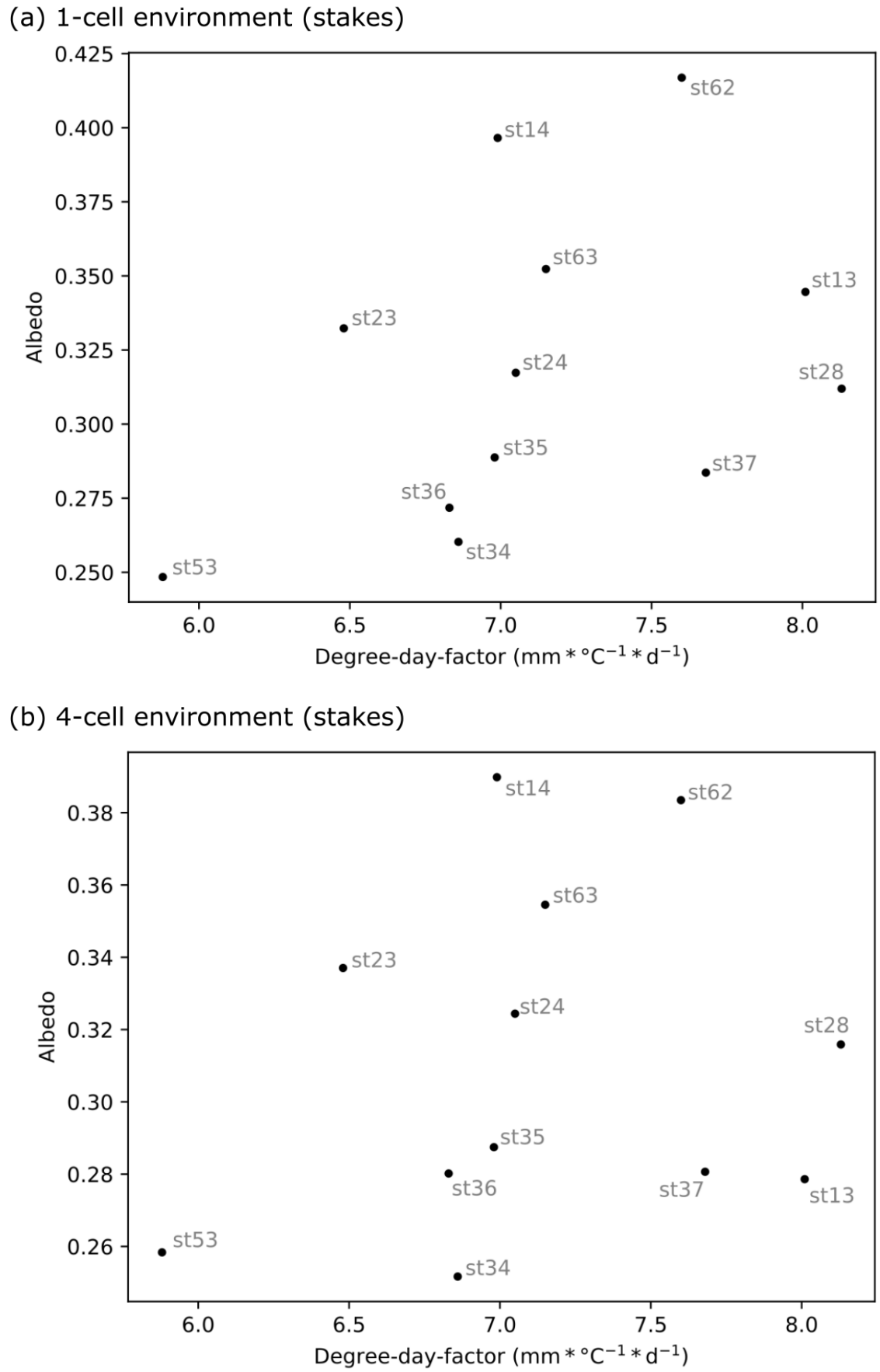

Fig. 17: Albedo and DDF of the stakes: (a) shows the results of the 1-cell environment method; (b) shows the results of the 4-cell environment method.

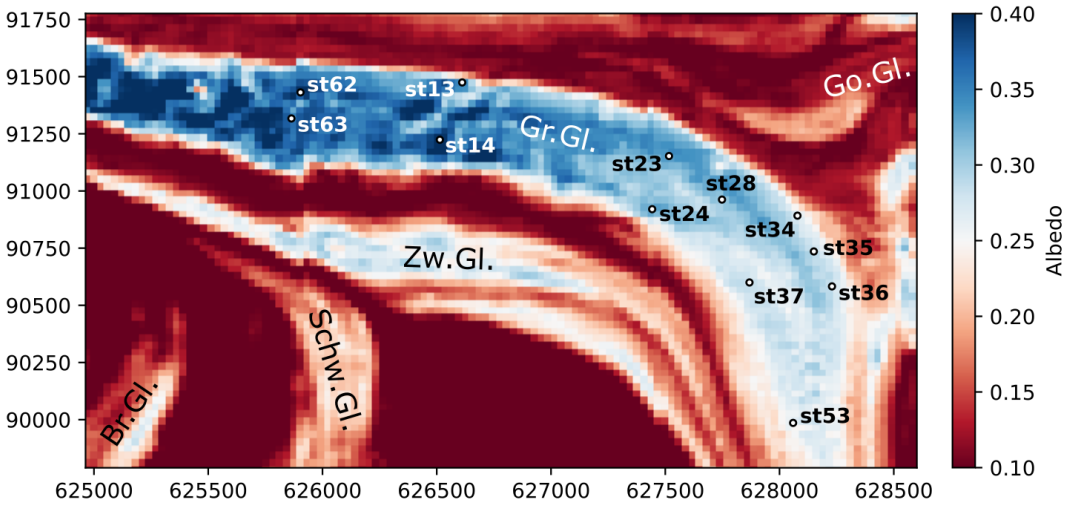

Fig. 18: The positions of the stakes on the Grenzgletscher (Gr. Gl.). The albedo is calculated as the average albedo of the ($\bar{\alpha}_{\text{annual min}}$) from the time span 2005-2007. Parts of the Zwillingsgletscher (Zw. Gl.) and the tongues of Gornergletscher (Go. Gl.), Schwärzegletscher (Schw. Gl.) and Breithorngletscher (Br. Gl.) are visible.

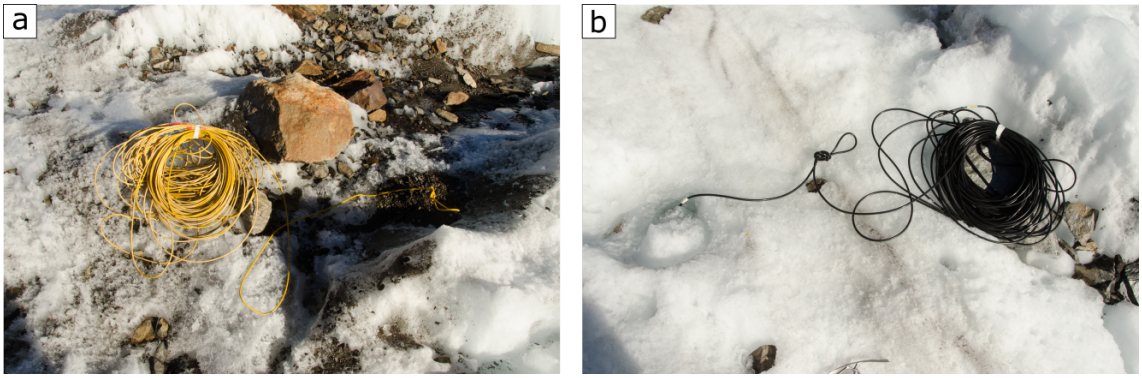

Fig. 19: Comparison between the immediate surroundings of (a) 'bh1-05' and (b) 'bh4-05'. 'bh1-05' is located in slush and dirt. 'bh4-05' is located in relatively clean ice.

Tab. 8: The mean albedo values in the test areas categorized by month.

	A1	A2	A3	A4
July	0.25	0.29	0.33	0.38
August	0.27	0.31	0.34	0.40
September	0.28	0.32	0.35	0.43
October	0.33	0.37	0.39	0.47

one scene (08.07.2016). The average of all mean albedos of all scenes in the time period 1990-2018 is 0.31 and 0.34 in A2 and A3, respectively.
In order to detect trends and to minimize seasonal fluctuations, the mean values were summarized in groups. The groups are defined by a time interval of five (Fig. 21) and ten years (Fig. 49 in the Appendix). They are presented in boxplots. The boxplots of both time intervals adapted on all scenes are also included in the appendix (Fig. 50 and Fig. 51). There is a trend towards rising albedo values in all test areas in the observed time period. The rise of the albedo was most pronounced in the 1990s and around the millenia change. In between 2003 and 2010, the trend of the rising albedo was much weaker or even stagnated. The values in 2011 and 2013 were the highest in the whole observation period.However, this trend got weaker and is even inverted during the last years (Fig. 21). From 2014-2018, the values were much lower again. This inversion is stronger when only using the end-of-summer scenes compared to using all scenes.

5.3 Spatial Change of Albedo Patterns

The albedo composite images which are used to detect spatial change in the albedo patterns over the last three decades are presented in Fig. 22. There is an error in the upper left corner of the image of 1995-1999 due to missing data. An aerial scene of SwissImage is used to correctly identify the features visible in the albedo images (Fig. 52).
First, some general characteristics of the pictures are pointed out. The albedo in the lower ablation of the Grenzgletscher is always higher than the albedo on the surrounding glaciers. The Zwillingsgletscher shows the highest albedo besides Grenzgletscher and there is also a large channel visible in the albedo images. The lower ablation area of the Grenzgletscher is very heterogeneous on the albedo images mainly due to a supraglacial channel system. The lower end of the heavily crevassed zone of the upper ablation area of the Grenzgletscher is clearly visible in the lower right corner of the images. In the confluence area, the albedo is generally lower closer to the medial moraine than at the outer glacier margins.

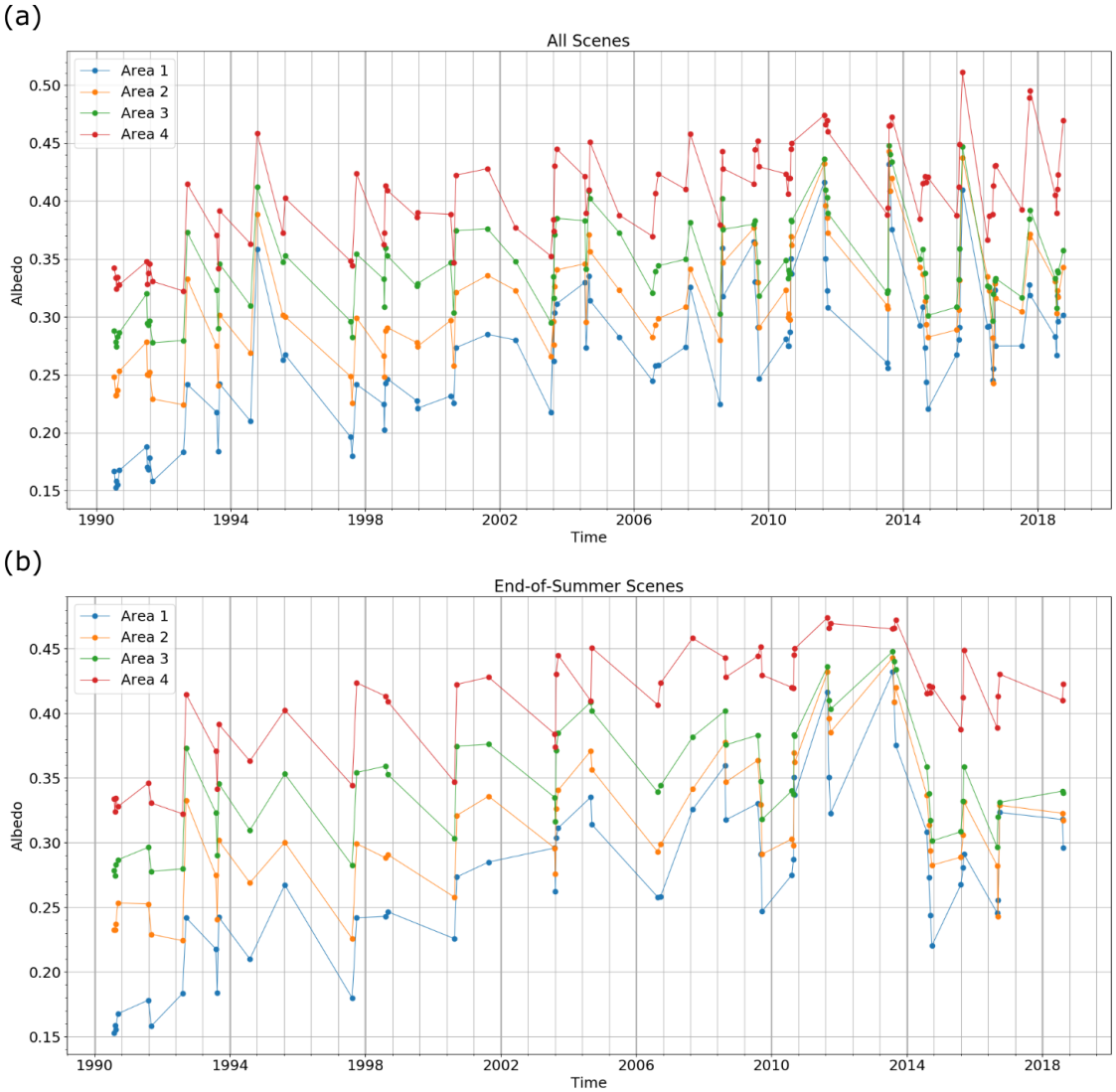

Fig. 20: Temporal Change of the Albedo: (a) shows the temporal evolution including all albedo images; (b) shows the temporal evolution including all end-of-summer scenes.

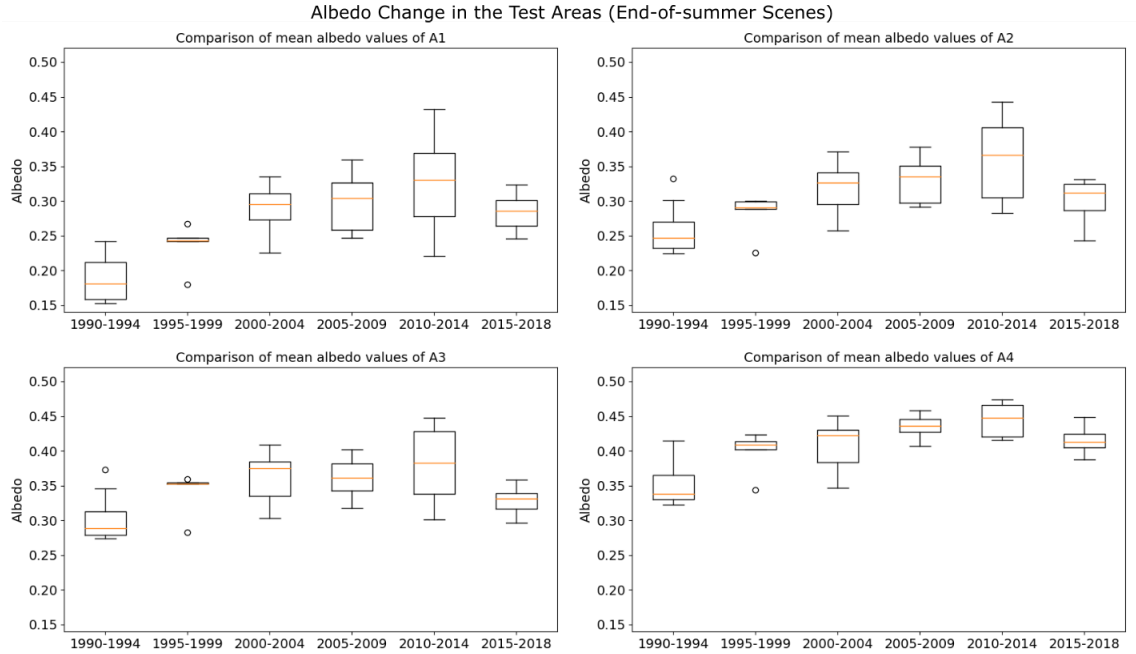

Fig. 21: Boxplots representing all mean albedos in certain time periods.

There are some general changes visible in the albedo images. All the glaciers are shrinking. The retreat of Gornergletscher, Schwärzegletscher and Breithorngletscher is clearly visible and goes along with a decline of the albedo in the affected areas. The Zwillingsgletscher shows the highest albedo besides Grenzgletscher. The width of the medial moraine between Zwillingsgletscher and Gornergletscher is increasing over the last decades.

The albedo images show some changing spatial patterns. In the 1990s, the higher albedo values (α>0.3) were restricted to the lower part of the confluence area and the area further down towards the terminus. In the 2000s, a large part of the glacier area up to the lower end of the ice fall of the upper ablation area had albedo values around 0.3. This trend of higher albedo values higher up in the ablation zone has continued in the first half of the last decade. However, this trend got weaker during the last few years.

While the albedo is generally increasing towards the tongue, there is a part of the glacier surface in the confluence area which does not follow this trend. There is a zone of relatively bright ice next to a crevasse zone, which is followed by a zone with darker ice further down the flowline. The wire measurement called 'hut' is located in this zone and it has a higher albedo value than other measurements much lower down.

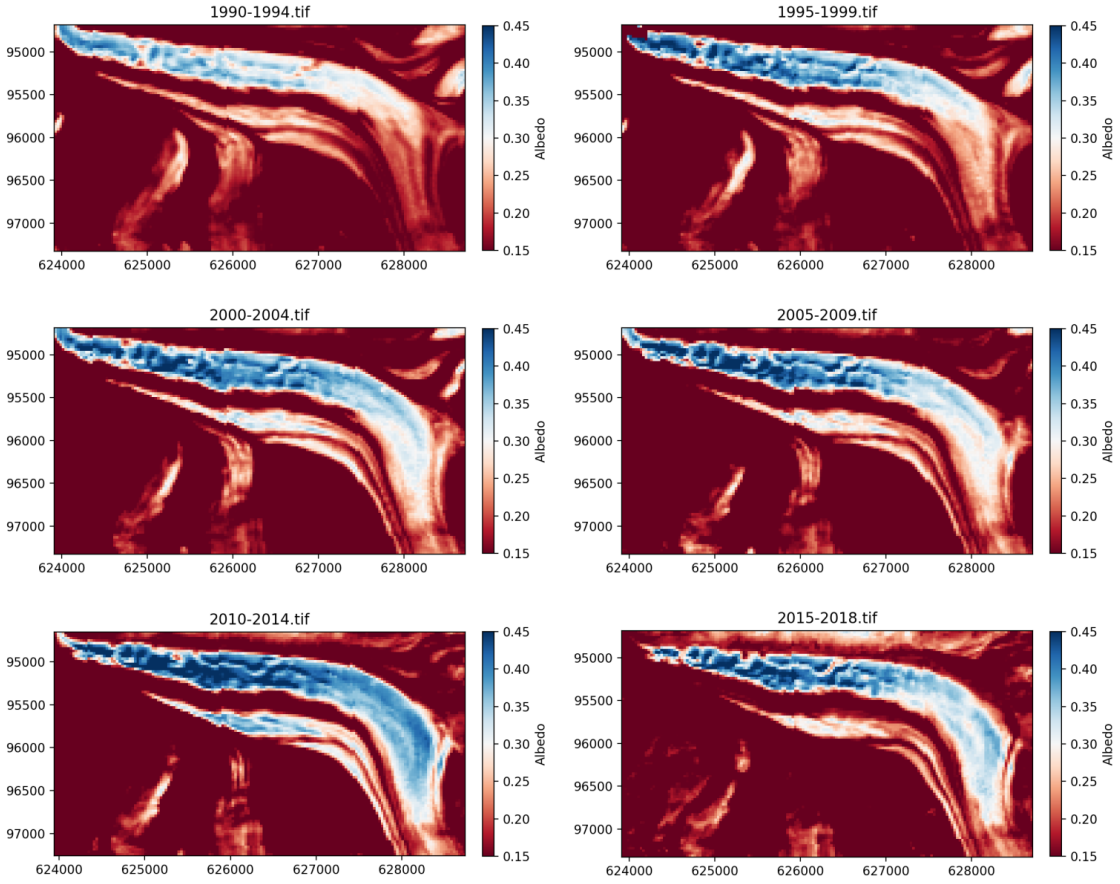

Fig. 22: Spatial change in albedo patterns since 1990, in 5 year intervals.

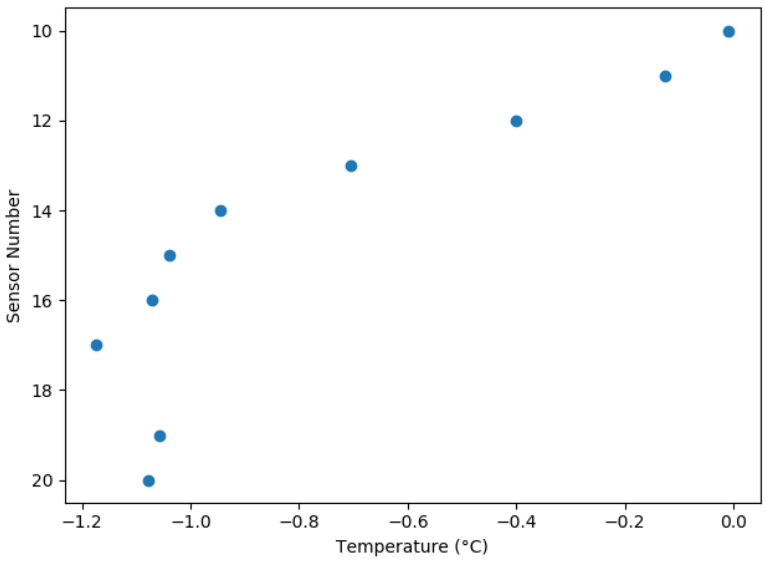

Fig. 23: Temperature measurements with a Thermistor string in the borehole next to 'bh3-07'. Sensor number 10 is the one closest to the glacier surface. Sensor number 18 is not displayed in the figure due to sensor malfunction.

5.4 Ice Temperature Measurement

The ice temperature measurement next to borehole 'bh3-07' was the only successful ice temperature measurement due to technical issues. The location of the measurement is about 20 m north of 'bh3-07', which was located at 627'317 / 91'239 at the 11th of September 2018. This zone is characterized by very bright and clean ice (α=0.39 on August 15th and α=0.44 on October 9th 2018) (see Fig. 14).

Sensor number 10 is the sensor which is located closest to the glacier surface. It is in a depth of 0 to 0.5 m. The spacing between the sensors is 0.5 m. Accordingly, sensor number 20 is located at a depth of approximately 5.0 to 5.5 m. Sensor number 18 is missing due to sensor malfunction. The measurement revealed negative ice temperatures close to the surface (see Fig. 23). Between the surface and a depth of about 2.0 to 2.5 m, the temperature gradient is relatively steep, before it flattens lower down, at a temperature a bit lower than -1 °C. The lowest temperature is measured by sensor number 17 (-1.173 °C) at a depth of 3.5 to 4.0 m. The temperatures measured lower down in the borehole are a bit warmer again.

6 Discussion

6.1 Albedo

6.1.1 Albedo Values

The absolute albedo values have to be interpreted with caution. The albedo is not corrected for the anisotropical reflection (BRDF correction) of glacier surfaces. Thus, the albedo of glacier ice is generally underestimated when observed from nadir (Klok et al., 2003). Despite these restrictions, the absolute albedo values are discussed and compared with examples from literature. Comparisons are often difficult because of differing observation periods, scales, definitions of terms like *ablation area* or *bare-ice* as well as characteristics of specific glaciers.

The average albedo values in A1-A4 in the whole observation period were in the range of 0.27-0.40. The mean albedo values of A1 (α=0.27), A2 (α=0.31) and A3 (α=0.34) are in line with bare-ice albedos presented in other studies. The value of 0.34 or 0.35 is often used as standard albedo for glacier ice (Oerlemans et al., 1998; Paul et al., 2005). Takeuchi (2002b) calculated a mean albedo of 0.32 for the ablation area of Gulkana Glacier in Alaska in 2000. Naegeli et al. (2015) determined a glacier-wide albedo of 0.29 ∓ 0.12 for Glacier de la Plaine Morte. Although this study considered the whole glacier surface, this value is still mentioned here. The research on Glacier de la Plaine Morte took place in August 2013, when the surface was mostly free of snow. Gabbi et al. (2014) calculated a mean ice albedo of 0.24 for Rhonegletscher in 2011. According to Paterson (1994), A1 and A2 are dominated by *slightly dirty ice*, while A3 is already dominated by *clean ice*. The mean albedo of A4 is 0.4 and thus clearly higher than in the other test areas. The value corresponds with *clean ice* according to Paterson (1994).

The maximum albedo values in certain parts of the lower ablation zone are exceptionally high, although the BRDF effect has a lower influence on very bright ice than on dirtier ice (Naegeli et al., 2017). The single cell maximum albedo in A4 exceeds 0.51 several times, which is the upper albedo limit for *clean ice* according to (Paterson, 1994). The frequency with which maximum values exceed 0.51 increases over the observation period. Since 2013, 12 of 28 scenes include maximum values higher than 0.51. On the other side, such elevated values have only been measured in 7 out of 65 scenes during the period 1990-2013. There are some explanations of the increase in the frequency of such maxima. The use of Landsat OLI data (since 2013) could result in higher maximum values than the use of Landsat TM data. However,

as the Landsat Surface Reflectance product is intercalibrated between the sensors, this seems unlikely. An other possibility is that the altered narrow-to-broadband conversion is responsible for these maxima. Naegeli et al. (2017) state that they found a few unrealistically high values when using the formula of Liang (2000) for Landsat 8 OLI data (Eq. 7). However, all four scenes of 2011, which are the last TM scenes used for this study, contain albedo values higher than 0.51. Thus, these values might not be a product of inaccurate computation but the albedo maxima might increase even stronger than the average albedo during the past few years.

The lowest minimum albedo values are found in A1 in the beginning of the 1990s. Also during a few other years of the observation period, a few values in the range of 0.10-0.15 are found, which corresponds to *debris-covered ice* according to Paterson (1994). Paul et al. (2005) found similar values in ablation areas during conditions of extreme summer melt in 2003. However, the minimum values on Grenzgletscher were often substantially higher a few weeks later (sometimes in the range of 0.1). As such an extraordinary short-term occurrence of LAIs and debris cover is unlikely, these extreme minima were interpreted as errors in the processing.

6.1.2 Albedo Computation

The albedo images are the basis of all analyses in this study. However, there are many factors that affect the accuracy of these images. According to Naegeli et al. (2019), uncertainties, which are hard to quantify, arise from the input data, the albedo computation, the data availability and environmental factors, mainly the meteorological conditions.

The Landsat Surface Reflectance Level-2 science product provides the input data for the computation of the albedo images. The product already includes an atmospheric correction (USGS, 2019a,b). It is suitable for temporal analysis (Claverie et al., 2015; Vermote et al., 2016), even at cell level according to the USGS (Naegeli et al., 2019). However, this product is not corrected for cloud shadows and topography (Young et al., 2017). Cloud shadows are not an issue because the scenes were selected manually, ignoring cloudy scenes. The missing correction for topography is also a minor problem, because the study area is rather flat (e.g. Naegeli et al., 2019).

The albedo computation was conducted with validated formulas which produce albedo images of good accuracy (Naegeli et al., 2017, 2019). The effect of the BRDF function was neglected. The BRDF effect is material dependent (Naegeli et al., 2015) and it exceeds the scope of this study to perform an accurate surface type classification which would have reduced the uncertainties. According to Naegeli et al.

(2017), the BRDF correction is negligible and its absence usually leads to a small underestimation of the albedo (Tab. 4). Albedo computation without anisotropy correction is not sufficient for computing absolute albedo values. However, as the focus of this thesis lies on relative temporal and spatial variations in the albedo, such a basic albedo retrieval approach is sufficient. According to Naegeli et al. (2019), relative changes are represented reliably.

The biggest problem presumably results from the limited temporal availability of data. The glacier albedo is subject to variations at different temporal scales (Section 2.2.4) and the images show only a few moments of the temporal evolution. Naegeli et al. (2019) call the uncertainty arising from the limited data availability *snapshot uncertainty*. The meteorological conditions prior to the acquisition of the Landsat scene are of great importance (Fugazza et al., 2016) because they can alter the albedo significantly (Naegeli et al., 2017). The effects of different meteorological conditions on the albedo were described in Section 2.2. However, it is not always obvious to identify the meteorological conditions prior to the acquisition of a specific scene, which are responsible for the glacier albedo in the corresponding albedo image.

6.2 Ablation

6.2.1 Ablation Values

The DDFs are mostly in the range of 5-8 mm $°C^{-1}$ d^{-1}. In literature, DDFs of glaciers in the range of 5.4 mm $°C^{-1}$ d^{-1} to 20.0 mm $°C^{-1}$ d^{-1} are found (Hock, 2003; Zhang et al., 2006). However, the values in most studies are lower than 12 mm $°C^{-1}$ d^{-1} (Hock, 2003). Lang (1986) made ablation measurements on the Aletschgletscher during August 1965. The DDF was 11.7 mm $°C^{-1}$ d^{-1}. They conducted their measurement at 2200 m a.s.l.. At this altitude, the Aletschgletscher is slightly wider and the valley is much more open towards the south compared to the lower ablation zone of Grenzgletscher (swisstopo, 2019). These factors favour high solar irradiation. In contrast, the low DDFs obtained in this study reflect the high albedo in the lower ablation zone of Grenzgletscher. In conclusion, the DDFs seem reasonable.

6.2.2 Comparison of Albedo and Ablation

Solar radiation is the most important energy source for ablation in the European Alps (e.g. Paul et al., 2005). The albedo determines the part of the solar radiation

which is available for melt (Section 2.1.4). Thus, a correlation between albedo values and melt seems likely. The lower ablation zone of Grenzgletscher is suitable to conduct a study which examines this relationship (Section 3.5).

Despite the suitable study area, this study was not able to find a correlation between albedo and ablation on the lower ablation zone of Grenzgletscher, whether with the stake measurements nor with the wire measurements. Accordingly, no difference in the ablation rate between zones of cold ice and zones of temperate ice was observed, which answers research question 1. However, several problems concerning methods and data were identified. These problems are discussed in order to contextualise this observation.

The ablation measurements performed with the direct glaciological method deliver values which represent the melt during a certain time period (e.g. Benn and Evans, 2010). Therefore, in contrast to satellite images, they are not snapshots in time. However, as there are only a few stakes and wires on the glacier, they could be seen as snapshots in space. Bare-ice surfaces are highly heterogeneous (e.g. Naegeli et al., 2015) and point measurements represent conditions which potentially can be very local.

Significant differences exist between the ablation measurements on the lower ablation zone of Grenzgletscher. The highest total ablation (98.57 m between June 2005 and October 2018) as well as the highest melt rate (8.67 mm $°C^{-1}$ d^{-1}) was measured at 'bh1-05' (see Tab. 9 and Fig. 25). The ablation at 'bh1-05' exceeds the ablation at nearby 'bh4-05' (62.03 m between June 2005 and October 2018) by almost 60%. They are both located close to the medial moraine. According to Paterson (1994), 'bh1-05' is located in *dirty ice* and 'bh4-05' is located in *slighly dirty ice* (see Tab. 3). But, as the absolute values are subject to large uncertainties, the focus lies more on the difference between the two sites. The albedo difference of less than 0.06 between the respective cells in the albedo image cannot explain such a huge difference in ablation. However, when we take a closer look at these locations in the field (Fig. 19), the difference is much more extreme than one expects from the albedo image. While 'bh1-05' is in the middle of a little mud basin filled with slush and surrounded by dirty ice and several stones, the ice at 'bh4-05' is much cleaner. At 'bh4-05', only some small streaks of relatively higher LAI concentration among very clean ice are visible and there are only a few small stones. This example of 'bh1-05' and 'bh4-05' shows that a stake that is randomly placed in a cell of 30 m side-length may not adequately represent this cell in terms of ablation. LAI concentrations, exposure to glaciohydrological processes, small-scale topography and other factors make comparison difficult.

The use of multi-annual measurements made the comparison with the albedo images even more difficult. The glacier flow continuously alters the measurement positions. The average flow velocity is about 30 m year^{-1} (Ryser et al., 2013). For the stakes, this is a minor problem as the measurement period is shorter. Especially with the 4-cell method, the extracted albedo is representative for the stake environment during a large part of the measurement period. However, the wires have much more time to travel. The distance between the 2006 and the 2018 position of the wire 'center', for example, is roughly 280 m. The methods used in this study likely do not adequately represent the different albedo values encountered on this long journey.

Another weakness of the study is the low number of ablation data points. The data of 12 stakes and 10 wires were analysed. Many more ablation measurements for the Grenzgletscher would be existing, however, they are not in cells which represent bare ice in the Landsat data. As the aim of this study is to detect differences in ablation between cold ice and temperate ice, these ablation measurements were ignored.

A future study about the influence of cold ice on the ablation should include more ablation measurements on bare-ice and more ice temperature measurements at the surface. Additionally, a shorter observation period (for example some weeks during July and August), but with good knowledge about the surrounding conditions (for example solar radiation, air temperature, in-situ albedo measurements, characteristics of each stake location), might contribute to better results.

6.3 Ice Temperature at the Glacier Surface

In this study, high albedo values in the ablation area are assumably associated with the presence of cold ice. In order to support this assumption, it was planned to carry out several temperature measurements in the surface ice. Due to technical problems, only one measurement was successful. Despite extensive studies on the thermal structure of the Grenzgletscher (Eisen et al., 2009; Ryser et al., 2013), it is not known exactly where the cold ice emerges at the surface. Therefore, different approaches are discussed, which allow conclusions to be drawn about the extent of cold ice at the surface.

The ice temperature measurement in the borehole took place on the 11$^{\text{th}}$ of September 2018. Because no suitable Landsat scenes are available in September, the scenes from 9$^{\text{th}}$ of October, 2018 and 15$^{\text{th}}$ of August, 2018 are used for comparison. The albedo of the cell in which the borehole measurement took place is $\alpha = 0.43$ in the October scene and $\alpha = 0.39$ in the August scene. Since cold ice has been detected

in this cell and albedo is used as a proxy for cold ice, it is assumed that cold ice is also found on the surface in all cells with the same or higher albedo (Fig. 24). This is probably a conservative estimation, as it is likely that there are cells with a lower albedo which still have cold surface ice.

The presence of supraglacial water channels is known as an indicator for cold ice (Hodgkins, 1997; Boon and Sharp, 2003; Ryser et al., 2013). Around the large meltwater channels, the albedo is high. However, there is also a smaller meltwater channel[6] in the confluence area, in a part with a lower albedo. On the lower ablation area of the Zwillingsgletscher, there is also a channel but the albedo values are not as high (0.30-0.35) as around the large channel system of the Grenzgletscher. In contrast, there is also a zone with high albedo values in the confluence area (Fig. 52). This high-albedo zone is free of meltwater channels but contains some large crevasses. Crevasses and fractures enable the water to get from the surface into the glacier and to the glacier bed. Thus, they may hinder the development of pronounced supraglacial channels.

Another indicator for cold ice is bright and clean ice (Suter et al., 2001; Ryser et al., 2013). The ice around the large channels is exceptionally bright and clean. In general, the zones of bright ice agree very well with zones of high albedo. This is not surprising as the biggest difference between clean and dirty glacier ice is in the visible part of the solar spectrum (Fig. 4).

There are two features which could indicate cold ice at the surface in the confluence zone. The first one is the zone with clearly elevated albedo values compared to the surrounding ice. The second one is the above mentioned melt water channel. In the confluence area, Ryser et al. (2013) detected a central band of cold ice that occupies a width of 400 m. Cold ice has been detected in the deep boreholes besides the channel. The high-albedo zone partly extends beyond the margins of the cold ice band inferred by Ryser et al. (2013, Fig. 10).

In conclusion, is is difficult to clearly determine a border which separates cold ice surfaces from temperate ice surfaces. However, it is very likely that there is cold ice at the surface along the central flowline from a few hundred meters upwards of the marked borehole position in Fig. 24 until close to the terminus. According to Ryser et al. (2013, Fig. 10), there is temperate ice close to the glacier margins. Also the parts of very bright ice in the confluence area are likely to be cold. Furthermore, it is

---

[6] This channel can be seen in Fig. 9 above the *G* of the label *Grenzgletscher*.

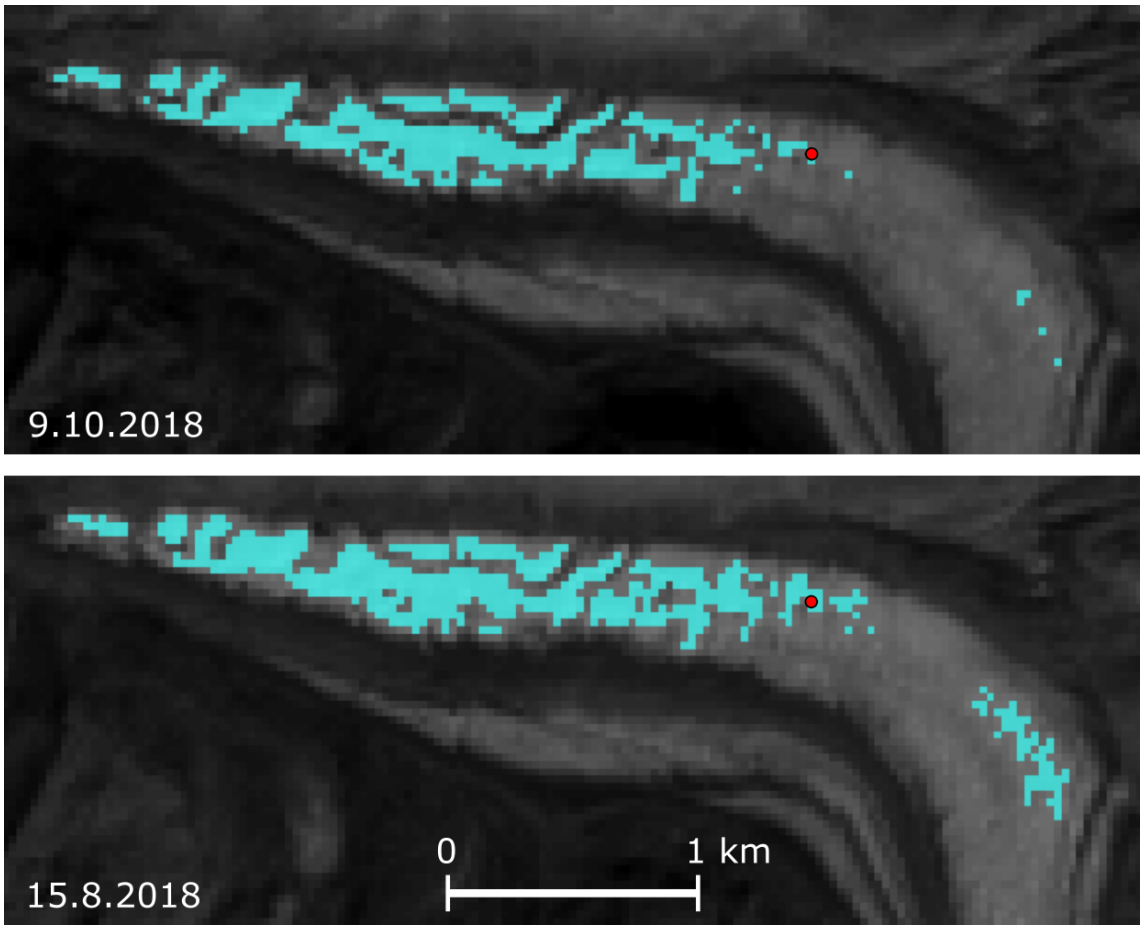

Fig. 24: Two albedo images of the lower ablation zone of the Grenzgletscher. The red dot marks the location of the temperature measurement that was conducted in a borehole next to 'temp3-07' on the 11th September 2018. The Landsat scenes, from which the two albedo images were calculated, are closest in time to the temperature measurement in the borehole. As this study makes the assumption that the albedo can be used as a proxy for the ice temperature, all cells which have the same or a higher albedo are colored in light blue. The thresholds, above which the cells are coloured, are $\alpha = 0.43$ on October 9, 2018 and $\alpha = 0.39$ on August 15, 2018.

probable that more parts of the confluence area are cold, as there exist pronounced channels.

For future investigations it would be very interesting to conduct more ice temperature measurements close to the surface according to the one presented in this study. While a few measurements lower down on the glacier may be sufficient to confirm the presence of cold ice, more detailed measurements in the confluence area would be interesting to gain detailed insight into the patterns of cold ice in this more complex area.

6.4 Seasonality of the Bare-Ice Albedo

Seasonal fluctuations of the glacier surface albedo are pronounced in all test areas. The albedo is clearly lower during the summer months than during autumn. Solar radiation and air temperature are higher in the summer than in autumn what causes higher melt rates. Therefore it is likely that these seasonal fluctuations are mostly due to the variations in the presence of liquid water on the glacier. A thin meltwater layer can substantially lower the bare-ice albedo (Naegeli et al., 2017). Furthermore, strong ablation possibly reduces the surface roughness and thus also the albedo (Cathles et al., 2011; Rippin et al., 2015). In contrast, prolonged periods with temperatures below freezing reduce melt in autumn and less liquid water is present on the glacier surface. Additionally, the holes and basins that contain cryoconite are covered by an ice layer if the temperatures are cold enough. The ice layer often contains air bubbles. The transition from cryoconite holes to clean, air-bubble rich water ice is expected to have a pronounced effect on the albedo in the lower ablation zone. Thus, periods of little irradiation and low air temperatures are likely to cause a positive feedback and reduce melt further. On the contrary, periods of pronounced ablation are likely to cause a positive feedback due to the meltwater layer and the temporally and spatially extended exposure of cryoconite.

The redistribution of LAIs is assumed to have less impact on the seasonal cycle. In Summer, when water availability for LAI evacuation is highest, the albedo is low. Vice versa, in autumn, when water availability is limited and LAIs are less likely to be flushed into depressions, the albedo is high. However, there are many relationships between meteorological conditions and LAIs which are still poorly understood (Naegeli et al., 2019). Further research is needed to get more knowledge about the LAI redistribution processes. Additionally, it could be interesting to see if seasonal albedo variations correspond to melt, solar irradiation and air temperature. If this assumed linkage exists, the missing albedo values between the acquisition dates of remote-sensing imagery could be interpolated and the snapshot uncertainty could be reduced.

In order to optimise multi-annual intercomparison, Naegeli et al. (2019) suggested the temporal restriction to end-of-summer. They used scenes from August and September, when the extent of bare-ice areas is largest. On Grenzgletscher, the magnitude of the seasonal albedo fluctuations between July and August as well as between August and September are relatively similar. The lower ablation zone of Grenzgletscher is also free of snow in July, as long as there are no summer snow fall events. Thus, the selection of scenes from July for the intercomparison over multiple

years is also likely to work. However, the fluctuations usually become much greater between September and October. October scenes are therefore less suitable for multi-annual intercomparison.

6.5 Brightening and Changing Albedo Patterns

The albedo images show brightening and changing albedo patterns in the lower ablation zone of the Grenzgletscher between 1990 and 2014, which answers research question 2 and 3. Areas 1-4 showed higher values during the last decade than in the 1990s (Fig. 49 and 51). However, this trend of rising albedo values seems to be inverted since 2014 (Fig. 20). The reason for this inversion remains unclear.

According to the albedo images, the cold ice seems to emerge earlier at the surface, under the assumption that high albedo values corresponds to cold ice. This contradicts with Ryser et al. (2013), who expect the cold ice to emerge at the surface downstream of their borehole measurements, where the large meltwater channels and the strikingly white ice are found.

However, it is possible that there is already cold ice at the surface in some parts of the confluence zone. The confluence zone and the upper accumulation area are home to some crevassed zones. Crevasse zones enable access to deeper parts of the glacier for energy fluxes (Pfeffer and Bretherton, 1987). Furthermore, crevasse zones allow the development of moulins in cold-ice zones, which are otherwise almost free of moulins (Ryser et al., 2013). Moulins with continuous water supply can warm cold ice to the pressure-melting point (Ryser et al., 2013). Crevasse zones and moulins might explain parts of the spatial heterogeneity of the albedo in the confluence zone.

Furthermore, the ice contains different concentrations of LAIs at different places on the glacier. These differences might arise for example due to crevasse zones, which enable englacial dust deposition, active scree slopes, which provide dust supply, or from ancient periods with high dust deposition. Spatial and temporal variations in englacial LAIs consequently cause changes in the surface albedo.

The topography of the glacier surface alters the glacier albedo in two ways. First, changing surface topography changes the incident angle of solar radiation. Second, the surface topography has an impact on LAI redistribution. It seems reasonable that the evacuation of LAIs during strong precipitation events is stronger from elevated areas. For example, the high-albedo zone in the confluence area is slightly elevated compared to the surrounding glacier surface (about 1-2 m higher).

In conclusion, it is very difficult to link albedo changes on the glacier surface to changes observed on the glacier. The explanations presented in this section are hypothetical. Further investigations are needed to understand the spatial heterogeneity as well as the temporal evolution of the glacier albedo.

7 Conclusion and Outlook

This study analyses 93 albedo images of the lower ablation zone of Grenzgletscher. The lower ablation zone of Grenzgletscher is known for supraglacial hydrological features like deeply incised meltwater channels as well as relatively large lakes. These features are linked to the presence of cold ice (Hodgkins, 1997; Boon and Sharp, 2003). The Grenzgletscher is the only glacier in the European Alps where these features can be observed (Ryser et al., 2013). The glacier ice in the ablation zone changes its appearance along the flowline and becomes strikingly white towards the terminus. The emergence of cold ice at the glacier surface is responsible for this transition. The spectral differences between clean and dirty ice are most pronounced in the visual part of the solar spectrum. Thus, the differences perceived by the human eye roughly represent the differences in the albedo images.

At the glacier surface, the albedo determines the amount of the incoming solar radiation that is available for glacier melting. In order to analyse the linkages between albedo and melt, the albedo images were compared with ablation measurements. This study, however, was not able to find a correlation between albedo and ablation on Grenzgletscher. The albedo images show a trend of rising albedo values since 1990. However, this trend is inverted since 2014. The reason for this sudden trend inversion remains unclear. In the course of the observation period, increasing albedo values are observed in greater distance to the terminus. This could be associated with cold ice emerging earlier at the surface as the temperate layer melts faster. However, the cold ice is present in the lower ablation zone for a long time and it is difficult to explain the variations in the albedo images with cold ice only. Furthermore, the albedo undergoes significant seasonal fluctuations. It is lowest in July and raises in the range of 0.06-0.09 until October. This seasonal cycle is most likely linked to the presence of liquid water and the exposure of cryoconite holes.

According to Naegeli et al. (2019), the relative differences between the different albedo scenes are reliable and robust. However, the temporal analysis suffers from snapshot uncertainty as the albedo images are strongly dependent on the meteorological conditions prior to the time of acquisition. Furthermore, there arise uncertainties from the input data and the albedo computation. It is difficult to quantify these uncertainties. More knowledge could be gained by additional measurements of the ice surface temperature as well as short-term ablation measurements, where all surrounding conditions are known. Insight gained by such a study might improve the understanding of the melt behaviour of polythermal glaciers and, consequently, the ice shields.

8 Acknowledgements

Sincere thanks go to Dr. Martin Lüthi for the supervision of this Master's thesis, for all the hours he's been helping me, for the support in the field work, for his very quick email replies and especially for the patience for my lack of programming skills. Furthermore, I want to say thank you to Andrea Walter for the support in the field work. Special thanks goes to Laura Büchler, who supported me extensively in the field and in general.

9 Bibliography

Aerts, J. C. J. H. (2017). Climate-induced migration: Impacts beyond the coast. *Nature Climate Change*, 7(5).

Alean, J., Haeberli, W., and Schadler, B. (1983). Snow accumulation, firn temperature and solar radiation in the area of the colle gnifetti core drilling site (monte rosa, swiss alps): distribution patterns and interrelationships. *Zeitschrift fur Gletscherkunde und Glazialgeologie*, 19(2):131–147.

Alexander, P. M., Tedesco, M., Fettweis, X., van de Wal, R. S. W., Smeets, C. J. P. P., and van Den Broeke, M. R. (2014). Assessing spatio-temporal variability and trends in modelled and measured Greenland Ice Sheet albedo (2000–2013). *The Cryosphere*, 8(6):2293–2312.

Amann, M., Pozzoli, L., Demkine, V., Dingenen, R. V., Raes, F., Anenberg, S. C., Ramanathan, V., Janssens-Maenhout, G., Schwartz, J., West, J. J., Faluvegi, G. S., Kuylenstierna, J., Muller, N. Z., Vignati, E., Williams, M., Emberson, L., Shindell, D. T., Klimont, Z., and Hicks, W. K. (2012). Global air quality and health co-benefits of mitigating near-term climate change through methane and black carbon emission controls.

Aoki, T., T, A., Fukabori, M., Hachikubo, A., Tachibana, Y., and F, N. (2000). Effects of snow physical parameters on spectral albedo and bidirectional reflectance of snow surface. *Journal of Geophysical Research: Atmospheres*, 105(D8):10219–10236.

Arendt, A., Bolch, T., Cogley, J., Gardner, A., Hagen, J., Hock, R., Kaser, G., Pfeffer, W., Moholdt, G., Paul, F., Radić, V., Andreassen, L. M., Bajracharya, S., Beedle, M., Berthier, E., Bhambri, R., Bliss, A., Brown, I., Burgess, E., and Zheltyhina, N. (2012). Randolph glacier inventory [v2. 0]: A dataset of global glacier outlines. global land ice measurements from space, boulder colorado, usa.

Azzoni, R., Senese, A., Zerboni, A., Maugeri, M., Smiraglia, C., and Diolaiuti, G. (2016). Estimating ice albedo from fine debris cover quantified by a semi-automatic method: The case study of forni glacier, italian alps. *The Cryosphere*, 10:665–679.

Beniston, M. (2003). Climatic change in mountain regions: A review of possible impacts. *Climatic Change*, 59(1):5–31.

Benn, D. and Evans, D. (2010). *Glaciers and Glaciation*. Routledge, 2 Park Square, Milton Park, Abingdon, Oxon OX14 4RN.

Benn, D. I., Wiseman, S., and Hands, K. A. (2001). Growth and drainage of supraglacial lakes on debrismantled Ngozumpa Glacier, Khumbu Himal, Nepal. *Journal of Glaciology*, 47(159):626–638.

Benning, L. G., Anesio, A. M., Lutz, S., and Tranter, M. (2014). Biological impact on greenland's albedo. *Nature Geoscience*, 7(10).

Benoit, L., Aurélie, G., Raphaël, V., Inigo, I., Mathieu, G., Benjamin, L., Gunther, P., Dominik, G., Frederic, H., and Gregoire, M. (2018). A high-frequency and high-resolution image time series of the gornergletscher - swiss alps - derived from repeated uav surveys.

Bøggild, C. E., Oerter, H., and Tukiainen, T. (1996). Increased ablation of wisconsin ice in eastern north greenland: observations and modelling. *Annals of Glaciology*, 23:144–148.

Blatter, H. and Haeberli, W. (1984). Modelling temperature distribution in alpine glaciers. *Annals of Glaciology*, 5:18–22.

Blatter, H. and Hutter, K. (1991). Polythermal conditions in Arctic glaciers. *Journal of Glaciology*, 37(126):261–269.

Bocchiola, D., Senese, A., Mihalcea, C., Mosconi, B., C, D., Smiraglia, C., and Diolaiuti, G. (2015). An ablation model for debris-covered ice: the case study of venerocolo glacier (italian alps). *Geografia Fisica e Dinamicca Quaternaria*, 38:113–128.

Bøggild, C. E., Brandt, R. E., Brown, K. J., and Warren, S. G. (2010). The ablation zone in northeast Greenland: ice types, albedos and impurities. *Journal of Glaciology*, 56(195):101–113.

Bohren, C. F. (1986). Applicability of effective-medium theories to problems of scattering and absorption by nonhomogeneous atmospheric particles. *Journal of the Atmospheric Sciences*, 43(5):468–475.

Boon, S. and Sharp, M. (2003). The role of hydrologically-driven ice fracture in drainage system evolution on an arctic glacier. *Geophysical Research Letters*, 30(18):1916.

Box, J. E., Fettweis, X., Stroeve, J. C., Tedesco, M., Hall, D. K., and Steffen, K. (2012). Greenland ice sheet albedo feedback: thermodynamics and atmospheric drivers.

Braithwaite, R. J. (1995). Positive degree-day factors for ablation on the Greenland ice sheet studied by energy-balance modeling. *Journal of Glaciology*, 41(137):153–160.

Braithwaite, R. J., Konzelmann, T., Marty, C., and Olesen, O. B. (1998). Reconnaissance study of glacier energy balance in north greenland, 1993–94. *Journal of Glaciology*, 44(147):239–247.

Braithwaite, R. J. and Olesen, O. B. (1990). A simple energy-balance model to calculate ice ablation at the margin of the greenland ice sheet. *Journal of Glaciology*, 36(123):222–228.

Brock, B., Willis, I., Sharp, M., and Arnold, N. (2000). Modelling seasonal and spatial variations in the surface energy balance of haut glacier d'arolla, switzerland. *Annals Of Glaciology, Vol 31, 2000*, 31:53–62.

Brock, B. W. (2004). An analysis of short-term albedo variations at haut glacier d'arolla, switzerland. 86(1):53–65.

Brun, F., Dumont, M., Wagnon, P., Berthier, E., Azam, M. F., Shea, J. M., Sirguey, P., Rabatel, A., and Ramanathan, A. (2015). Seasonal changes in surface albedo of himalayan glaciers from modis data and links with the annual mass balance. *The Cryosphere*, 9(1):341–355.

Casey, K. A., Polashenski, C. M., Chen, J., and Tedesco, M. (2017). Impact of MODIS sensor calibration updates on Greenland Ice Sheet surface reflectance and albedo trends. *The Cryosphere*.

Catania, G. A., Neumann, T. A., and Price, S. F. (2008). Characterizing englacial drainage in the ablation zone of the Greenland ice sheet. *Journal of Glaciology*, 54(187):567–578.

Cathles, L. M., Abbot, D. S., Bassis, J. N., and Macayeal, D. R. (2011). Modeling surface-roughness/solar-ablation feedback: application to small-scale surface channels and crevasses of the greenland ice sheet. *Annals of Glaciology*, 52(59):99–108.

Chandler, D. M., Alcock, J. D., Wadham, J. L., Mackie, S. L., and Telling, J. (2015). Seasonal changes of ice surface characteristics and productivity in the ablation zone of the greenland ice sheet. *The Cryosphere*, 9(2):487–504.

Chiarle, M., Iannotti, S., Mortara, G., and Deline, P. (2007). Recent debris flow occurrences associated with glaciers in the alps. 56(1-2):123–136.

Choi, M., Hamins, A., Mulholland, G., and Kashiwagi, T. (1994). Simultaneous optical measurement of soot volume fraction and temperature in premixed flames. *Combustion and Flame*, 99(1).

Chylek, P., Ramaswamy, V., and Srivastava, V. (1983). Albedo of soot-contaminated snow. *Journal of Geophysical Research: Oceans*, 88(C15):10837–10843.

Cierniewski, J., Karnieli, A., Kuśnierek, K., Goldberg, A., and Herrmann, I. (2012). Approximating the average daily surface albedo with respect to soil roughness and latitude. *International Journal of Remote Sensing*, 34(9):1–9.

Claverie, M., Vermote, E. F., Franch, B., and Masek, J. G. (2015). Evaluation of the landsat-5 tm and landsat-7 etm + surface reflectance products. *Remote Sensing of Environment*, 169:390–403.

Cogley, J. G. (2009a). Geodetic and direct mass-balance measurements: comparison and joint analysis. *Annals of Glaciology*, 50(50):96–100.

Cogley, J. G. (2009b). A more complete version of the world glacier inventory. *Annals of Glaciology*, 50(53):32–38.

Cogley, J. G., Hock, R., Rasmussen, L. A., Arendt, A. A., Bauder, A., Braithwaite, R. J., Jansson, P., Kaser, G., Möller, M., Nicholson, L., and Zemp, M. (2011). *Glossary of glacier mass balance and related terms*.

Cook, J. M., Edwards, A., Bulling, M., Mur, L. A. J., Cook, S., Gokul, J. K., Cameron, K. A., Sweet, M., and Irvine-Fynn, T. D. L. (2016). Metabolome-mediated biocryomorphic evolution promotes carbon fixation in greenlandic cryoconite holes. 18(12):4674–4686.

Dahl-Jensen, D., Gundestrup, N. S., Keller, K., Johnsen, S. J., Gogineni, S. P., Allen, C. T., Chuah, T. S., Miller, H., Kipfstuhl, S., and Waddington, E. D. (1997). A search in north Greenland for a new ice-core drill site. *Journal of Glaciology*, 43(144):300–306.

Das, S. B., Joughin, I., Behn, M. D., Howat, I. M., King, M. A., Lizarralde, D., and Bhatia, M. P. (2008). Fracture propagation to the base of the Greenland Ice Sheet during supraglacial lake drainage. *Science*, 320.

Davaze, L., Rabatel, A., Arnaud, Y., Sirguey, P., Six, D., Letreguilly, A., and Dumont, M. (2018). Monitoring glacier albedo as a proxy to derive summer and annual surface mass balances from optical remote-sensing data. *The Cryosphere*, 12(1):271–286.

Deconto, R. M. and Pollard, D. (2016). Contribution of antarctica to past and future sea-level rise. *Nature*, 531(7596).

Dieser, M., Greenwood, M., and Foreman, C. M. (2010). Carotenoid pigmentation in antarctic heterotrophic bacteria as a strategy to withstand environmental stresses. *Arctic, Antarctic, and Alpine Research*, 42(4):396–405.

Dumont, M., Brun, E., Picard, G., Michou, M., Libois, Q., Petit, J.-R., Geyer, M., Morin, S., and Josse, B. (2014). Contribution of light-absorbing impurities in snow to greenland's darkening since 2009. *Nature Geoscience*, 7(7).

Dyurgerov, M. and Meier, M. (2005). Glaciers and the changing earth system: A 2004 snapshot. 58.

Eisen, O., Bauder, A., Lüthi, M., Riesen, P., and Funk, M. (2009). Deducing the thermal structure in the tongue of Gornergletscher, Switzerland, from radar surverys and borehole measurements. *Annals of Glaciology*, 50(51):63–70.

Etzelmüller, B., Vatne, G., Ødegård, R. S., and Sollid, J. L. (1993). Dynamics of two subpolar valley glaciers—erikbreen and hannabreen, liefdefjorden, northern spitsbergen. *Geografiska Annaler: Series A, Physical Geography*, 75(1-2):41–54.

Evans, S. G. and Clague, J. J. (1994). Recent Climatic Change and Catastrophic Geomorphic Processes in Mountain Environments. *Geomorphology*, 10:107–128.

Faillettaz, J., Sornette, D., and Funk, M. (2011). Climate warming and stability of cold hanging glaciers: Lessons from the gigantic 1895 Altels break-off.

Falconer, R. E. and Hogan, A. W. (1971). Capture of aerosol particles by ice crystals. *Proc. Eastern Snow Conference*, pages 1–8.

Fisher, J. E. (1953). The cold ice tunnel on the Silbersattel, Monte Rosa. *Journal of Glaciology*, 2(13):195–196.

Fisher, J. E. (1954). The cold ice tunnel on the Silbersattel, Monte Rosa (progress 1953). *Journal of Glaciology*, 2(15):341.

Fitzpatrick, A. A. W., Hubbard, A. L., Box, J. E., Quincey, D. J., van As, D., Mikkelsen, A. P. B., Doyle, S. H., Dow, C. F., Hasholt, B., and Jones, G. A. (2014). A decade (2002-2012) of supraglacial lake volume estimates across russell glacier, west greenland. *The Cryosphere*, 8(1):107–121.

Fountain, A. G., Nylen, T. H., Macclune, K. L., and Dana, G. L. (2006). Glacier mass balances (1993–2001), taylor valley, mcmurdo dry valleys, antarctica. *Journal of Glaciology*, 52(178):451–462.

Fountain, A. G., Tranter, M., Nylen, T. H., Lewis, K. J., and Mueller, D. R. (2004). Evolution of cryoconite holes and their contribution to meltwater runoff from glaciers in the mcmurdo dry valleys, antarctica. *Journal of Glaciology*, 50(168):35–45.

Frey, H., Haeberli, W., Linsbauer, A., Huggel, C., and Paul, F. (2010). A multi-level strategy for anticipating future glacier lake formation and associated hazard potentials. 10(2):339–352.

Fuentes, I., Padarian, J., Van Ogtrop, F., and Willem Vervoort, R. (2019). Spatiotemporal evaluation of inundated areas using modis imagery at a catchment scale. *Journal of Hydrology*, 573:952–963.

Fugazza, D., Senese, A., Azzoni, R., Maugeri, M., and Diolaiuti, G. (2016). Distribution of surface albedo at the forni glacier (stelvio national park, central italian alps). *Cold Reg. Sci. Technol.*, 125:128–137.

Fugazza, D., Senese, A., Azzoni, R. S., Maugeri, M., Maragno, D., and Diolaiuti, G. A. (2019). New evidence of glacier darkening in the ortles-cevedale group from landsat observations. *Global and Planetary Change*, 178:35–45.

Gabbi, J., Carenzo, M., Pellicciotti, F., Bauder, A., and Funk, M. (2014). A comparison of empirical and physically-based glacier surface melt models for long-term simulations of glacier response. *Journal of Glaciology*, 60(224):1140–1154.

Gajda, R. (1958). Cryoconite phenomena on the greenland ice cap in the thule area. *The Canadian Geographer/Le Géographe Canadien*, 12.

Gardner, A., Moholdt, G., Cogley, J., Wouters, B., Arendt, A., Wahr, J., Berthier, E., Hock, R., Pfeffer, T., Kaser, G., Ligtenberg, S., Bolch, T., Sharp, M., Hagen, J., van den Broeke, M., and Paul, F. (2013). A reconciled estimate of glacier contributions to sea level rise: 2003 to 2009. *Science*, 340(6134):852–857.

Gardner, A. S. and Sharp, M. J. (2010). A review of snow and ice albedo and the development of a new physically based broadband albedo parameterization. *Journal of Geophysical Research: Earth Surface*, 115(F1):n/a–n/a.

Gratton, D. J., Howarth, P. J., and Marceau, D. J. (1993). Using landsat-5 thematic mapper and digital elevation data to determine the net radiation field of a mountain glacier. 43(3):315–331.

Grenfell, T. C., Light, B., and Sturm, M. (2002). Spatial distribution and radiative effects of soot in the snow and sea ice during the sheba experiment. *Journal of Geophysical Research: Oceans*, 107(C10):SHE 7–1–SHE 7–7.

Greuell, W. (2000). Melt-water accumulation on the surface of the greenland ice sheet: Effect on albedo and mass balance. *Geografiska Annaler. Series A, Physical Geography*, 82(4):489–498.

Greuell, W. and de Ruyter de Wildt, M. (1999). Anisotropic reflection by melting glacier ice: Measurements and parametrizations in landsat tm bands 2 and 4. *Remote Sensing of Environment*, 70(3):265–277.

Greuell, W. and Knap, W. (2000). Remote sensing of the albedo and detection of the slush line on the greenland ice sheet. *Journal of Geophysical Research: Atmospheres*, 105(D12):15567–15576.

Greuell, W., Knap, W. H., and Smeets, P. C. (1997). Elevational changes in meteorological variables along a midlatitude glacier during summer. *Journal of Geophysical Research: Atmospheres*, 102(D22):25941–25954.

Greuell, W., Reijmer, C. H., and Oerlemans, J. (2002). Narrowband-to-broadband albedo conversion for glacier ice and snow based on aircraft and near-surface measurements. *Remote Sensing of Environment*, 82(1):48–63.

Greve, R. (1997). Application of a polythermal three-dimensional ice sheet model to the Greenland ice sheet: response to a steady-state and transient climate scenarios. *Journal of Climate*, 10(5):901–918.

Gusmeroli, A., Jansson, P., Pettersson, R., and Murray, T. (2012). Twenty years of cold surface layer thinning at Storglaciaren, sub-Arctic Sweden, 1989–2009. *Journal of Glaciology*, 58(207):3–10.

Haeberli, W. (1976). Eistemperaturen in den Alpen. *Zeitschrift für Gletscherkunde und Glazialgeologie*, 11(2):203–220.

Haeberli, W. and Funk, M. (1991). Borehole temperatures at the Colle Gnifetti core drilling site (Monte Rosa, Swiss Alps). *Journal of Glaciology*, 37(125):37–46.

Haeberli, W., Iken, A., and Siegenthaler, H. (1979). Glaziologische Aspekte beim Bau der Fernmelde-Mehrzweckanlage der PTT auf dem Chli Titlis. *Hydrol. Glaziol. Mitt.*, 41:59–75.

Haefeli, R. and Brentani, F. (1955). Observations in a cold ice cap. *Journal of Glaciology*, 2(18):571–581.

Hall, D. K., Bindschadler, R. A., Foster, J. L., Chang, A. T. C., and Siddalingaiah, H. (1990). Comparison of in situ and satellite-derived reflectances of forbindels glacier, greenland. *International Journal of Remote Sensing*, 11(3):493–504.

Hall, D. K., Chang, A. T., and Siddalingaiah, H. (1988). Reflectances of glaciers as calculated using landsat-5 thematic mapper data. *Remote Sensing of Environment*, 25(3):311,IN1,313–312,IN1,321.

Hammer, C. (1977). Dating of greenland ice cores by microparticle concentration analyses. pages 297–301.

Hanson, A. M. (1965). Studies of the mass budget of arctic pack-ice floes. *Journal of Glaciology*, 5(41):701–709.

Hauer, M. E. (2017). Migration induced by sea-level rise could reshape the us population landscape. *Nature Climate Change*, 7(5).

He, T., Liang, S., Yu, Y., Wang, D., Gao, F., and Liu, Q. (2013). Greenland surface albedo changes in july 1981–2012 from satellite observations. *Environmental Research Letters*, 8(4).

Hock, R. (2003). Temperature index melt modelling in mountain areas. *Journal of Hydrology*, 282:104–115.

Hock, R. (2005). Glacier melt: a review of processes and their modelling. *Progress in Physical Geography*, 29(3):362–391.

Hodgkins, R. (1997). Glacier hydrology in Svalbard, Norwegian high arctic. *Quaternary Science Reviews*, 16:957–973.

Hodson, A., Anesio, A. M., Tranter, M., Fountain, A., Osborn, M., Priscu, J., Laybourn Parry, J., and Sattler, B. (2008). Glacial ecosystems. *Ecological Monographs*, 78(1):41–67.

Huggel, C., Clague, J. J., and Korup, O. (2012). Is climate change responsible for changing landslide activity in high mountains? 37(1):77–91.

Huss, M., Bookhagen, B., Huggel, C., Jacobsen, D., Bradley, R., Clague, J., Vuille, M., Buytaert, W., Cayan, D., Greenwood, G., Mark, B., Milner, A., Weingartner, R., and Winder, M. (2017). Toward mountains without permanent snow and ice. *Earth's Future*, 5(5):418–435. 2016EF000514.

Huss, M., Funk, M., and Ohmura, A. (2009). Strong alpine glacier melt in the 1940s due to enhanced solar radiation. *Geophysical Research Letters*, 36(23):n/a–n/a.

Huss, M. and Hock, R. (2018). Global-scale hydrological response to future glacier mass loss. *Nature Climate Change*.

Huss, M., Hock, R., Bauder, A., and Funk, M. (2012). Conventional versus reference-surface mass balance. *Journal of Glaciology*, 38(208):278–286.

Hutter, K. (1983). *Theoretical glaciology; material science of ice and the mechanics of glaciers and ice sheets*. D. Reidel Publishing Company/Tokyo, Terra Scientific Publishing Company.

IPCC (2013). Climate Change 2013: The Physical Science Basis. Contribution of Working Group I to the Fifth Assessment Report of the Intergovernmental Panel on Climate Change. Technical report, WMO/UNEP. Authors: T.F. Stocker, D. Qin, G.-K. Plattner, M. Tignor, S.K. Allen, J. Boschung, A. Nauels, Y. Xia, V. Bex and P.M. Midgley.

Jouvet, G., Huss, M., Funk, M., and Blatter, H. (2011). Modelling the retreat of Grosser Aletschgletscher, Switzerland, in a changing climate. *Journal of Glaciology*, 57(206):1033–1044.

Kaser, G., Cogley, J. G., Dyurgerov, M. B., Meier, M. F., and Ohmura, A. (2006). Mass balance of glaciers and ice caps: Consensus estimates for 1961–2004. *Geophysical Research Letters*, 33(19):n/a–n/a.

Kayastha, R. B., Ohata, T., and Ageta, Y. (1999). Application of a mass-balance model to a himalayan glacier. *Journal of Glaciology*, 45(151):559–567.

Kääb, A., Chiarle, M., Raup, B., and Schneider, C. (2007). Climate change impacts on mountain glaciers and permafrost. *Global and Planetary Change*, 56(1–2):56–58.

Klok, E. J., Greuell, W., and Oerlemans, J. (2003). Temporal and spatial variation of the surface albedo of morteratschgletscher, switzerland, as derived from 12 landsat images. *Journal of Glaciology*, 49(167):491–502.

Knap, W. and Oerlemans, J. (1996). The surface albedo of the greenland ice sheet: Satellite-derived and in situ measurements in the sondre stromfjord area during the 1991 melt season. *Journal Of Glaciology*, 42(141):364–374.

Knap, W., Reijmer, C., and Oerlemans, J. (1999). Narrowband to broadband conversion of Landsat TM glacier albedos. *Int. J. Remote Sensing*, 20(10):2091–2110.

Koelemeijer, R., Oerlemans, J., and Tjemkes, S. (1993). Surface reflectance of hintereisferner, austria, from landsat 5 tm imagery. *Annals of Glaciology*, 17:17–22.

Kohno, S. and Maeno, N. (1979). Migration of solid particles in melting snow. *Low Temperature Sciences*, 38:81–92.

Kohshima, S., SEKO, K., and Yoshimura, Y. (1993). Biotic acceleration of glacier melting in yala glacier 9 langtang region, nepal himalaya. *IAHS Publ*, 208.

Körner, H. J. (1977). Flow mechanisms and resistences in the debris streams of rock falls. *Bull. Internat. Ass. Eng. Geol.*, 16:101–104.

Krimmel, R. M. and Meier, M. F. (1975). Glacier applications of erts images. *Journal of Glaciology*, 15(73):391–402.

Kumai, M. (1976). Identification of nuclei and concentrations of chemical species in snow crystals sampled at the south pole. *Journal of Atmospheric Sciences*, 33:833–841.

Kumai, M. (1977). Electron microscope analysis of aerosols in snow and deep ice cores from greenland. *Isotopes and Impurities in Snow and Ice*, 118:341–350.

LaChapelle, E. R. (1969). *Field guide to snow crystals*. University of Washington Press, Seattle.

Lang, H. (1986). Forecasting meltwater runoff from snow–covered areas and from glacier basins. In Kraijenhoff, D. A. and Moll, J. R., editors, *River flow modelling and forecasting*, pages 99–127.

Langway, C., Klouda, A., Herron, M., and Cragin, J. (1977). Seasonal variations in chemical constituents in annual layers of Greenland deep ice deposits. *Isotopes and Impurities in Snow and Ice*, 38:302–306.

Legleiter, C. J., Tedesco, M., Smith, L. C., and Overstreet, B. T. (2013). Mapping the bathymetry of supraglacial lakes and streams on the greenland ice sheet using field measurements and high resolution satellite images. *The Cryosphere Discussions*, 7(5):4741–4773.

Liang, S. (2000). Narrowband to broadband conversions of land surface albedo i Algorithms. *EOS*, 76:213–238.

Lindberg, J. (1976). The composition and optical absorption coefficient of atmospheric particulate matter. *Opt. Quant. Electron.*, 7:131–139.

Lliboutry, L. (1996). Temperate ice permeability, stability of water veins and percolation of internal meltwater. *Journal of Glaciology*, 42(141):201–211.

Lliboutry, L., Briat, M., Creseveur, M., and Pourchet, M. (1976). 15m deep temperatures in the glaciers of mont blanc (french alps). *Journal of Glaciology*, 16(74):197–203.

Lüthje, M., Pedersen, L., Reeh, N., and Greuell, W. (2006). Modelling the evolution of supraglacial lakes on the west greenland ice-sheet margin. *Journal of Glaciology*, 52(179):608–618.

Lüthi, M. P. and Funk, M. (2001). Modelling heat flow in a cold, high altitude glacier: interpretation of measurements from Colle Gnifetti, Swiss Alps. *Journal of Glaciology*, 47(157):314–324.

Lutz, S., Anesio, A. M., Jorge Villar, S. E., and Benning, L. G. (2014). Variations of algal communities cause darkening of a greenland glacier. *FEMS Microbiology Ecology*, 89(2):402–414.

Macdonell, S. and Fitzsimons, S. (2008). The formation and hydrological significance of cryoconite holes. 32(6):595–610.

Magono, C., Endoh, T., Ueno, F., Kubota, S., and Itasaka, M. (1979). Direct observations of aerosols attached to falling snow crystals. *Tellus*, 31(2):102–114.

McGranahan, G., Balk, D., and Anderson, B. (2007). The rising tide: assessing the risks of climate change and human settlements in low elevation coastal zones. *Environment and Urbanization*, 19(1):17–37.

Meier, M., Rasmussen, L., Krimmel, R., Olsen, R., and Frank, D. (1985). Photogrammetric determination of surface altitude, terminus position, and ice velocity of Columbia Glacier, Alaska. *U.S. Geological Survey Professional Paper*.

Meier, M. F. (1984). Contribution of small glaciers to global sea level. *Science*, 226(4681):1418–21.

Mullen, P. and Warren, S. (1988). Theory of the optical properties of lake ice. *Journal of Geophysical Research*, 93(7):8403–8414.

Naegeli, K., Damm, A., Huss, M., Schaepman, M., and Hoelzle, M. (2015). Imaging spectroscopy to assess the composition of ice surface materials and their impact on glacier mass balance. *Remote Sensing and Environment*, 168:388–402.

Naegeli, K., Damm, A., Huss, M., Wulf, H., Schaepman, M., and Hoelzle, M. (2017). Cross-Comparison of Albedo Products for Glacier Surfaces Derived from Airborne and Satellite (Sentinel-2 and Landsat 8) Optical Data. *Remote Sensing*, 9(2).

Naegeli, K., Huss, M., and Hoelzle, M. (2019). Change detection of bare-ice albedo in the swiss alps. *The Cryosphere*, 13(1):397–412.

Nicholls, R. J., Marinova, N., Lowe, J. A., Brown, S., Vellinga, P., De Gusmo, D., Hinkel, J., and Tol, R. S. J. (2011). Sea-level rise and its possible impacts given a beyond 4c world in the twenty-first century. *Philosophical Transactions of the Royal Society A*, 369(1934):161–181.

Nordenskiöld, A. E. (1883). Nordenskiold on the Inland Ice of Greenland. *Science*, 2:732–738.

Nye, J. F. and Frank, F. C. (1973). Hydrology of the intergranular veins in a temperate glacier. In *Symposium on the Hydrology of Glaciers*, pages 157–161. Proceedings of the symposium held at Cambridge, England, 7–13 September 1969, IAHS Publication No. 95.

Oerlemans, J. (1993a). A meteorological experiment in the melting zone of the Greenland ice sheet. 74(3).

Oerlemans, J. (1993b). A model for the surface balance of ice masses: part i. alpine glaciers. *Zeitschrift fuÈr Gletscherkunde und Glazialgeologie*, 27:63–83.

Oerlemans, J., Anderson, B., Hubbard, A., Huybrechts, P., Johannesson, T., Knap, W., Schmeits, M., Stroeven, A., van de Wal, R., Wallinga, J., and Zuo, Z. (1998). Modelling the response of glaciers to climate warming. *Climate Dynamics*, 14:267–274.

Oerlemans, J., Giesen, R., and Van Den Broeke, M. (2009). Retreating alpine glaciers: increased melt rates due to accumulation of dust (vadret da morteratsch, switzerland). *Journal of Glaciology*, 55(192):729–736.

Oeschger, H., Schotterer, U., amd W. Haeberli, B. S., and Röthlisberger, H. (1978). First results from alpine core drilling projects. *Z. Gletscherkd. Glazialgeol.*, 13:193–208.

Paterson, W. S. B. (1994). *The Physics of Glaciers*. Pergamon, New York, third edition.

Paul, F., Machguth, H., and Kääb, A. (2005). On the impact of glacier albedo under conditions of extreme glacier melt: The summer of 2003 in the alps. *EARSeL eProc*, 4:13–149.

Pellikka, P. and Rees, G. (2010). *Remote sensing of glaciers : techniques for topographic, spatial and thematic mapping of glaciers*. CRC Press/Balkema, Leiden.

Pfeffer, W. T. and Bretherton, C. S. (1987). The effect of crevasses on the solar heating of a glacier surface. In *The Physical Basis of Ice Sheet Modelling*, volume 170, pages 191–205. International Association of Hydrological Sciences.

Phillips, T., Rajaram, H., and Steffen, K. (2010). Cryo-hydrologic warming: A potential mechanism for the thermal response of ice sheets. *Geophysical Research Letters*, 37(L20503).

Pope, E., Willis, I., Pope, A., Miles, E., Arnold, N., and Rees, W. (2016). Contrasting snow and ice albedos derived from modis, landsat etm+ and airborne data from langjökull, iceland. *Remote Sens. Environ.*, 175:183–195.

Radić, V. and Hock, R. (2014). Glaciers in the earth's hydrological cycle: Assessments of glacier mass and runoff changes on global and regional scales. *Surveys in Geophysics*, 35(3):813–837.

Remias, D., Schwaiger, S., Aigner, S., Leya, T., Stuppner, H., and Lütz, C. (2012). Characterization of an uv- and vis-absorbing, purpurogallin-derived secondary pigment new to algae and highly abundant in m esotaenium berggrenii (z ygnematophyceae , chlorophyta), an extremophyte living on glaciers. *FEMS Microbiology Ecology*, 79(3):638–648.

Renaud, A. (1936). Les entonnoirs du glacier de Gorner. *Denkschriften der Schweizerischen Naturforschenden Gesellschaft*, 71(1):pp. 27.

Rignot, E., Box, J. E., Burgess, E., and Hanna, E. (2008). Mass balance of the Greenland ice sheet from 1958 to 2007. *Geophysical Research Letters*, 35(L20502).

Rippin, D. M., Pomfret, A., and King, N. (2015). High resolution mapping of supra-glacial drainage pathways reveals link between micro-channel drainage density, surface roughness and surface reflectance. 40(10):1279–1290.

Röthlisberger, H. and Lang, H. (1987). Glacial Hydrology. In *A.M. Gurnell and M.J. Clark (Ed.), Glacio-Fluvial Sediment Transfer - An Alpine Perspective*, pages 207–284. John Wiley and Sons, Chichester, New York, Toronto, Singapore.

Ryan, J., Hubbard, A., Box, J., Todd, J., Christoffersen, P., Carr, J., Holt, T., and Snooke, N. (2015). UAV photogrammetry and structure from motion to assess calving dynamics at Store Glacier, a large outlet draining the Greenland ice sheet. *The Cryosphere*, 9:1–11.

Ryan, J., Hubbard, A., Stibal, M., Irvine-Fynn, T., Cook, J., Smith, L., Cameron, K., and Box, J. (2018). Dark zone of the greenland ice sheet controlled by distributed biologically-active impurities. *Nat Commun*, 9(1):1065–1065.

Ryser, C., Lüthi, M., Blindow, N., Suckro, S., Funk, M., and Bauder, A. (2013). Cold ice in the ablation zone: its relation to glacier hydrology and ice water content. *Journal of Geophysical Research*, 118(F02006):693–705.

Schaepman-Strub, G., Schaepman, M., Painter, T., Dangel, S., and Martonchik, J. (2006). Reflectance quantities in optical remote sensing—definitions and case studies. *Remote Sensing of Environment*, 103(1):27–42.

Shimada, R., Takeuchi, N., and Aoki, T. (2016). Inter-annual and geographical variations in the extent of bare ice and dark ice on the greenland ice sheet derived from modis satellite images. *Frontiers in Earth Science*, 4.

Sicart, J. E., Hock, R., and Six, D. (2008). Glacier melt, air temperature, and energy balance in different climates: The bolivian tropics, the french alps, and northern sweden. *Journal of Geophysical Research: Atmospheres*, 113(D24):n/a–n/a.

Sirguey, P., Mathieu, R., Arnaud, Y., Khan, M., and Chanussot, J. (2008). Improving modis spatial resolution for snow mapping using wavelet fusion and arsis concept. *IEEE Geoscience and Remote Sensing Letters*, 5(1):78–82.

Sold, L., Huss, M., Machguth, H., Joerg, P. C., Leysinger Vieli, G., Linsbauer, A., Salzmann, N., Zemp, M., and Hoelzle, M. (2016). Mass balance re-analysis of Findelengletscher, Switzerland; benefits of extensive snow accumulation measurements. *Frontiers in Earth Science*, 4(18).

Sorg, A., Bolch, T., Stoffel, M., Solomina, O., and Beniston, M. (2012). Climate change impacts on glaciers and runoff in tien shan (central asia). *Nature Climate Change*, 2(10).

Soruco, A., Vincent, C., Rabatel, A., Francou, B., Thibert, E., Sicart, J. E., and Condom, T. (2015). Contribution of glacier runoff to water resources of la paz city, bolivia (16° s) (book review). *Annals of Glaciology*, 56(70):147–154.

Stibal, M., Box, J. E., Cameron, K. A., Langen, P. L., Yallop, M. L., Mottram, R. H., Khan, A. L., Molotch, N. P., Chrismas, N. A. M., Calì Quaglia, F., Remias, D., Smeets, C. J. P. P., Broeke, M. R., Ryan, J. C., Hubbard, A., Tranter, M., As, D., and Ahlstrøm, A. P. (2017). Algae drive enhanced darkening of bare ice on the greenland ice sheet. 44(22):11,463–11,471.

Stoffel, M. and Huggel, C. (2012). Effects of climate change on mass movements in mountain environments. *Progress in Physical Geography*, 36(3):421–439.

Strauss, B. H., Kulp, S., and Levermann, A. (2015). Carbon choices determine us cities committed to futures below sea level. *Proceedings of the National Academy of Sciences*, 112(44).

Stroeve, J., Box, J. E., Wang, Z., Schaaf, C., and Barrett, A. (2013). Re-evaluation of modis mcd43 greenland albedo accuracy and trends. *Remote Sensing of Environment*, 138:199–214.

Sugiyama, S., Bauder, A., Riesen, P., and Funk, M. (2010). Surface ice motion deviating toward the margins during speed-up events at Gornergletscher, Switzerland. *Journal of Geophysical Research*, 115(F03010).

Suter, S., Laternser, M., Haeberli, W., Frauenfelder, R., and Hoelzle, M. (2001). First results from alpine core drilling projects. *Journal of Glaciology*, 47(156):85–96.

swisstopo (2019). Karten der Schweiz - Schweizerische Eidgenossenschaft [online]. Available from: https://map.geo.admin.ch [Accessed 30.08.2019]. .

Takeuchi, N. (2002a). Optical characteristics of cryoconite (surface dust) on glaciers: the relationship between light absorbency and the property of organic matter contained in the cryoconite. *Annals of Glaciology*, 34(1):409–414.

Takeuchi, N. (2002b). Surface albedo and characteristics of cryoconite (biogenic surface dust) on an Alaska glacier, Gulkana glacier in the Alaska Range. *Bull. Glaciol. Res.*, 19:63–70.

Takeuchi, N., Kohshima, S., and Seko, K. (2001). Structure, formation, and darkening process of albedo-reducing material (cryoconite) on a himalayan glacier: A granular algal mat growing on the glacier. *Arctic, Antarctic, and Alpine Research*, 33(2):115–122.

Tedesco, M., Doherty, S., Fettweis, X., Alexander, P., Jeyaratnam, J., and Stroeve, J. (2016). The darkening of the greenland ice sheet: trends, drivers, and projections (1981-2100). *The Cryosphere*, 10(2):477–496.

Tedesco, M., Fettweis, X., van den Broeke, M. R., van de Wal, R. S. W., Smeets, C. J. P. P., van de Berg, W. J., Box, J. E., and Serreze, M. C. (2011). The role of albedo and accumulation in the 2010 melting record in greenland.

Tedstone, A. J., Bamber, J. L., Cook, J. M., Williamson, C. J., Fettweis, X., Hodson, A. J., and Tranter, M. (2017). Dark ice dynamics of the south-west greenland ice sheet. *The Cryosphere*, 11(6):2491–2506.

Toon, O., Pollack, J., and B, K. (1976). The optical constants of several atmospheric aerosol species: Ammonium sulfate, aluminium oxide and sodium chloride. *Annals of Glaciology*, 81:5733–5748.

USGS (2016). Landsat—earth observation satellites (ver. 1.1, august 2016). *U.S. Geological Survey Fact Sheet*, 2015(3081):1–4.

USGS (2019a). Landsat 4-7 surface reflectance (ledaps) product guide. *LANDSAT PRODUCT GUIDE*, 2(2):1–32.

USGS (2019b). Landsat 8 surface reflectance code (lasrc) product guide. *LANDSAT PRODUCT GUIDE*, 2(2):1–33.

Vallot, J. (1913). Valeur et variation de la température profonde du glacier, au Mont Blanc. *Comptes Rendus Hebdomadaires des Séances de l'Académie des Sciences*, 156(20):1575–1578.

van den Broeke, M., Bamber, J., Ettema, J., Rignot, E., Schrama, E., van de Berg, W. J., van Meijgaard, E., Velicogna, I., and Wouters, B. (2009). Partitioning recent Greenland mass loss. *Science*, 326:984–986.

Van den Broeke, M., Bamber, J., Lenaerts, J., and Rignot, E. (2011). Ice Seets and Sea Level: Thinking Outside the Box. *Surv Geophys*, 32:495–505.

Vermote, E., Justice, C., Claverie, M., and Franch, B. (2016). Preliminary analysis of the performance of the landsat 8/oli land surface reflectance product. *Remote Sensing of Environment*, 185(C):46–56.

Vincent, C., Vallon, M., Pinglot, J., Funk, M., and Reynaud, L. (1997). Snow accumulation and ice flow at dome du gouter (4300m), mont blanc, french alps. *Journal Of Glaciology*, 43(145):513–521.

Warren, S. (1982). Optical properties of snow. *Reviews of Geophysics and Space Physics*, 20(1):67–89.

Warren, S. G. and Wiscombe, W. J. (1980). A model for the spectral albedo of snow. ii: Snow containing atmospheric aerosols. *Journal of the Atmospheric Sciences*, 37(12):2734–2745.

Werder, M., Hewitt, I., Schoof, C., and Flowers, G. (2013). Modeling channelized and distributed subglacial drainage in two dimensions. *Journal of Geophysical Research*, 118:2140–2158.

Werder, M. A., Loye, A., and Funk, M. (2009). Dye tracing a jökulhlaup: I. Subglacial water transit speed and water-storage mechanism. *Journal of Glaciology*, 55:889–898.

Westerling, A. L., Hidalgo, H. G., Cayan, D. R., and Swetnam, T. W. (2006). Warming and earlier spring increase western u.s. forest wildfire activity. *Science (New York, N.Y.)*, 313(5789).

WGMS (1989). *World glacier inventory : status 1988 : a contribution to the Global Environment Monitoring System (GEMS) and the International Hydrological Programme*. IAHS (ICSI) [etc.], Wallingford, Oxfordshire.

Wharton, R. A., Mckay, C. P., Simmons, G. M., and Parker, B. C. (1985). Cryoconite holes on glaciers. *Bioscience*, 35(8).

Wientjes, I. and Oerlemans, J. (2010). An explanation for the dark region in the western melt zone of the greenland ice sheet. *The Cryosphere*, 4:261–268.

Wientjes, I., Van de Wal, R., Reichart, G., Sluijs, A., and Oerlemans, J. (2011). Dust from the dark region in the western ablation zone of the Greenland ice sheet. *The Cryosphere*, 5:589–601.

Wientjes, I., van de Wal, R., Schwikowski, M., Zapf, A., Fahrni, S., and Wacker, L. (2012). Carbonaceous particles reveal that Late Holocene dust causes the dark region in the western ablation zone of the Greenland ice sheet. *Journal of Glaciology*, 58(210):787–794.

Winther, J.-G. (1993). Landsat tm derived and in situ summer reflectance of glaciers in svalbard. *Polar Research*, 12(1):37–55.

Wiscombe, W. J. and Warren, S. (1980). A model for the spectral albedo of snow. i: Pure snow. *Journal of the Atmospheric Sciences*, 37(12):2712–2733.

Worni, R., Stoffel, M., Huggel, C., Volz, C., Casteller, A., and Luckman, B. (2012). Analysis and dynamic modeling of a moraine failure and glacier lake outburst flood at ventisquero negro, patagonian andes (argentina). *Journal of Hydrology*, 444-445:134–145.

Yallop, M. L., Anesio, A. M., Perkins, R. G., Cook, J., Telling, J., Fagan, D., Macfarlane, J., Stibal, M., Barker, G., Bellas, C., Hodson, A., Tranter, M., Wadham, J., and Roberts, N. W. (2012). Photophysiology and albedo-changing potential of the ice algal community on the surface of the greenland ice sheet. *The ISME Journal*, 6(12).

Young, N. E., Anderson, R. S., Chignell, S. M., Vorster, A. G., Lawrence, R., and Evangelista, P. H. (2017). A survival guide to Landsat preprocessing. *Ecology*, 98(4):920–932.

Zhang, Y., Liu, S., and Ding, Y. (2006). Observed degree-day factors and their spatial variation on glaciers in western china. *Annals of Glaciology*, 43:301–306.

Zuo, Z. and Oerlemans, J. (1996). Modelling albedo and specific balance of the greenland ice sheet: calculations for the søndre strømfjord transect. *Journal of Glaciology*, 42(141):305–317.

Zwally, H. J., Abdalati, W., Herring, T., Larson, K., Saba, J., and Steffen, K. (2002). Surface melt-induced acceleration of Greenland ice-sheet flow. *Science*, 297(5579):218–222.

10 Appendix

10.1 Appendix 1: Degree-Day-Factors

10.1.1 Appendix 1.1: Degree-Day-Factors for the Wires

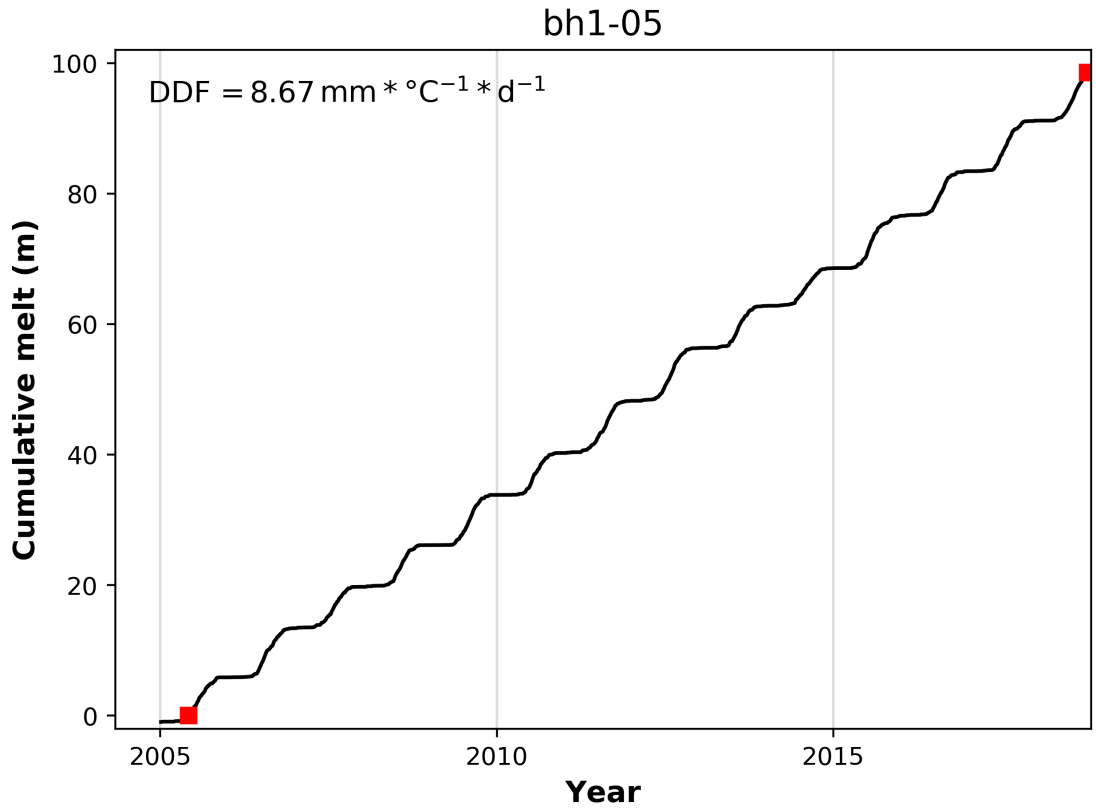

Fig. 25: Degree-Day-Factor 'bh1-05'.

Tab. 9: Ablation 'bh1-05'

Date	Ablation (m)
2005-06-04	0
2018-10-13	98.57

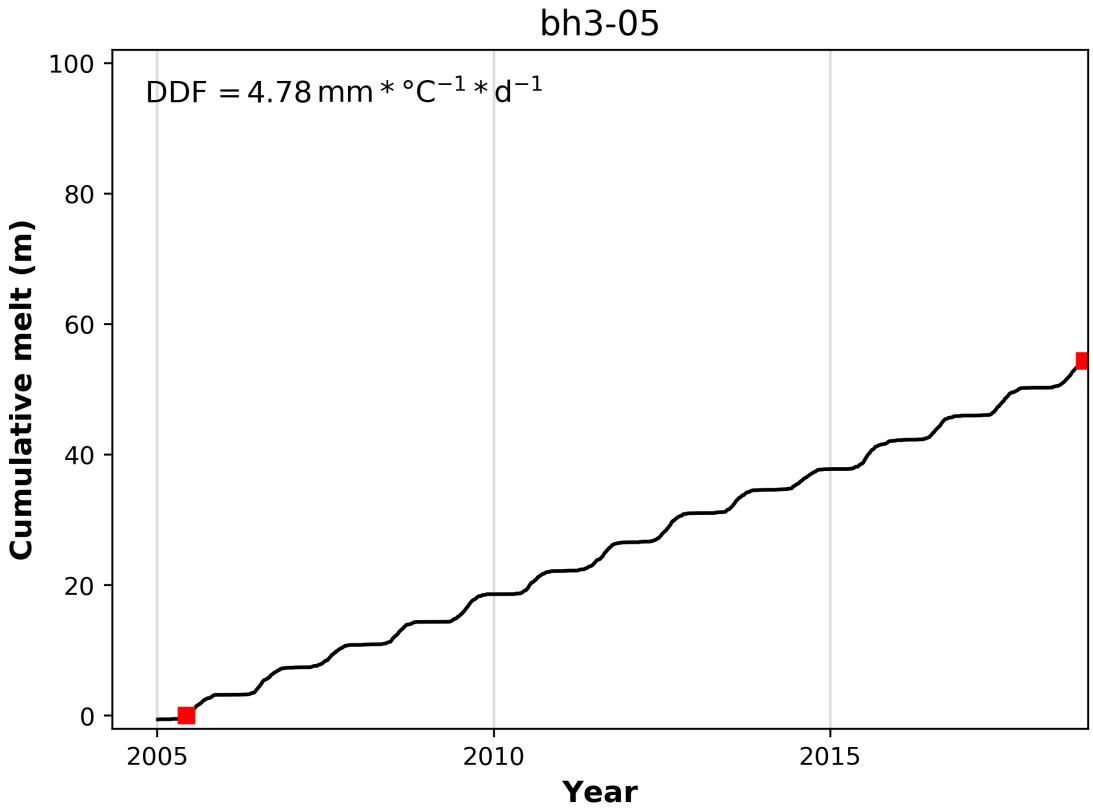

Fig. 26: Degree-Day-Factor 'bh3-05'.

Tab. 10: Ablation 'bh3-05'

Date	Ablation (m)
2005-06-08	0
2018-10-13	54.34

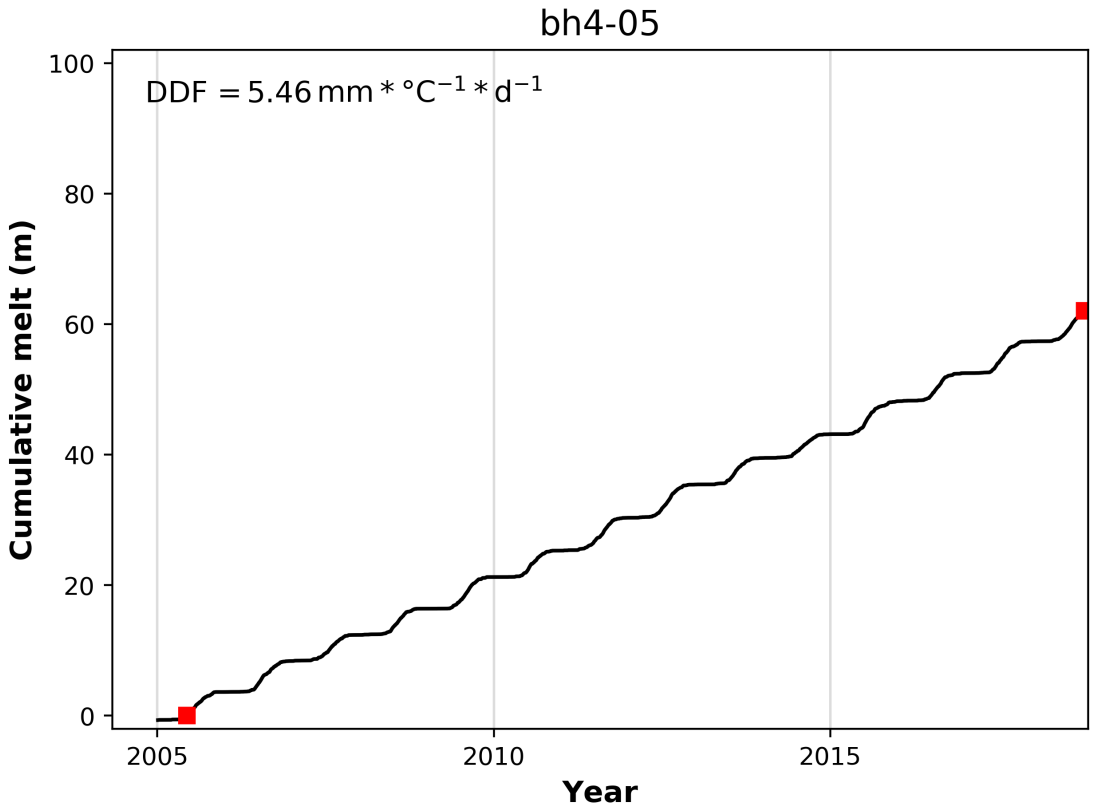

Fig. 27: Degree-Day-Factor 'bh4-05'.

Tab. 11: Ablation 'bh4-05'

Date	Ablation (m)
2005-06-11	0
2018-10-13	62.03

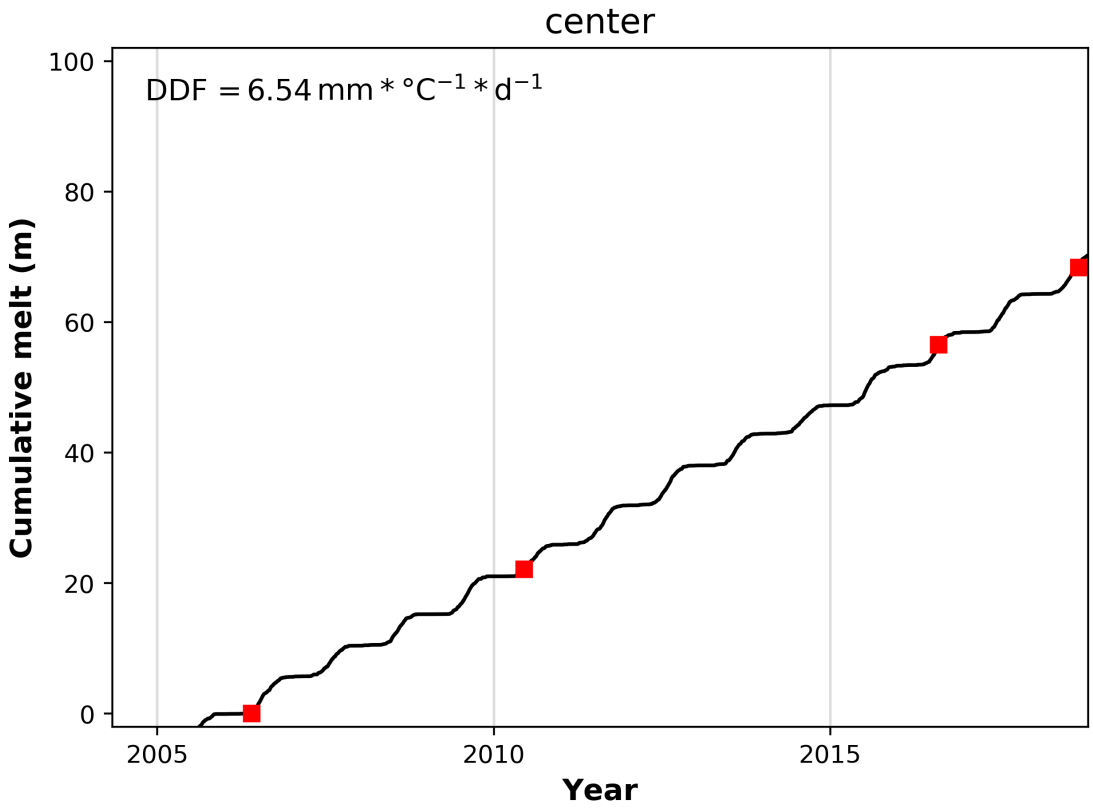

Fig. 28: Degree-Day-Factor 'center'.

Tab. 12: Ablation 'center'

Date	Ablation (m)
2006-05-28	0
2010-06-15	22.10
2016-08-12	56.55
2018-09-11	68.37

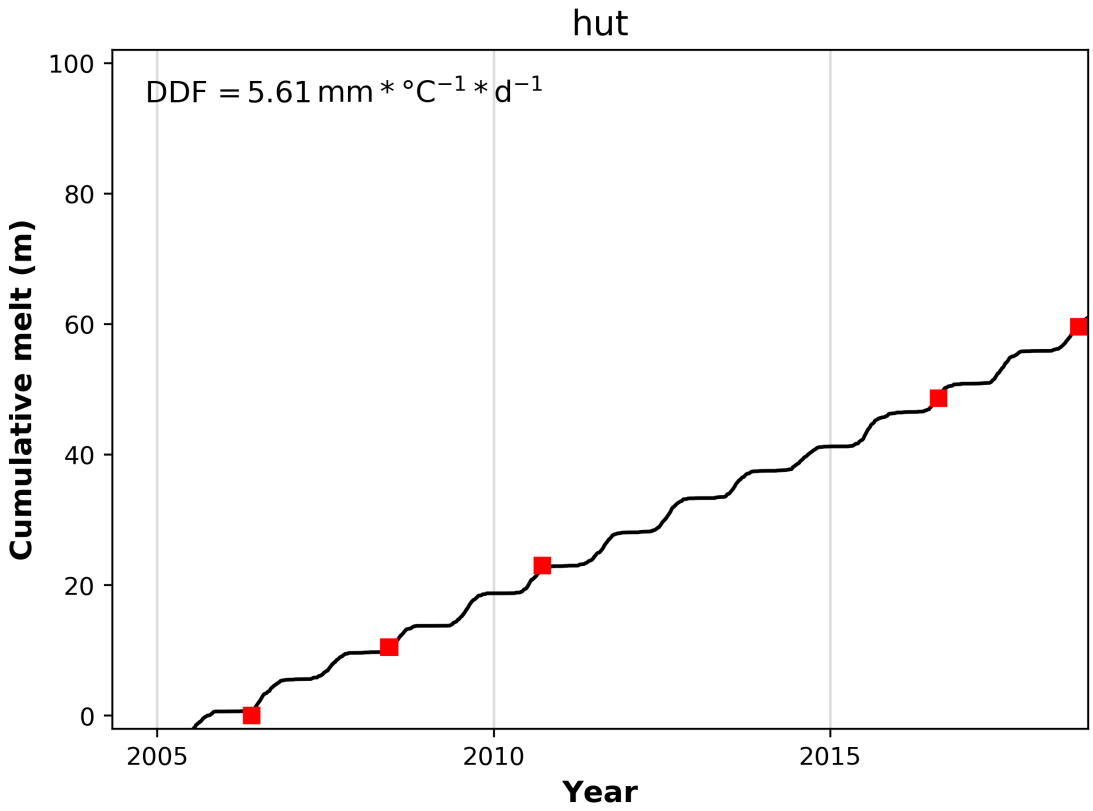

Fig. 29: Degree-Day-Factor 'hut'.

Tab. 13: Ablation 'hut'

Date	Ablation (m)
2006-05-29	0
2008-06-11	10.51
2010-09-22	23.02
2016-08-12	48.67
2018-09-11	59.57

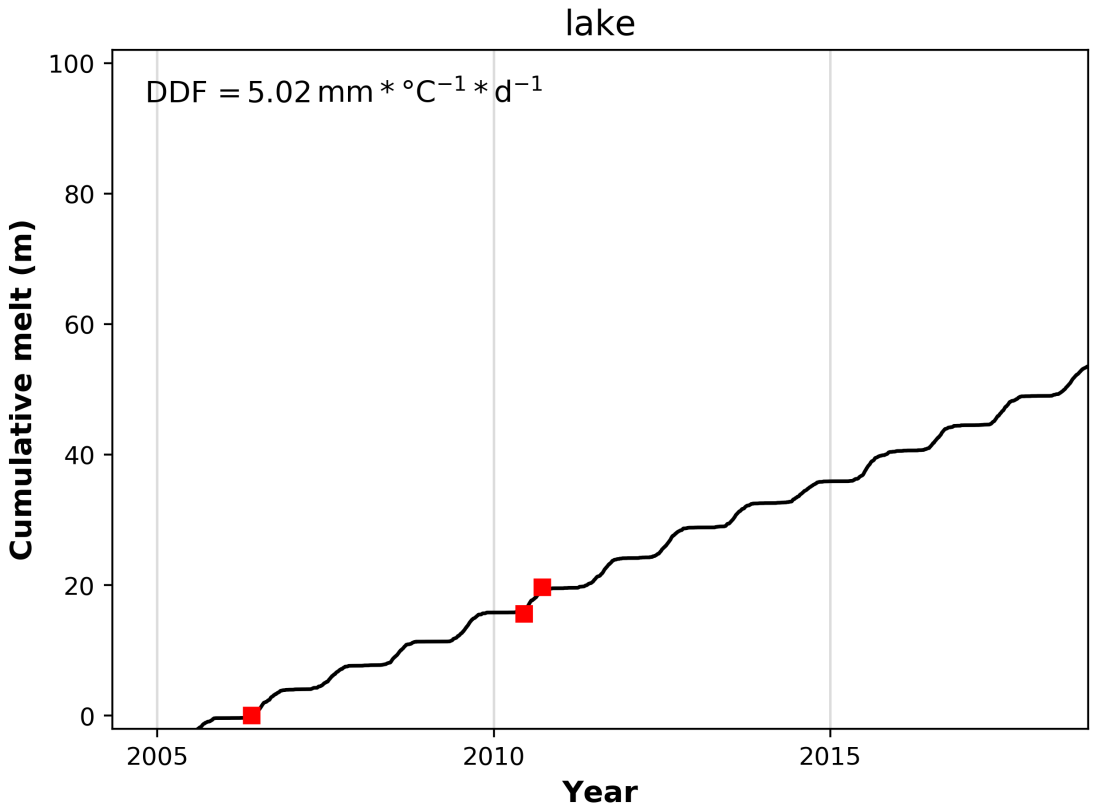

Fig. 30: Degree-Day-Factor 'lake'.

Tab. 14: Ablation 'lake'

Date	Ablation (m)
2006-05-27	0
2010-06-15	15.59
2010-09-22	19.69

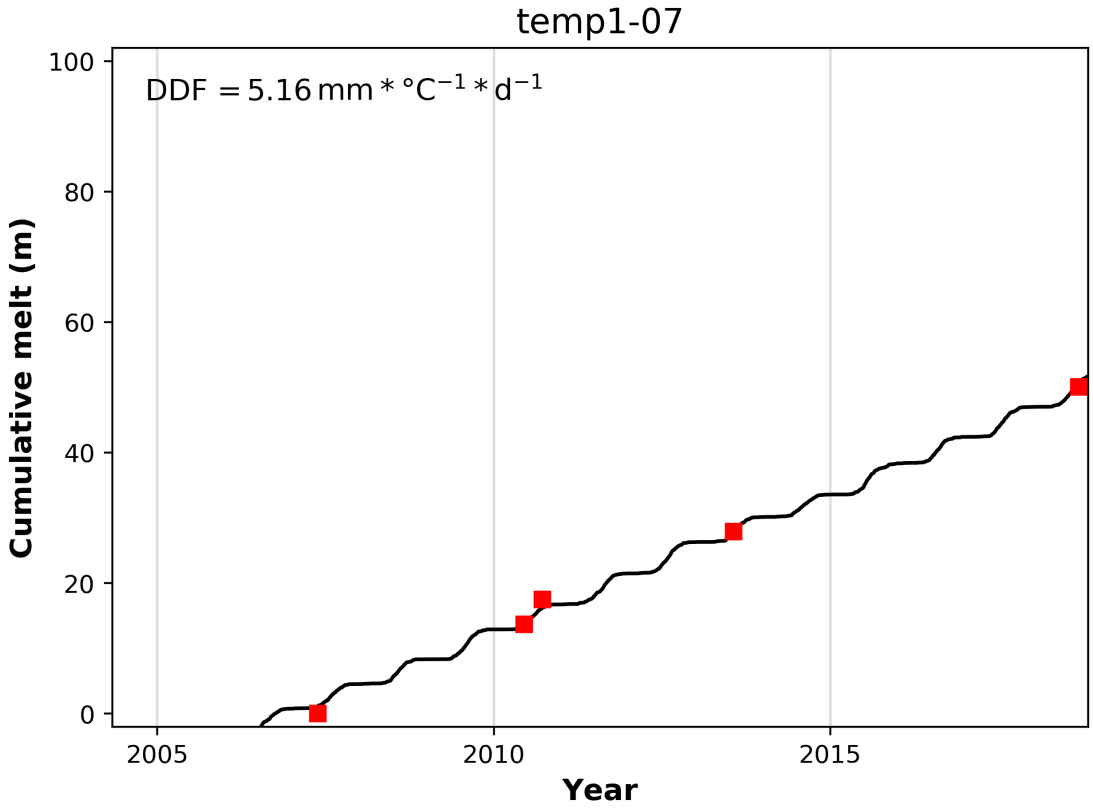

Fig. 31: Degree-Day-Factor 'temp1-07'.

Tab. 15: Ablation 'temp1-07'

Date	Ablation (m)
2007-05-21	0
2010-06-15	13.70
2010-09-22	17.50
2013-07-26	27.90
2018-09-11	50.08

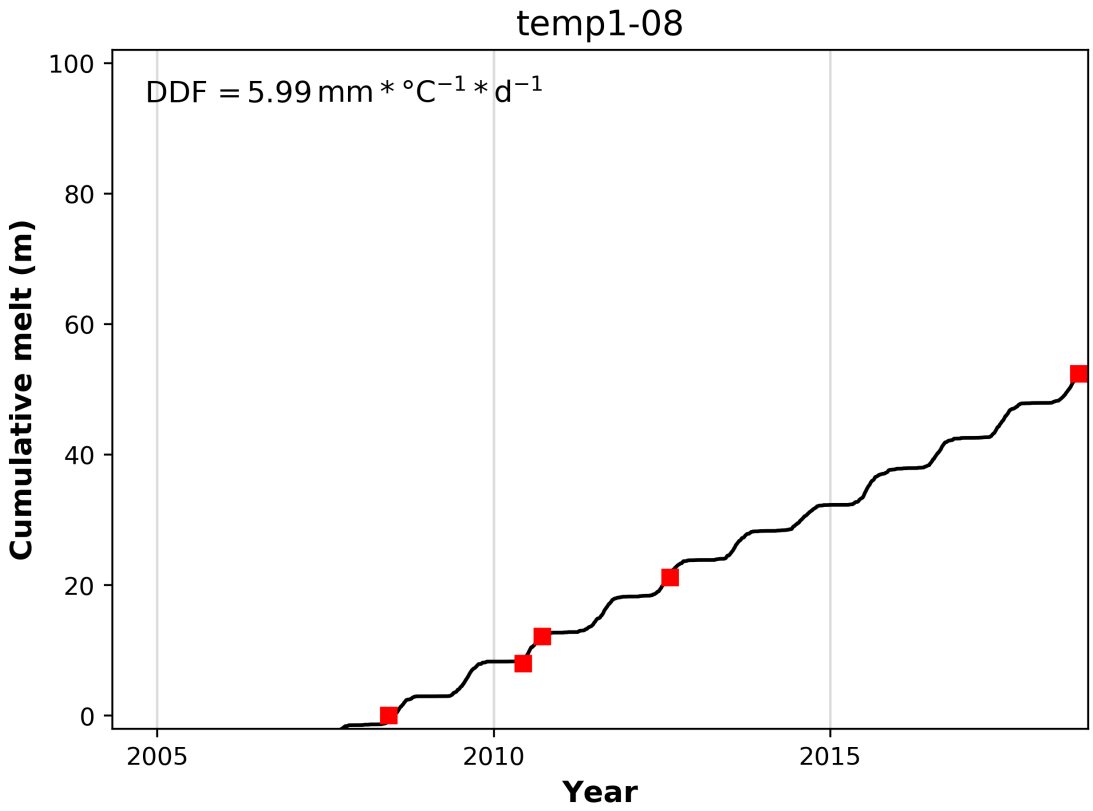

Fig. 32: Degree-Day-Factor 'temp1-08'.

Tab. 16: Ablation 'temp1-08'

Date	Ablation (m)
2008-06-11	0
2010-06-11	8.00
2010-09-22	12.12
2012-08-15	21.17
2018-09-11	52.40

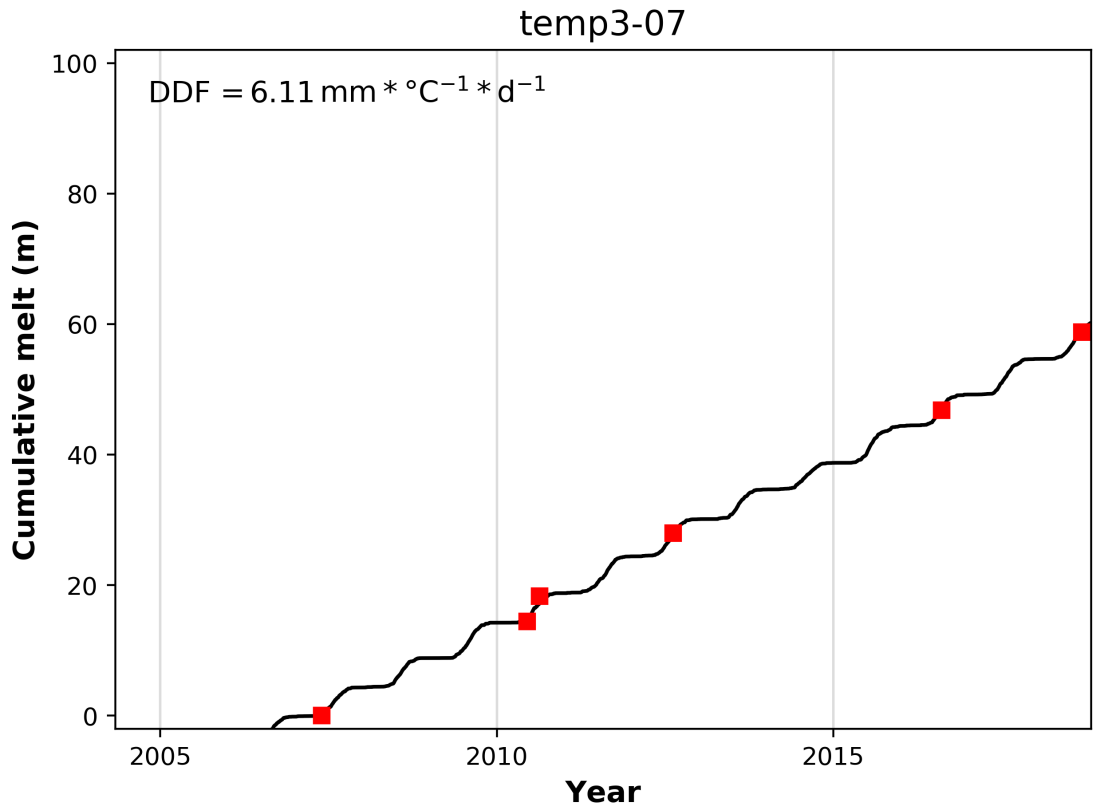

Fig. 33: Degree-Day-Factor 'temp3-07'.

Tab. 17: Ablation 'temp3-07'

Date	Ablation (m)
2007-05-27	0
2010-06-15	14.46
2010-08-22	18.30
2012-08-15	27.95
2016-08-12	46.79
2018-09-11	58.79

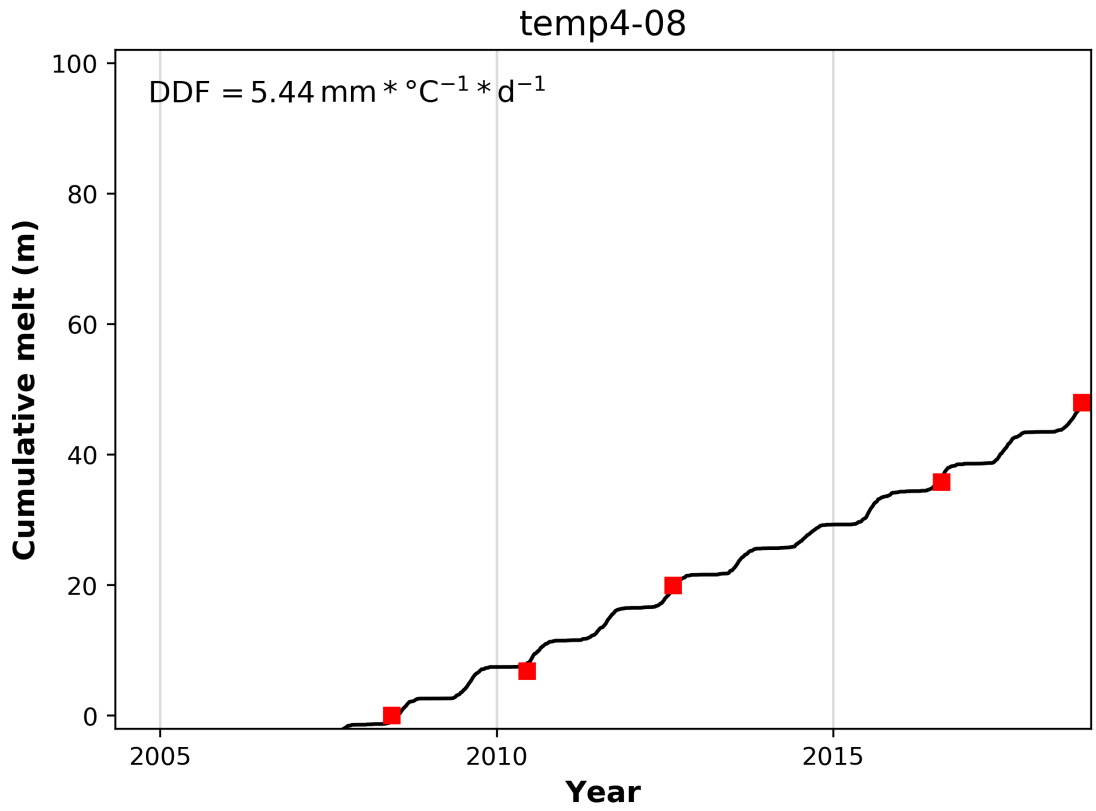

Fig. 34: Degree-Day-Factor 'temp4-08'.

Tab. 18: Ablation 'temp4-08'

Date	Ablation (m)
2008-06-10	0
2010-06-15	6.85
2012-08-15	19.95
2016-08-12	35.77
2018-09-11	47.97

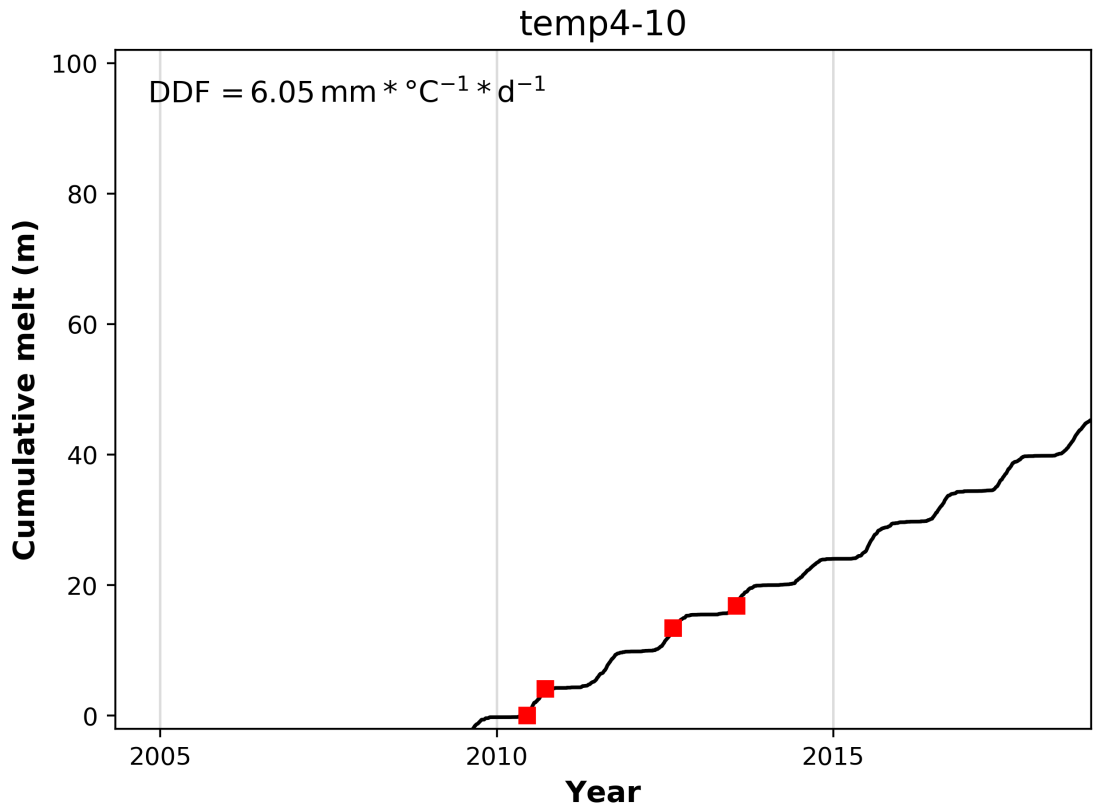

Fig. 35: Degree-Day-Factor 'temp4-10'.

Tab. 19: Ablation 'temp4-10'

Date	Ablation (m)
2010-06-15	0
2010-09-22	4.10
2012-08-15	13.46
2013-07-25	16.80

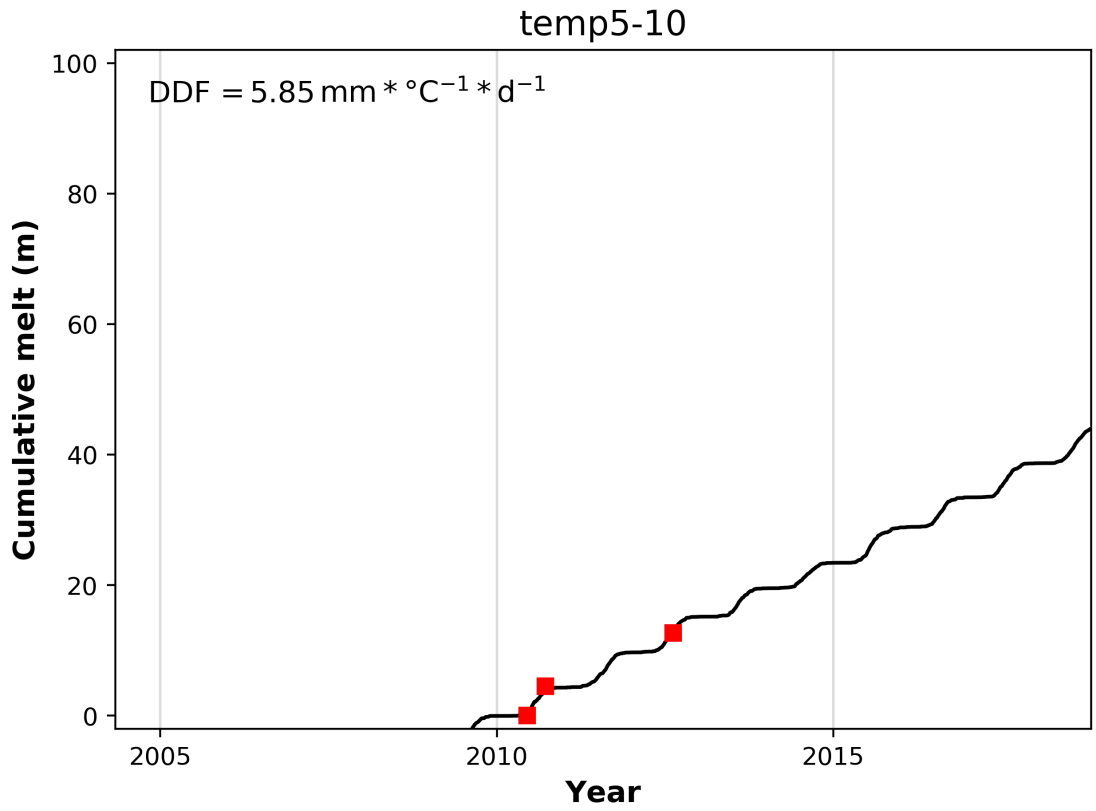

Fig. 36: Degree-Day-Factor 'temp5-10'.

Tab. 20: Ablation 'temp5-10'

Date	Ablation (m)
2010-06-15	0
2010-09-22	4.53
2012-08-15	12.70

10.1.2 Appendix 1.2: Degree-Day-Factors for the Stakes

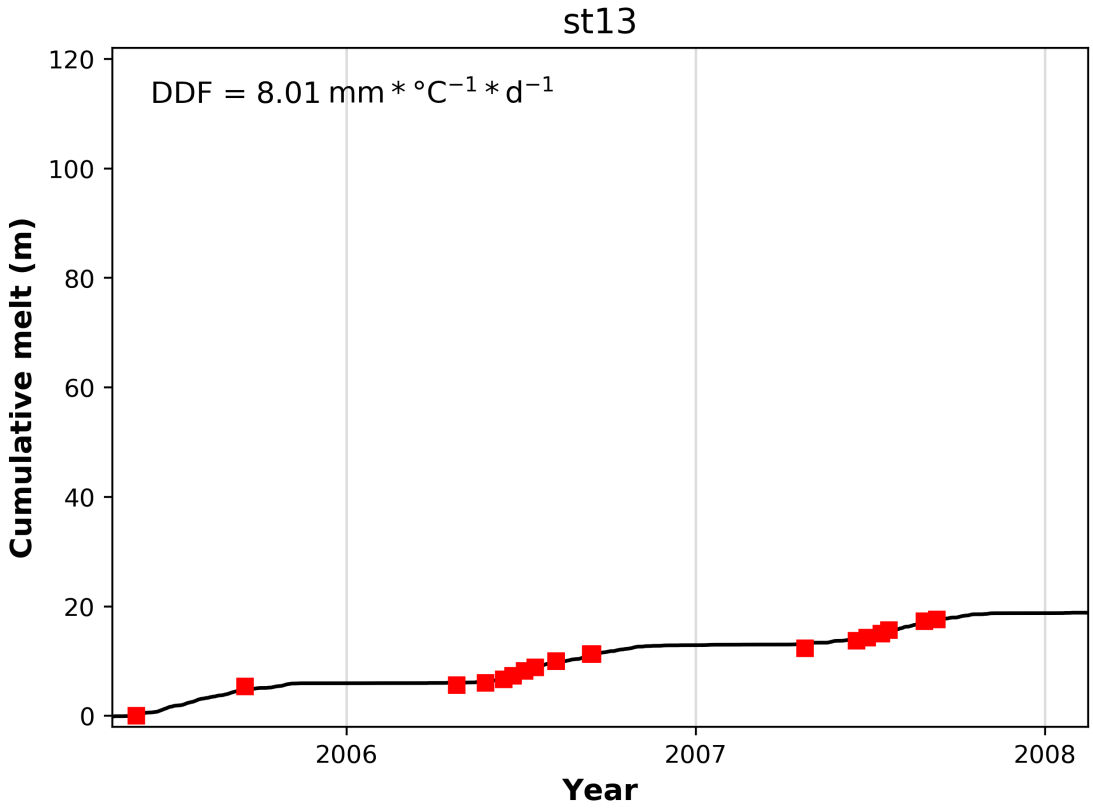

Fig. 37: Degree-Day-Factor 'st13'.

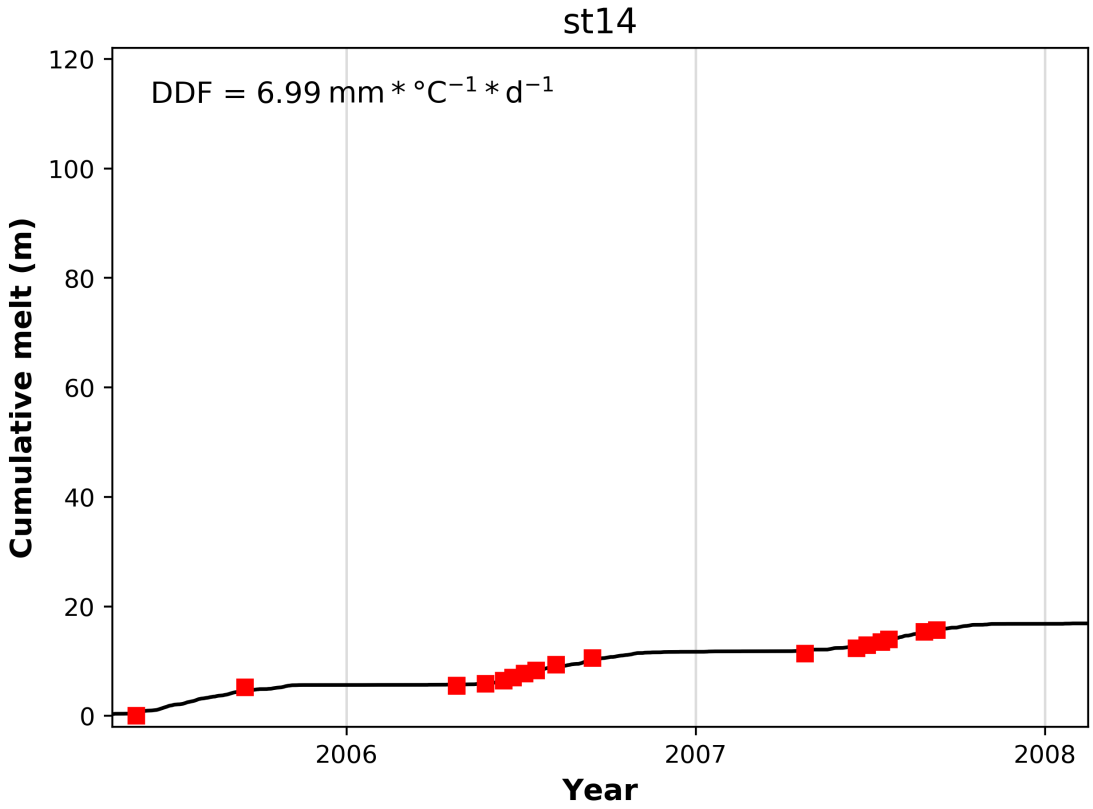

Fig. 38: Degree-Day-Factor 'st14'.

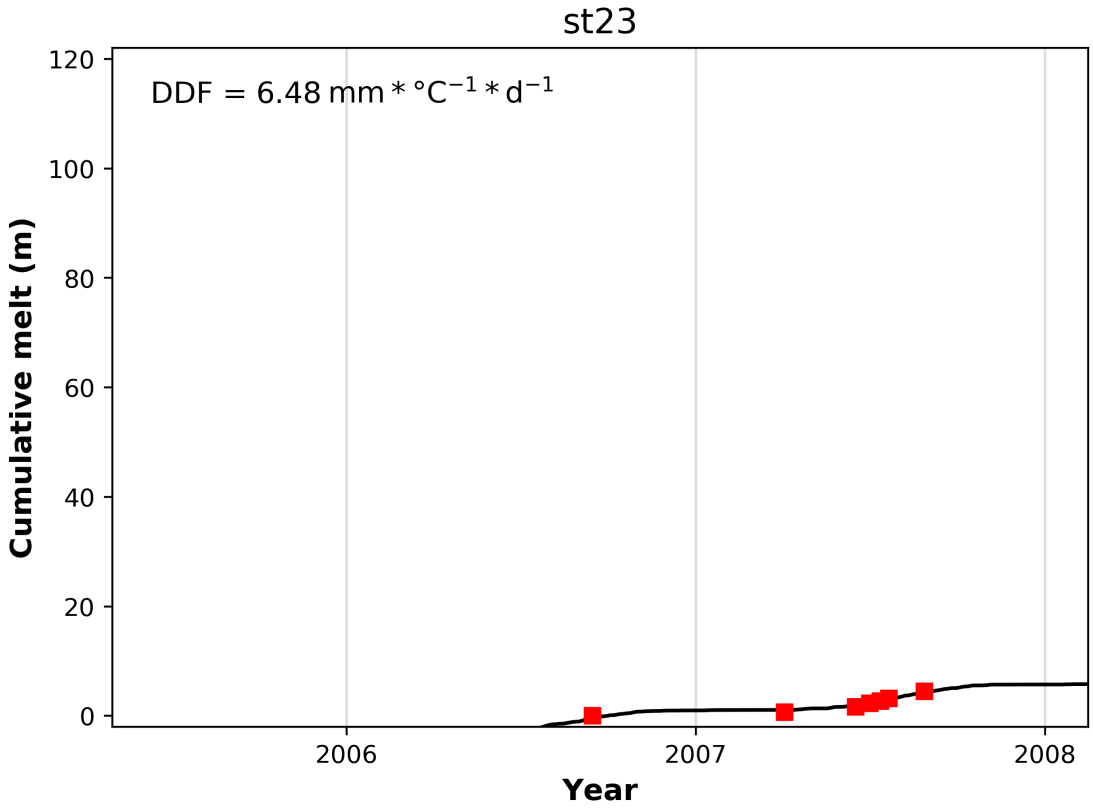

Fig. 39: Degree-Day-Factor 'st23'.

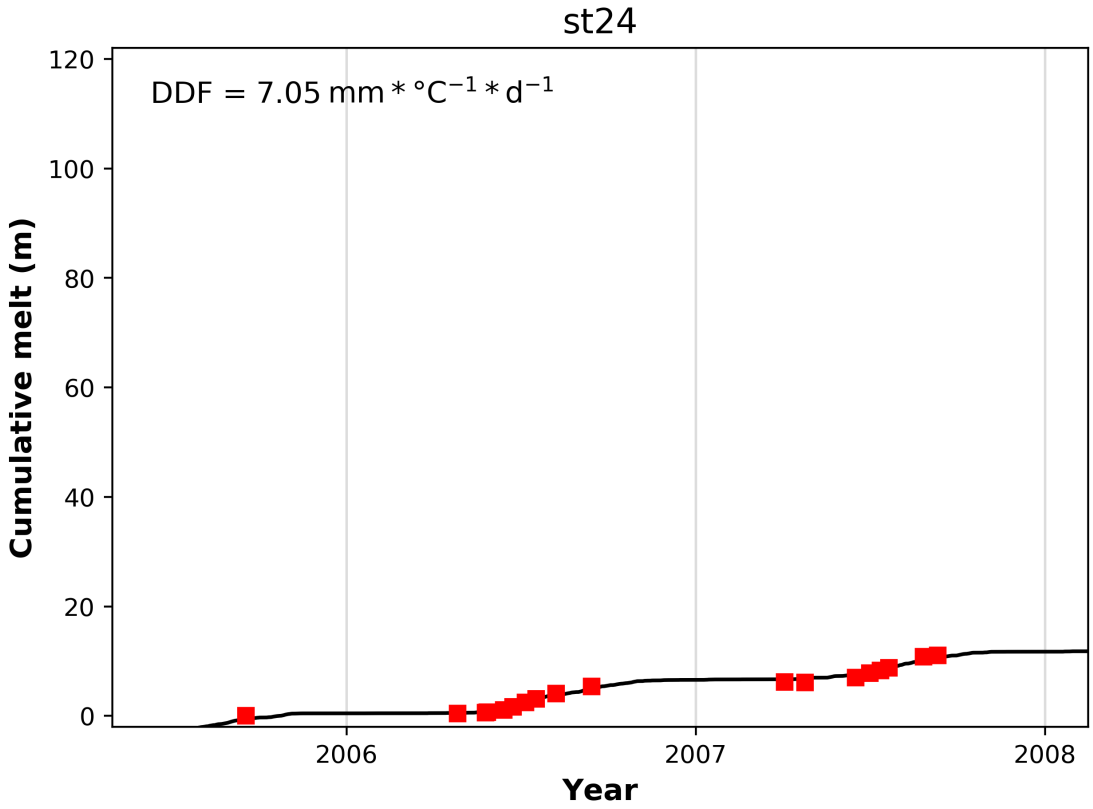

Fig. 40: Degree-Day-Factor 'st24'.

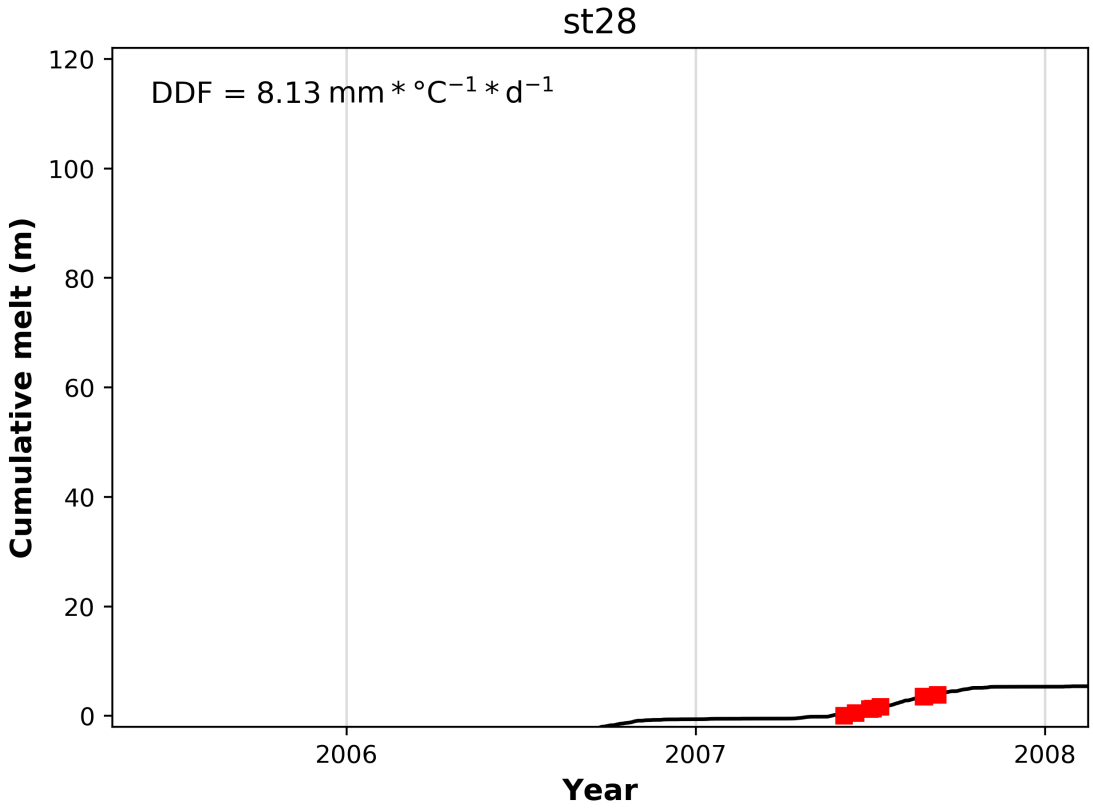

Fig. 41: Degree-Day-Factor 'st28'.

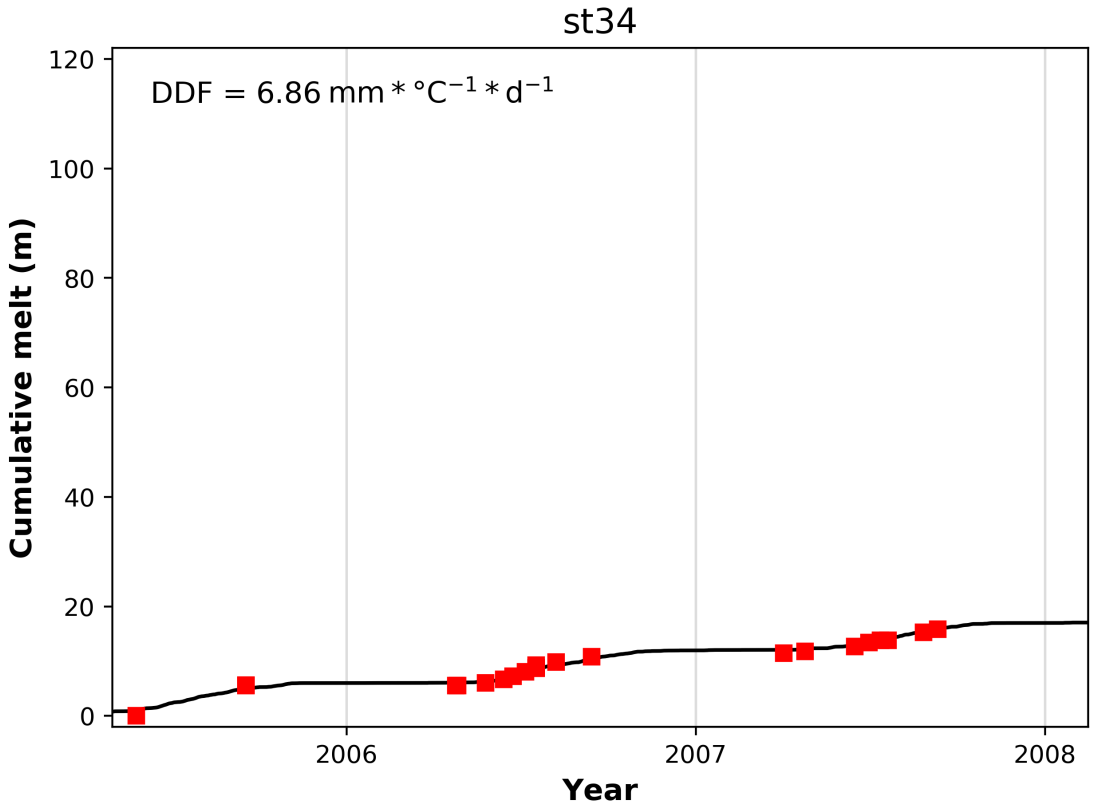

Fig. 42: Degree-Day-Factor 'st34'.

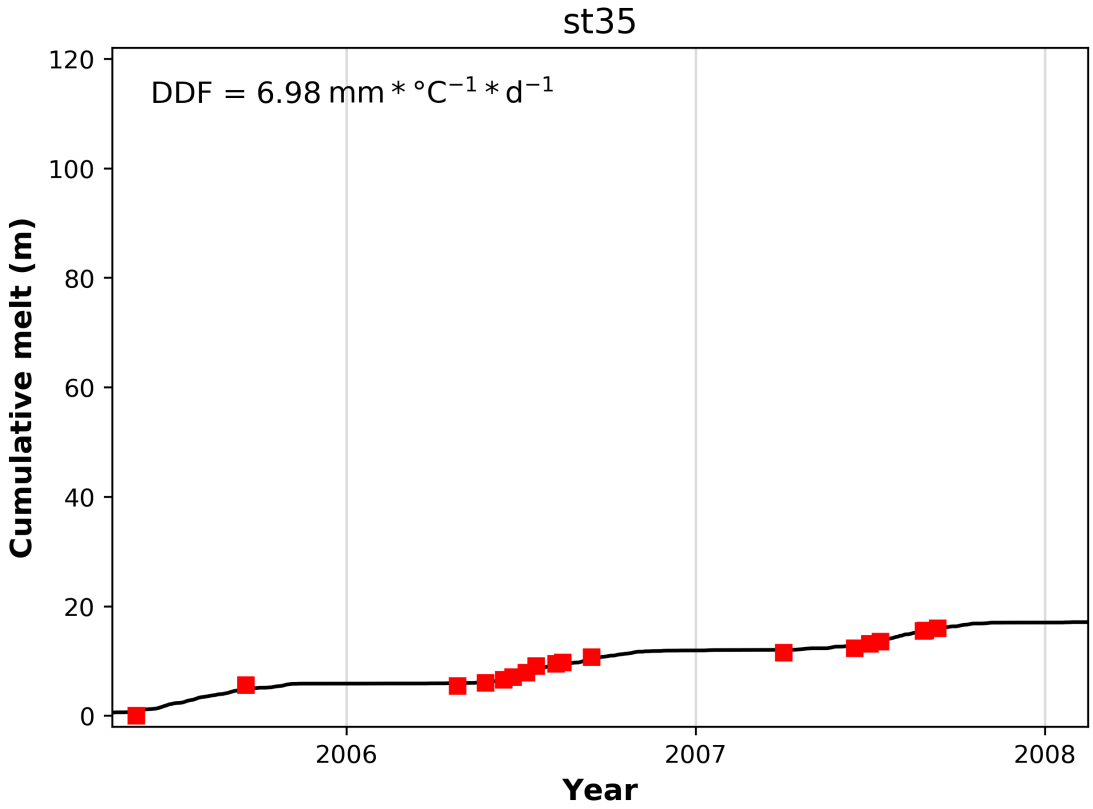

Fig. 43: Degree-Day-Factor 'st35'.

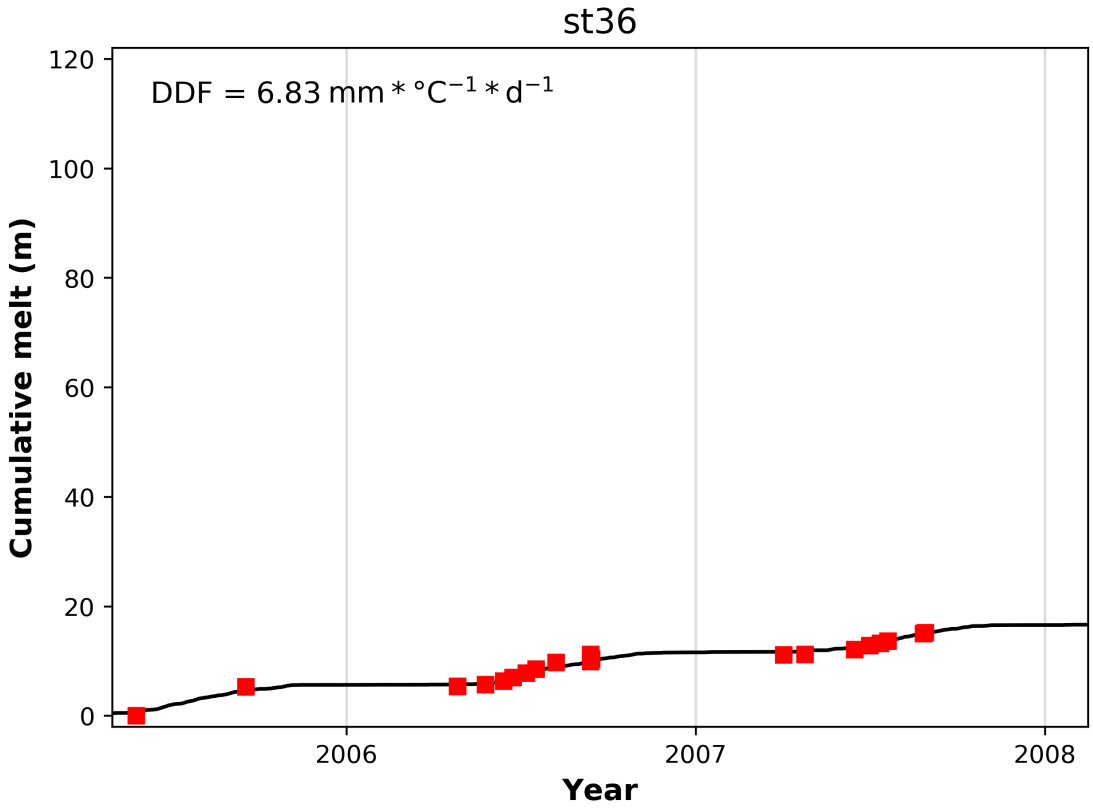

Fig. 44: Degree-Day-Factor 'st36'.

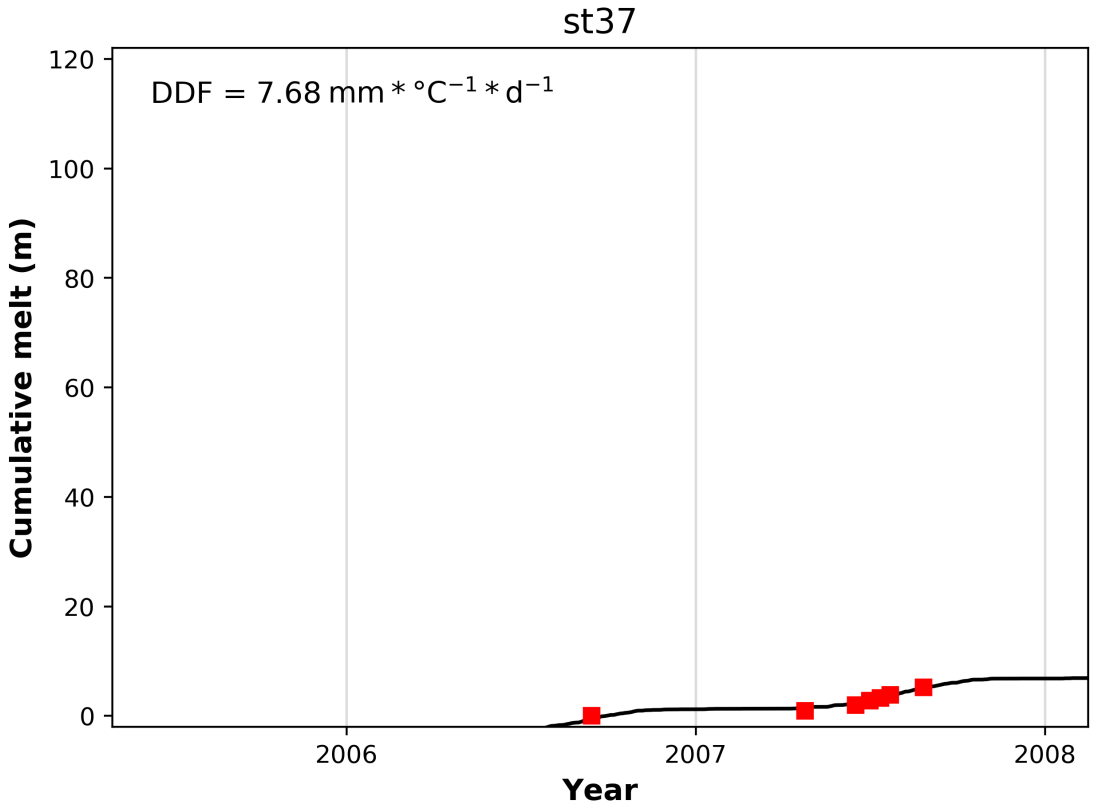

Fig. 45: Degree-Day-Factor 'st37'.

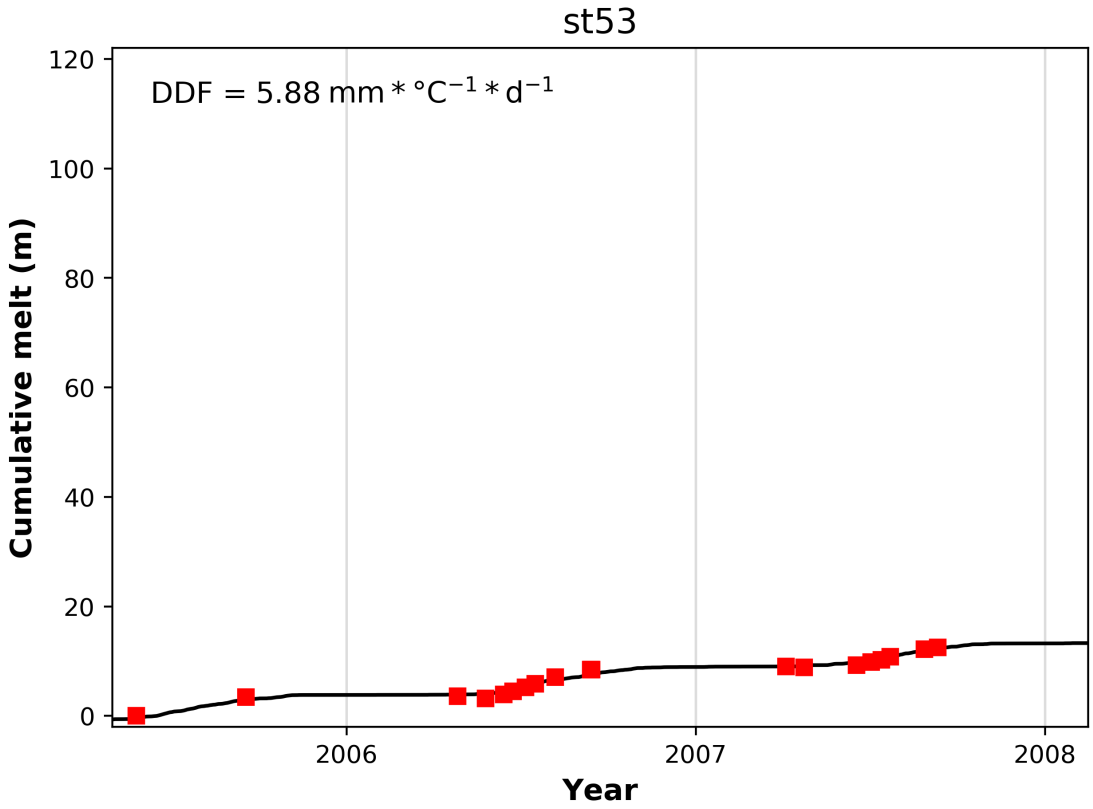

Fig. 46: Degree-Day-Factor 'st53'.

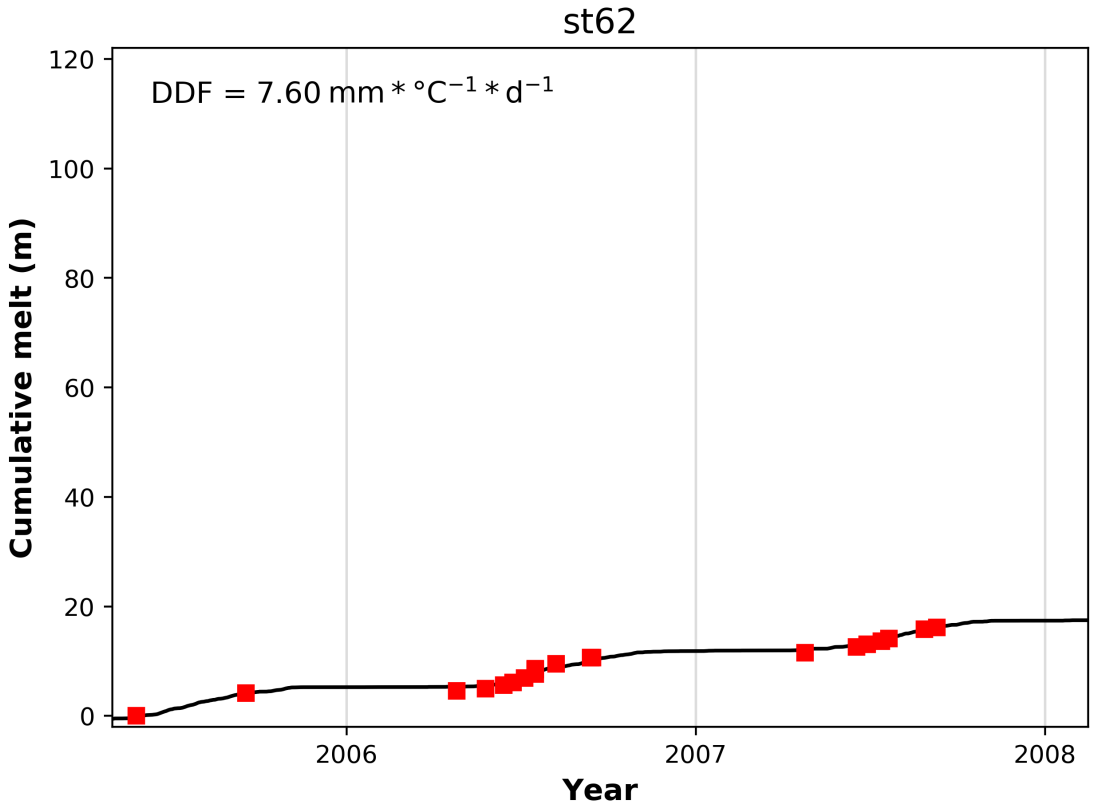

Fig. 47: Degree-Day-Factor 'st62'.

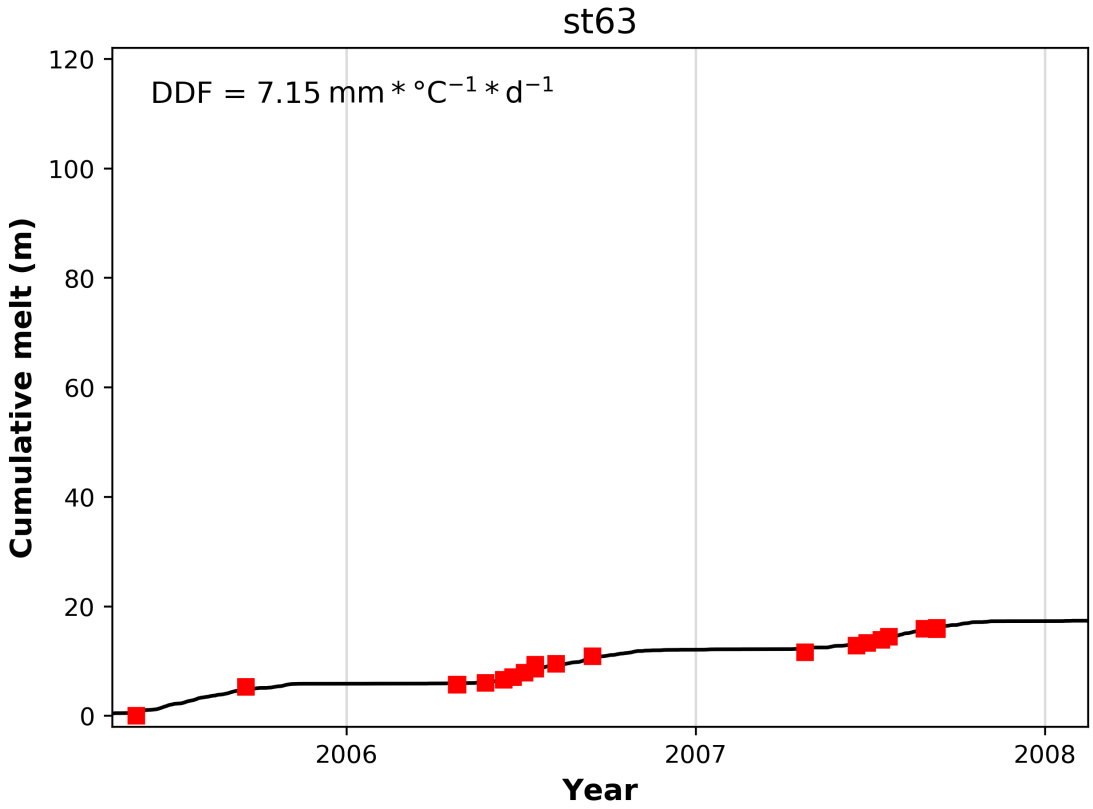

Fig. 48: Degree-Day-Factor 'st63'.

10.2 Appendix 2: Additional Material

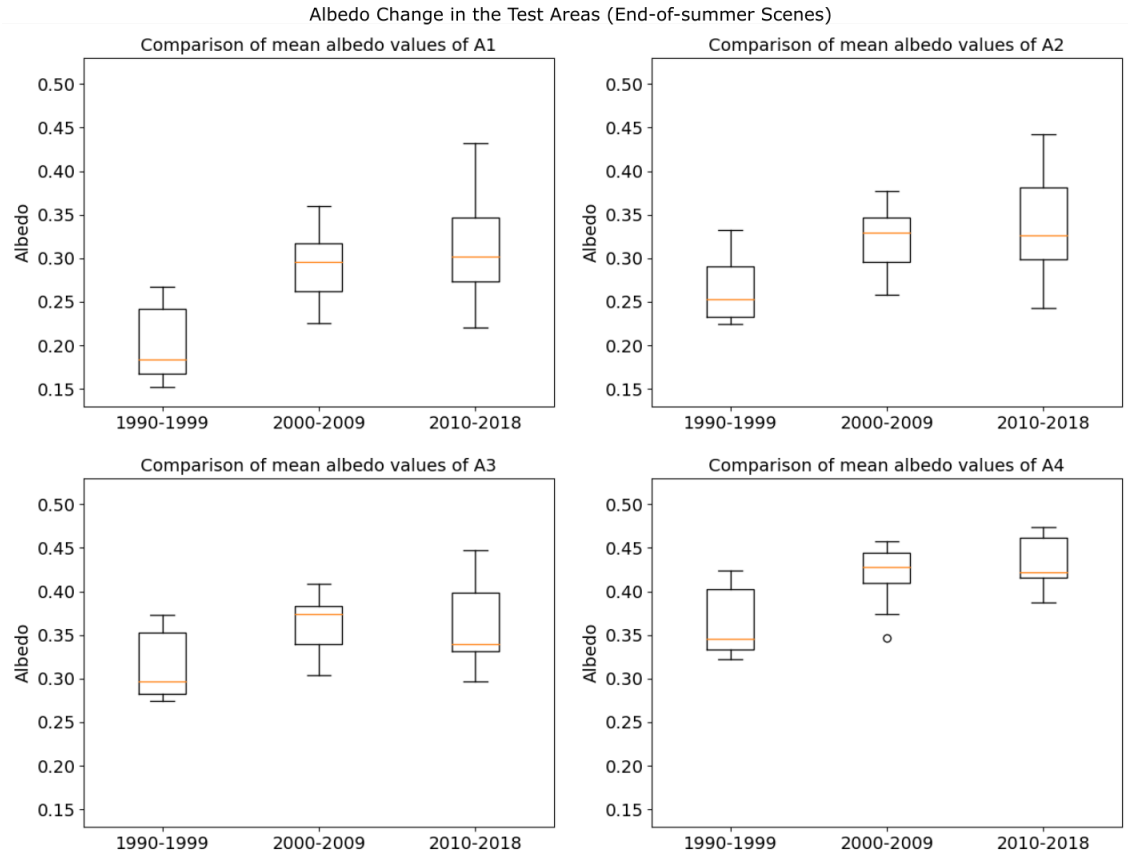

Fig. 49: Boxplots representing the mean albedo values of the end-of-summer scenes in certain time periods.

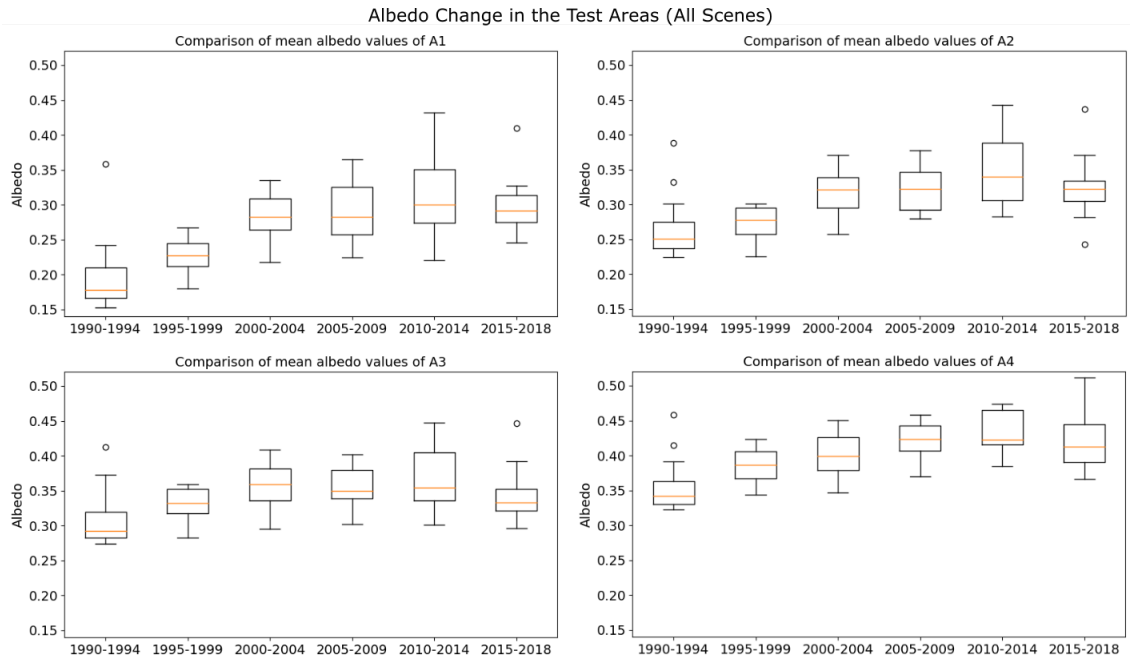

Fig. 50: Boxplots representing all mean albedos in certain time periods.

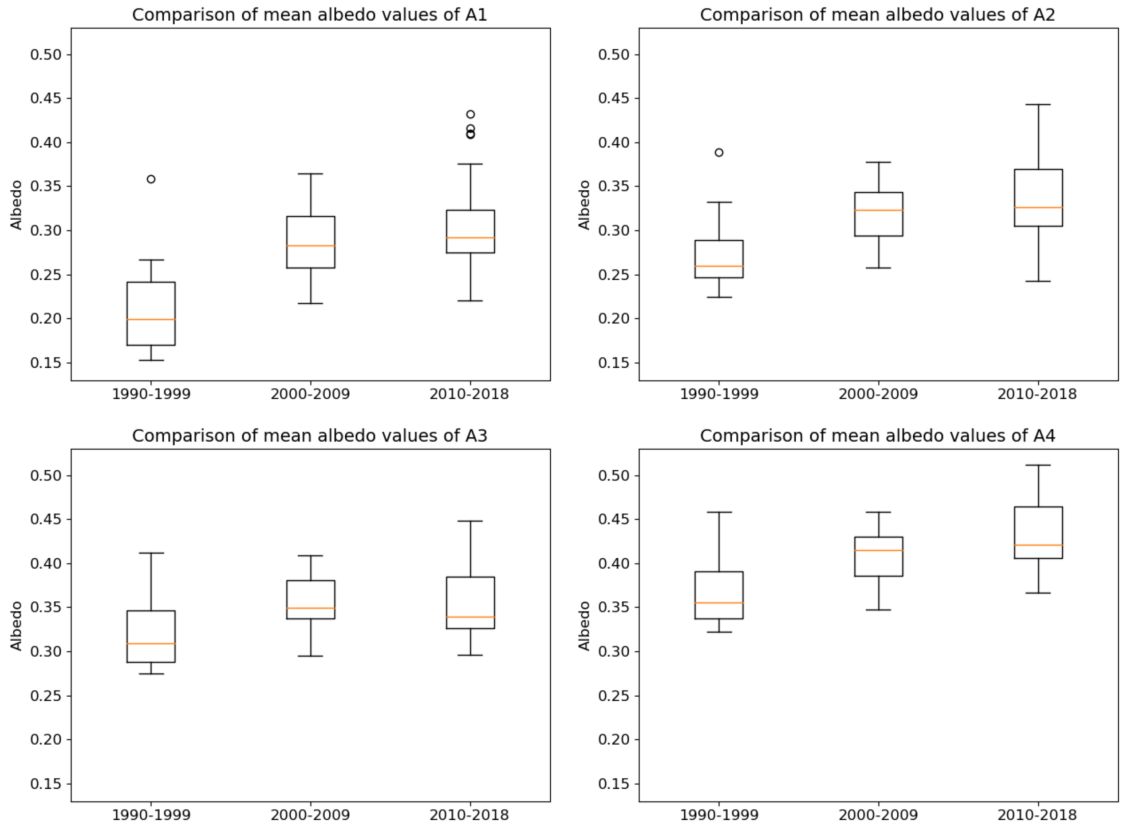

Fig. 51: Boxplots representing all mean albedos in certain time periods.

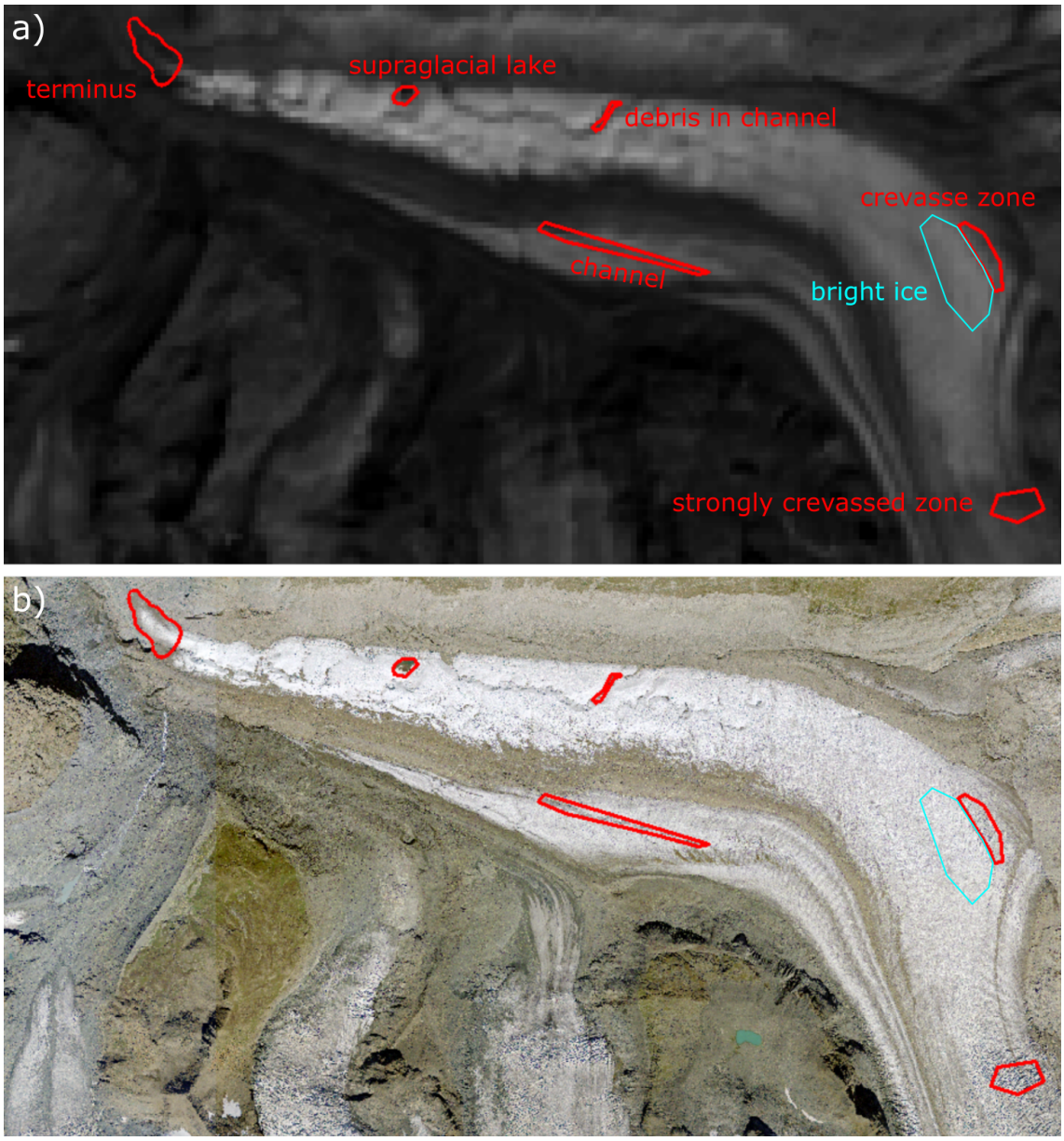

Fig. 52: Comparison of albedo image and SwissImage (swisstopo, 2019).

11 Personal Declaration

I hereby declare that the material contained in this thesis is my own original work. And quotation or paraphrase in this thesis from the published or unpublished work of another individual or institution has been duly acknowledged. I have not submitted this thesis, or any part of it, previously to any institution for assessment purposes.

Zürich, 30.09.2019, Michael Thalmann